INFORMATION TO USERS

This manuscript has been reproduced from the microfilm master. UMI films the text directly from the original or copy submitted. Thus, some thesis and dissertation copies are in typewriter face, while others may be from any type of computer printer.

The quality of this reproduction is dependent upon the quality of the copy submitted. Broken or indistinct print, colored or poor quality illustrations and photographs, print bleedthrough, substandard margins, and improper alignment can adversely affect reproduction.

In the unlikely event that the author did not send UMI a complete manuscript and there are missing pages, these will be noted. Also, if unauthorized copyright material had to be removed, a note will indicate the deletion.

Oversize materials (e.g., maps, drawings, charts) are reproduced by sectioning the original, beginning at the upper left-hand corner and continuing from left to right in equal sections with small overlaps. Each original is also photographed in one exposure and is included in reduced form at the back of the book.

Photographs included in the original manuscript have been reproduced xerographically in this copy. Higher quality 6" x 9" black and white photographic prints are available for any photographs or illustrations appearing in this copy for an additional charge. Contact UMI directly to order.

UMI

A Bell & Howell Information Company
300 North Zeeb Road, Ann Arbor MI 48106-1346 USA
313/761-4700 800/521-0600

Université d'Ottawa · University of Ottawa

A Photoluminescence Study of Intermixed III/V Semiconductor Quantum Well Structures

By

Paul Garrett Piva

Submitted to the School of Graduate Studies in
partial fulfillment of the requirements for the degree of M.Sc. in Physics

Paul Garrett Piva
University of Ottawa
Ottawa, Canada
1996

National Library of Canada

Bibliothèque nationale du Canada

Acquisitions and Bibliographic Services

Acquisitions et services bibliographiques

395 Wellington Street
Ottawa ON K1A 0N4
Canada

395, rue Wellington
Ottawa ON K1A 0N4
Canada

Your file Votre référence

Our file Notre référence

The author has granted a non-exclusive licence allowing the National Library of Canada to reproduce, loan, distribute or sell copies of this thesis in microform, paper or electronic formats.

L'auteur a accordé une licence non exclusive permettant à la Bibliothèque nationale du Canada de reproduire, prêter, distribuer ou vendre des copies de cette thèse sous la forme de microfiche/film, de reproduction sur papier ou sur format électronique.

The author retains ownership of the copyright in this thesis. Neither the thesis nor substantial extracts from it may be printed or otherwise reproduced without the author's permission.

L'auteur conserve la propriété du droit d'auteur qui protège cette thèse. Ni la thèse ni des extraits substantiels de celle-ci ne doivent être imprimés ou autrement reproduits sans son autorisation.

0-612-26357-6

Canadä

To Nanny and Madeleine

ABSTRACT

Vacancy enhanced compositional mixing of quantum well (QW) structures induced by ion beam implantation has shown itself to be a useful technique for achieving spatially selective tuning of the QW bandgap. As QWs form the active region of most optoelectronic devices, this method is being actively pursued as a means of monolithically integrating many such components onto a single substrate.

This work presents a novel variation on this technique allowing one to deliver several times the maximum QW bandgap shift traditionally attributed to a single implant/RTA (rapid thermal anneal) cycle. This is achieved by distributing the total implanted ion dose over multiple sequential ion implantation and RTA cycles. Continuous-wave photoluminescence (CWPL) measurements are used to monitor the extent of QW intermixing taking place, and demonstrate the success of this innovation in various material systems (GaAs/AlGaAs, InGaAs/GaAs, InGaAs/InP).

In another experiment, the effectiveness of high energy (8 MeV As^{4+}) implantation in intermixing GRINSCH (graded-index separate confinement heterostructure) QW laser structures grown in InGaAs/GaAs was demonstrated. Preliminary investigations were carried out on the effects of sample temperature, and ion current density during implantation on the intermixed QWs. Results from CWPL measurements suggest that

better quality intermixed material can be obtained by implanting at elevated sample temperatures, and low ion current densities.

Finally the effect of ion implantation induced intermixing on the effective radiative lifetimes in GaAs/AlGaAs quantum wells is investigated using the technique of time-resolved photoluminescence (TRPL). Below the critical dose (required to initiate disordering), the carrier lifetimes appear enhanced by the processing although no changes are discernible in the CWPL spectra. Above the critical dose, carrier lifetimes are reduced by residual defects created in the intermixed wells by the implantation procedure. These observations reflect the greater sensitivity of TRPL in detecting residual damage produced by intermixing QW material over CWPL.

STATEMENT OF ORIGINALITY

The experimental results presented in this thesis were obtained either directly by the author or through his collaborations during the period of his M.Sc. research project, and is to the best of his knowledge original. This encompasses in particular:

(1) The photoluminescence (PL) study of enhanced quantum well intermixing achieved by multiple ion implantations and RTAs in GaAs/AlGaAs, InGaAs/GaAs, and InGaAs/InP QW structures.

(2) A PL study of high energy (8 MeV As^{4+}) implantation induced intermixing of GRINSCH (graded-index separate confinement heterostructure) InGaAs/GaAs QW laser structures; and a preliminary investigation on the influence of sample temperature, and ion current density during implantation on the intermixing process.

(3) The effect of ion implantation induced disordering on carrier lifetimes in GaAs/AlGaAs quantum well structures both above and below the critical dose.

No portion of this work has been previously submitted to any other academic institution for credit.

PUBLICATIONS RELATED TO THESIS

*<u>**Bandgap Tuning of Semiconductor Quantum Well Structures Using Ion Implantation**</u>. P.G. Piva, P.J. Poole, S. Charbonneau, E.S. Koteles, M. Buchanan, G. Aers, A.P. Roth, Z.R. Wasilewski, J. Beauvais, R.D. Goldberg. *Superlattices and Microstructures*, **15** (4) 385, 1994.

*<u>**Enhanced Compositional Disordering of Quantum Wells in GaAs/AlGaAs and InGaAs/GaAs using focused Ga ion beams**</u>. P.G. Piva, P.J. Poole, M. Buchanan, I. Templeton, G.C. Aers, R. Williams, Z.R. Wasilewski, E.S. Koteles, S. Charbonneau. *Appl. Phys. Lett.* **65** (5) 621, 1994.

*<u>**The Enhancement of Quantum Well Intermixing Through Repeated Ion Implantation**</u>. P.J. Poole, P.G. Piva, M. Buchanan, G.C. Aers, A.P. Roth, M. Dion, Z.R. Wasilewski, E.S. Koteles, S. Charbonneau, J. Beauvais. *Semiconductor Sci. Technol.* **9** 2134, 1994.

*<u>**Enhanced Quantum Well Intermixing Using Multiple Ion Implantation**</u>. P.J. Poole, P.G. Piva, M. Buchanan, G. Champion, I. Templeton, G. Aers, R. Williams, A.P. Roth, Z.R. Wasilewski, E.S. Koteles, S. Charbonneau. *SPIE Conference Proceedings*, Vol. 2139 130, 1994.

*<u>**Effect of Implantation Dose on Photoluminescence Decay Times in Intermixed GaAs/AlGaAs Quantum Wells**</u>. P.G. Piva, S. Charbonneau, I.V. Mitchell, R.D. Goldberg. *Appl. Phys. Lett.* **68** (16) 2252, 1996.

<u>**Quantum Well Intermixing for Optoelectronic Integration Using High Energy Ion Implantation**</u>. S. Charbonneau, P.J. Poole, P.G. Piva, G.C. Aers, E.S. Koteles, M. Fallahi, J.-J. He, J.P. McCaffrey, M. Buchanan, M. Dion, R.D. Goldberg, I.V. Mitchell. *J. Appl. Phys.* **78** (6) 3697, 1995.

<u>**Threshold Dose for Ion-Induced Intermixing in InGaAs/GaAs Quantum Wells**</u>. L.B. Allard, G.C. Aers, P.G. Piva, P.J. Poole, M. Buchanan, I.M. Templeton, T.E. Jackman, S. Charbonneau. *Appl. Phys. Lett.* **64** (18) 2412, 1994.

<u>**Bandgap Tuning of Semiconductor Quantum Well Laser Structures Using High Energy Ion Implantation**</u>. S. Charbonneau, P.J. Poole, P.G. Piva, M. Buchanan, R.D. Goldberg, I.V. Mitchell. *Nucl. Instr. and Methods in Phys. Research B.* **106** 457, 1995.

*included in Chapter IV of this work

AUTHOR'S CONTRIBUTIONS TOWARDS PUBLICATIONS PRESENTED IN THESIS

1)Bandgap Tuning of Semiconductor Quantum Well Structures Using Ion Implantation:

P.G. Piva: Author of first draft and all subsequent corrections, 50% of continuous wave photoluminescence (CWPL) work (low energy implanted samples) 100% CWPL (high energy implanted samples) and photoluminescence excitation measurements.

2)Enhanced Compositional Disordering of Quantum Wells in GaAs/AlGaAs and InGaAs/GaAs using focused Ga ion beams:

P.G. Piva: Author of first draft. Subsequent corrections to manuscript carried out by S. Charbonneau and G. C. Aers. 70% of CWPL work.

3)The Enhancement of Quantum Well Intermixing Through Repeated Ion Implantation:

P.G. Piva: Corrections and comments to manuscript. 50% of CWPL work.

4)Enhanced Quantum Well Intermixing Using Multiple Ion Implantation:

P.G. Piva: Corrections and comments to manuscript. 50% of CWPL work.

5)Effect of Implantation Dose on Photoluminescence Decay Times in Intermixed GaAs/AlGaAs Quantum Wells:

P.G. Piva: Author of first draft and all subsequent corrections. Responsible for design of experiments, selection and post-implantation annealing of samples. 100% of characterisation work in paper. (i.e. CWPL and time-resolved PL work)

ACKNOWLEDGMENTS

To begin with, I would like to thank Dr. Sylvain Charbonneau for his patience, generosity, and support both as a supervisor and friend. In the time I have spent in his group, I have come to deeply admire and respect the creativity and dynamism that characterise his daily activities as a researcher. From him, I depart with much.

I also wish to thank Dr. Philip Poole for his invaluable assistance in the laboratory. To Sylvain Raymond, I would like to say 'merci', both for his help early on with the time-resolved set-up, and for many lively debates - scientific and otherwise.

During my joint stay at the NRC and the University of Ottawa, I had the opportunity to exchange or collaborate with a host of people, among which I wish to single out: Geof Aers, Roberto Benzaquen, Margaret Buchanan, Mike Davies, Michel Dion, Simon Fafard, Paul Finnie, Bela Joos, Emil Koteles, Richard Normandin, Robert Parent, and Alain Roth. It has been a pleasure working with and knowing you all!

Finally, I would like to extend my gratitude to Sofia Zouroudis (and family), my family, and God for their unfailing support over the years.

The financial support of Dr. Sylvain Charbonneau, the National Research Council, the Natural Sciences and Engineering Research Council of Canada, and the University of Ottawa are greatfully acknowledged.

TABLE OF CONTENTS

Abstract iii
Statement of Originality v
Publications Related to Thesis vi
Author's Contributions Towards Publications Presented in Thesis vii
Acknowledgments viii
List of Figures x
Preface xi

Chapter 1 - Photoluminescence 1
1.1 Introduction to Radiative Recombination in III/V Semiconductors 1
1.2 Free and Bound Excitons 2
1.3 Donor-Acceptor Recombination 9
1.4 Radiative Recombination in Semiconductor Quantum Wells 11

Chapter 2 - Quantum Well Intermixing 17
2.1 Motivation 17
2.2 Quantum Well Intermixing 20
2.3 A Model for QW Interdiffusion 27

Chapter 3 - Experimental Techniques and Apparatus 32
3.1 Introduction 32
3.2 Samples 32
3.3 Ion Implantation 33
3.3.1 TRIM 35
3.4 Thermal Annealing 40
3.5 PL Characterization 43
3.5.1 Excitation Sources 43
3.5.2 Spectroscopic Instrumentation 48

Chapter 4 - Results 53
4.1 List of Presented Papers 53
Appendix A: *Bandgap Tuning of Semiconductor Quantum Well Structures Using Ion Implantation* 54
Appendix B: *Enhanced Compositional Disordering of Quantum Wells in GaAs/AlGaAs and InGaAs/GaAs Using Focused Ga^+ Ion Beams* 55
Appendix C: *The Enhancement of Quantum Well Intermixing Through Repeated Ion Implantation* 56
Appendix D: *Enhanced Quantum Well Intermixing Using Multiple Ion Implantation* 57
Appendix E: *Effect of Implantation Dose on Photoluminescence Decay Times in Intermixed GaAs/AlGaAs Quantum Wells* 58

Chapter 5 - Conclusions....59

References....62

LIST OF FIGURES

1.1 K-Space representation of the PL process in a bulk direct gap semiconductor....3

1.2 Principal electron-hole decay processes in semiconductors....3

1.3 Band-edge profile and energy gaps for a type 1 semiconductor QW structure....13

2.1 Bandgap requirement for the optimal integration of a laser, modulator and passive waveguide section on a single substrate....18

2.2 Schematic of QW crystal structures and associated energy band diagrams....21

2.3 Ion implantation induced intermixing of a QW structure....25

2.4 Time evolution of concentration-distance curves for a QW initially of width 2h and concentration C_o....31

3.1 Ion ranges for 8.56 MeV As^{4+} ions in $Al_{0.2}Ga_{0.8}As$....38

3.2 Vacancy Production Efficiencies for 8.56 MeV As^{4+} and and 8 MeV Bi^{4+}....39

3.3 Cross-sectional diagram of the RTA heating chamber and associated components....41

3.4 RTA temperature determination for InGaAs/GaAs QW structures....42

3.5 Schematic layout of pulsed laser system employed in performing time-resolved PL experiments....45

3.6 Schematic diagram of the Bomem Michelson spectrometer....50

3.7 Photoluminescence setup employed to obtain spectra in continuous wave, and time-resolved PL experiments....52

PREFACE

This thesis differs from the standard format in that it makes direct use of scientific publications as a means of presenting the experimental work completed during the tenure of the author's M.Sc. project. As such, the first three chapters of this thesis (Photoluminescence, Quantum Well Intermixing, and Experimental Techniques and Apparatus), as well as the final 'Conclusions' chapter, serve primarily to expand on background concepts and experimental techniques only hinted at in the publications. For this reason, the reader may gain a rapid overview of the thesis by beginning with an examination of the papers appearing in Chapter 4. This approach is also recommended as it will assist the reader in uncovering the common thread uniting the various chapters of this work. The task of presenting the experimental results has been left solely to the papers and has not been repeated elsewhere in the text.

CHAPTER 1

Photoluminescence

1.1 Introduction to Radiative Recombination in III/V Semiconductors[1.1]

In semiconductors, photoluminescence (PL) is the name given to the light emitted by the recombination of photo-excited electrons with holes in a crystalline solid. In a typical experiment, a sample is irradiated with light from an external source (such as a laser) possessing photons of energy roughly equal to or greater than the bandgap of the material under study. Electrons in the illuminated volume absorbing these photons are then promoted from the valence band (VB) to the conduction band (CB). These photo-excited carriers will then diffuse away from the illuminated surface while being depleted by both radiative and nonradiative processes. Since the absorption coefficient for both the above bandgap radiation and the recombination radiation is large, the corresponding PL will come from a region only a few microns in depth from the sample surface.

Once created, the electrons and holes, subject to Coulombic attraction, may form into excitons (X). These are essentially hydrogen like particles where the electrons and holes have become bound to one another. Once formed, the excitons may diffuse through the crystal, and are referred to as free excitons (FE). As excitons posses no net charge, their displacement does not constitute an electric current. Before the FEs recombine,

however, a portion of them may become trapped at donor (D) or acceptor (A) sites in either neutral or ionized states, and are then referred to as bound excitons (BE).

Another form of luminescence arises from photo-excited carriers which become localized at electrically active sites within the lattice. Electrons becoming bound to donors can recombine radiatively with holes on acceptors and result in what is known as donor-acceptor pair (DAP) luminescence. Other luminescence mechanisms may include the recombination of free electrons with holes (band to band luminescence), the recombination of free electrons with acceptors, and finally the recombination of holes with donors (see figures 1.1 and 1.2). In all cases, the energies of the released photons will be characteristic of the surroundings experienced by the carriers during their recombination. In such a way then, the PL spectrum emitted from a photo-excited semiconductor will contain a wealth of information regarding its internal structure and composition. As a result, PL lends itself as a powerful, non-destructive characterization tool in the development of optoelectronic semiconductor devices.

1.2 Free and Bound Excitons[1.1,1.2]

As mentioned earlier, excitons are formed when electrons in the CB become bound to holes in the VB though Coulombic attraction. Two different kinds of excitons exist. One is the tightly bound and relatively small (radius on the order of the lattice constant) Frenkel exciton which forms in ionic crystals with low mobilities and dielectric constants,

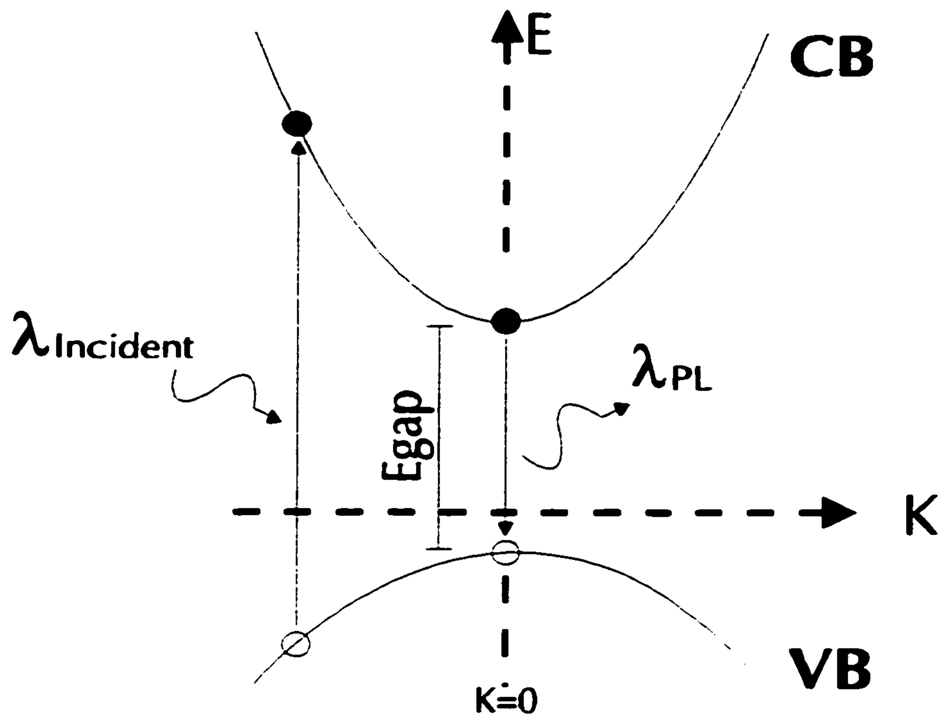

Fig. 1.1: K-space representation of the PL process in a bulk direct gap semiconductor. The optically excited carriers thermalize rapidly to their band extrema by emitting longitudinal optic and acoustic phonons and finally recombine by emitting a photon. [Taken from reference 1.4]

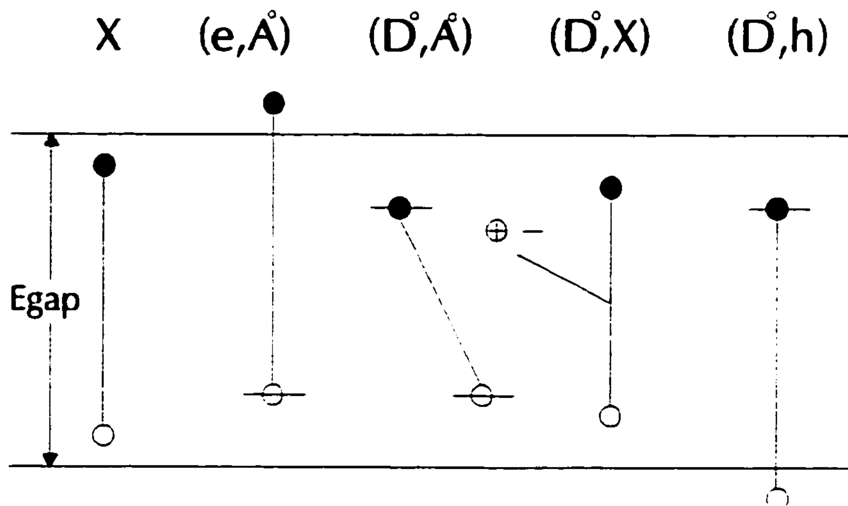

Fig. 1.2: Principal electron-hole decay processes in semiconductors: free exciton recombination X; free electron to neutral acceptor (e,A°); donor acceptor (D°,A°); bound exciton decay at a neutral donor (D°,X); and donor to free hole (D°,h). [Taken from reference 1.4]

such as the alkali halides. The other, called the Wannier-Mott exciton, is loosely bound (diameter extending over many unit cells of the crystal) and is formed in covalently bound crystals with high mobilities and dielectric constants such as III-V and type IV semiconductors. The following treatment shall limit itself to excitons of the latter type.

As the Wannier-Mott exciton closely resembles the hydrogen atom in structure, we may expect to find similar expressions for its energy structure. To begin, we may consider the masses of the electrons and holes to be given by effective masses m_e^* and m_h^* respectively. These values reflect the apparent masses of these particles in the crystalline environment, and incorporate the effects of the periodicity of the crystal potential and the dielectric constant on the carriers. We thus define a reduced mass for the system $\mu^{-1} = (m_e^*)^{-1} + (m_h^*)^{-1}$. Given the spatial extent of the Wannier-Mott exciton, the dielectric function may be assumed constant, allowing us to write for the attractive potential between the electron and hole

$$V(r) = -e^2/\varepsilon r \tag{1.1}$$

where e is the fundamental charge, r is the distance separating the electron-hole pair and ε is the dielectric constant of the semiconductor. The time independent Schrödinger equation for the system may then be written

$$\left[-\frac{h^2}{2\mu(2\pi)^2}\frac{\partial^2}{\partial r^2}+V(r)\right]\Psi_n(r)=E_n\Psi_n(r) \tag{1.2}$$

from which one obtains for the energy eigenvalues

$$E_n(K)=-\frac{(2\pi)^2e^4\mu}{2h^2\varepsilon^2n^2}+\frac{h^2K^2}{2\mu(2\pi)^2} \tag{1.3}$$

where $hK/2\pi$ is the exciton's centre of mass momentum and n is a positive integer. The n=1 binding energy for the exciton, or the 'exciton Rydberg' (R_x) follows from equation 1.3 with K=0 and can be written as follows

$$R_x=\frac{(2\pi)^2e^4\mu}{2h^2\varepsilon^2} \tag{1.4}$$

The total energy of the exciton complex E_x may then be expressed as

$$E_x(K)=E_{gap}-\frac{R_x}{n^2}+\frac{h^2K^2}{2\mu(2\pi)^2} \tag{1.5}$$

with E_{gap} corresponding to the energy of the bandgap. Equation 1.2 yields a ground state solution of

$$\psi_{1s}(r) = (\pi a_x^3)^{-1/2} \exp(-r/a_x) \quad (1.6)$$

Where a_x is known as the 'Bohr radius' and is given by

$$a_x = \frac{h^2 \varepsilon}{e^2 \mu (2\pi)^2} \quad (1.7)$$

For bulk GaAs, $\mu = 0.058m_o$ (where m_o is the free electron rest mass) and $\varepsilon = 12.5$, one obtains $R_x = 5$ meV and $a_x = 110$Å. When the thermal energy, kT (k being Boltzmann's constant), is on the order of the exciton binding energy, the excitons will dissociate into free electrons and holes. This means that excitonic features will only be observed at very low temperatures (i.e. below $T \approx R_x/k = 58$ Kelvin).

Like all recombination mechanisms, excitonic recombination must conserve momentum. As the emitted photons possess negligible momentum, we find that the only FEs that may recombine on their own are those possessing near zero kinetic energy. Recombination for excitons with non-zero momentum is possible, but only via added interactions with lattice phonons to satisfy the momentum conservation requirements.

The width of the FE recombination peak is influenced by the Heisenberg uncertainty relation $\Delta E \Delta t > h/2\pi$. Hence, the shorter the exciton lifetime, the broader the emission peak. Any processes which affect the time the exciton spends in the $\mathbf{K} = \mathbf{0}$ state

will contribute to altering the width of the luminescence peak (e.g. phonon scattering which transfers kinetic energy to $\mathbf{K} = \mathbf{0}$ excitons limiting time spent in $\mathbf{K} = \mathbf{0}$ state, or interactions with lattice defects). Alternatively, some broadening can occur from acoustical phonon (AP) assisted transitions. These transitions consist in the recombination of an exciton with slightly non-zero wavevector **K** with subsequent emission of a photon with wavevector **k** and AP with wavevector $\mathbf{q}_{AP}$. We may write this as

$$\mathbf{K} = \mathbf{k} + \mathbf{q}_{AP} \tag{1.8}$$

The emission energy is then shifted by

$$\frac{h}{2\pi}\omega_{emitted} = E_x - \frac{h}{2\pi}\omega_{AP} \tag{1.9}$$

where E_x is the exciton energy as defined in equation 1.5 and $\omega_{emitted}$ is the angular frequency of the emitted photon. As the energy of acoustical phonons is fairly small compared to the exciton energy, their effect is to spread out the zero phonon FE emission peak. A similar mechanism exists for longitudinal optical (LO) phonons but because their energies are a significant fraction of E_x (and their dispersion curves yield energies roughly independent of momentum within the first Brillouin zone), they act to generate phonon replica's of the no-phonon FE peak with little broadening, displaced by the LO phonon energy.

Bound excitons (BE) are formed by free excitons which have become localized on impurity or defect sites in the host semiconductor. When excitons bound to these sites eventually recombine, they emit photons of energy equivalent to that of FEs reduced by their localization energy. After a BE recombines at a donor (acceptor) site, the impurity is left with an electron (hole) in either a ground or excited state, the outcome of which altering somewhat the energy of the emitted photon. The predominant BE lines, however, result from transitions between the BE complex to the electronic ground states of the systems. The linewidths from BE recombination are narrower than those of free excitons as the BEs lack the Boltzmann tail associated with the thermal motion of free excitons.

The luminescence emerging from BE recombination in direct gap bulk semiconductors often overwhelms that coming from the FEs. On one hand, the relatively large size of the FE ensures that most of those created will encounter at least one of these impurity sites before recombining. For example, in GaAs $a_x \approx 100$Å for a FE and the Bohr radii for acceptors and donors are 30 Å and 100 Å respectively. At 2K, a FE has an average velocity of roughly $v \approx 10^6$ cm/s.[1.3] A FE - donor cross section of $\sigma \approx 10^{-12}$ cm^2 and a relatively low impurity donor concentration of $N \approx 10^{15}$ cm^{-3} yield an average time to encounter of about 10 ns ($[N\sigma v]^{-1}$). This value being comparable to the radiative lifetime of FEs in GaAs at these temperatures, implies that a significant portion of them will encounter such impurities before they may recombine as free excitons. A second determining factor for the dominance of the BE emission is a giant oscillator strength proportional to the volume of the BE wavefunction. The oscillator strength of an impurity

BE increases by a factor of 'a_x^3/v' times the oscillator strength for the FE (where v is the volume of the crystal's primitive cell and a_x is the Bohr radius for the BE wavefunction).[1.5] For semiconductors, this factor is on the order of 10^4 explaining why, when given a choice, excitons will preferentially recombine after having formed BE complexes.

1.3 Donor-acceptor Recombination[1.4]

This process is essentially described by the following

$$[(D^o,A^o) \rightarrow (D^+,A^-) + \text{photon}] \qquad (1.10)$$

and corresponds to the radiative transfer of an electron from a neutral donor impurity to a neutral acceptor. Of particular significance to this donor-acceptor pair (DAP) recombination is the dependence of the recombination energy on the distance between the donors and acceptors. We have for pairs separated by a distance r

$$E(r)=E_{gap} - (E_a+E_d) + (e^2/\varepsilon r) \qquad (1.11)$$

where E_a and E_d are the acceptor and donor binding energies, E_{gap} is the bandgap energy and ε is the low frequency dielectric constant. This expression can be understood by considering the energy required to form the (D^o,A^o) complex from (D^+,A^-). First we

require E_{gap} reduced by E_d to promote an electron from the VB to the donor. This quantity must be further increased by an amount '$e^2/\varepsilon r$' to compensate for the repulsive field of the A^-. Finally E_a is gained by letting the hole in the VB relax onto the A^- (and the now neutral D^0). Summing these stepwise contributions leads to equation 1.11.

As the donors and acceptors tend to occupy regular positions in the crystalline lattice, recombination between them for small r values result in discrete emission peaks (see equation 1.11). For larger values of r, however, the individual pair lines begin to merge together to form a continuum resulting from the $r \rightarrow \infty$ limit. Since small r values correspond to large emission energies, the better resolved donor-acceptor recombination peaks appear on the high energy side of the DAP peaks.

Identification of (D^0,A^0) recombination peaks can be made by varying the excitation intensity. The radiative transition probability for this type of recombination is given by[1.4]

$$W(r)=W_o\exp(-2r/a_o) \qquad (1.12)$$

where a_o is the Bohr radius, and W_o is the transition probability as $r \rightarrow 0$. Therefore, close pairs recombine more rapidly than distant pairs, and so are more difficult to saturate than the more distantly separated pairs. As a result, the high energy peaks belonging to the closely spaced pairs appear relatively enhanced to the more distantly spaced ones at higher

excitation levels. Similarly, time resolved PL spectra will show donor-acceptor peaks shifting to lower energy wavelengths for increasing time delays on the order of the DAP recombination time.

1.4 Radiative Recombination in Semiconductor Quantum Wells[1.6,1.7]

A quantum well (QW) is formed when a confinement potential restricts the motion, on a small scale, of an arbitrary number of particles, in one dimension. Effects associated with the wavelike nature of matter arise as the length scale of this confinement profile approaches that of the particles' De Broglie wavelengths. In this case, the trapped particles may only possess energies in the confinement direction corresponding to the formation of standing matter waves in the QW. This results in the creation of discrete energy levels allowed for the particles in the well which readily depend on the well thickness (L_z). In the simplest case, that of an infinitely deep rectangular potential well, the solution of Schrödinger equation leads to energy eigenvalues of

$$E_n = (h^2/8m^*)(n/L_z)^2 \quad n=1,2,3... \tag{1.13}$$

For L_z much larger than the De Broglie wavelength of the confined particles, a continuum of energy states results and we regain the classical behavior of the system.

Making use of semiconductors possessing differing bandgaps, it is possible to implement such a structure. If the lattice constants are closely matched, they can be grown epitaxially in alternating sequences to produce the desired QW heterostructures (the well/barrier regions being defined by the low/high bandgap semiconductors). Many different techniques exist today to do so. The most often employed methods are those of molecular beam epitaxy (MBE), chemical beam epitaxy (CBE), and metalorganic chemical vapour deposition (MOCVD). All of these techniques allow for the relatively rapid growth ($\approx 1\,\mu m/hr$) of high quality heterostructures possessing atomically sharp interfaces. The growth of QW structures can also be carried out in various material systems. GaAs/AlGaAs, InGaAs/GaAs and InGaAs/InP being examples of the more technologically relevant ones.

When a QW heterostructure is created, we must actually solve two separate confinement problems - one for the holes in the valence band, and another for the electrons in the conduction band. The band offset defines how much of the difference in bandgap will appear as a discontinuity in the CB (ΔE_C) and how much in the VB (ΔE_V). In type I semiconductors, the band-edge discontinuities ΔE_C and ΔE_V have opposite signs and result in the formation of attractive finite potential wells for both carrier types (see figure 1.3). Solutions for each of these are those of the Schrödinger wave equation applied to the finite square well problem. They are well known and will not be rederived here (the inquisitive reader is referred to G. Bastard's 'Wave Mechanics Applied to Semiconductor Heterostructures" in ref. 1.7 for a thorough treatment of the problem).

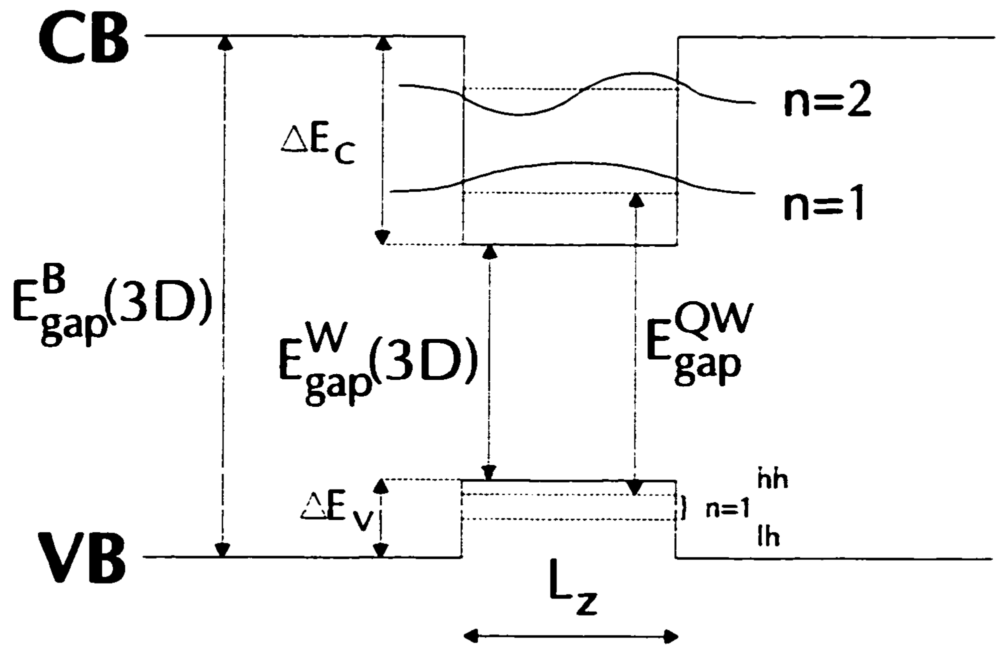

Fig. 1.3: Band-edge profile and energy gaps for a type 1 semiconductor QW structure. Superscripts 'B' and 'W' stand for barrier and well respectively. [Taken from reference 1.6]

Qualitatively, these solutions differ from those of the infinite square well problem by possessing a non zero probability of finding the bound particles outside of the QW. This is the uniquely non-classical phenomenon known as 'tunneling'. One also finds for the finite square well only a limited number of bound states. The eigenenergies of these, however, are reduced in comparison to their infinite square well counterparts by the relaxation of the particles' wavefunctions into the barrier regions.

The first optical study of GaAs/$Al_xGa_{(1-x)}As$ QW heterostructures was performed by Dingle et al. in 1974[1.8]. They studied QWs ranging in width from 200 to 4000 angstroms. Their results showed that the GaAs QWs behaved as finite potential wells with $\Delta E_C \approx 0.70\Delta E_{gap}$ and $\Delta E_V \approx 0.30\Delta E_{gap}$, where ΔE_{gap} = (1.879eV - 1.519eV) = 0.360eV for $Al_{.25}Ga_{.75}As$ barriers. For the 200 Å QW, an exciton binding energy was found to be roughly 7meV compared with a value of 5meV for bulk GaAs. These values are in fairly close agreement with what is commonly accepted today for the GaAs/AlGaAs system (i.e. a band offset of $\Delta E_C/\Delta E_V$=0.65/0.35 and a heavy hole exciton binding energy of 9meV).

This increased binding energy leads to an enhanced stability of the QW excitons at higher temperatures. In QW PL spectra, one detects similar structural features to those found in bulk samples. For low level excitation, however, FE recombination often dominates the emission spectra for QWs - quite contrary to what one finds for bulk material of presumably equivalent quality. Various mechanisms have been proposed to

explain this. Some point to the possible migration of impurities during growth to interfaces resulting in increased purity of the QW material. Also, a smoothing action of the interfaces during growth diminishes the propagation of structural defects through the epitaxial layers (it is standard to grow superlattice buffer layers before commencing the growth of desired structures for this reason).

There may also be an associated reduction in the 2D impurity capture efficiency when the impurity Bohr radius becomes comparable to the impurity-interface distance (in bulk GaAs a_{Bohr} = 100Å for donors and 30 Å for acceptors). As the impurity moves closer to the interface, the ground state wavefunction gradually changes from a 1S symmetry in bulk to a 2P symmetry at the interface and the overlap with FE wavefunctions is slowly reduced. This effect also influences the impurity binding energy and smears out the BE luminescence peaks.

A trend noted in QWs of diminishing thickness is a global broadening of peak linewidths. Taking the derivative of equation 1.13 results in

$$\Delta E_n = -\Delta L_z(h^2n^2/4m^*L_z^3) \quad n=1,2,3... \tag{1.14}$$

From which we see that a variation of ΔL_z in the width of a well results in a spreading of ΔE_n for the nth energy level. As L_z appears cubed in the denominator, this effect is enhanced for narrow QWs. If one assumes the 2D exciton density of states is occupied

over an energy range smaller than the spread described by equation 1.14, at low excitation intensities and temperatures, the luminescence features from the QW will be broadened into a distribution related to the roughness of the interface.[1.9]

CHAPTER 2

Quantum Well Intermixing

2.1 Motivation

Today, semiconductor quantum well structures find applications in a host of optoelectronic devices. In some applications, such as semiconductor lasers or detectors, the introduction of QWs in the active region allows for increased performance over that of their bulk semiconductor counterparts. In other instances, entirely novel devices have been created whose function rely entirely upon the quantum confinement inherent in QWs (e.g. quantum confined Stark effect modulators). Many of these devices are already being utilized commercially by the telecommunications sector, notably in their efforts to construct a fiber-optics based communications network. Although the transmission of gigabit per second data rates are routinely achieved over fiber-optic cables by single source lasers coupled with modulators,[2.1] even greater data rates could be achieved by multiplexing (demultiplexing) tens or hundreds of similar lasers (detectors), each sending (receiving) data streams at different wavelengths. To make the production of such multiplexing/demultiplexing systems economically viable, however, requires the development of an integration technology capable of placing entire arrays of lasers, detectors, and modulators (each operating at different wavelengths) on a single chip (see figure 2.1).

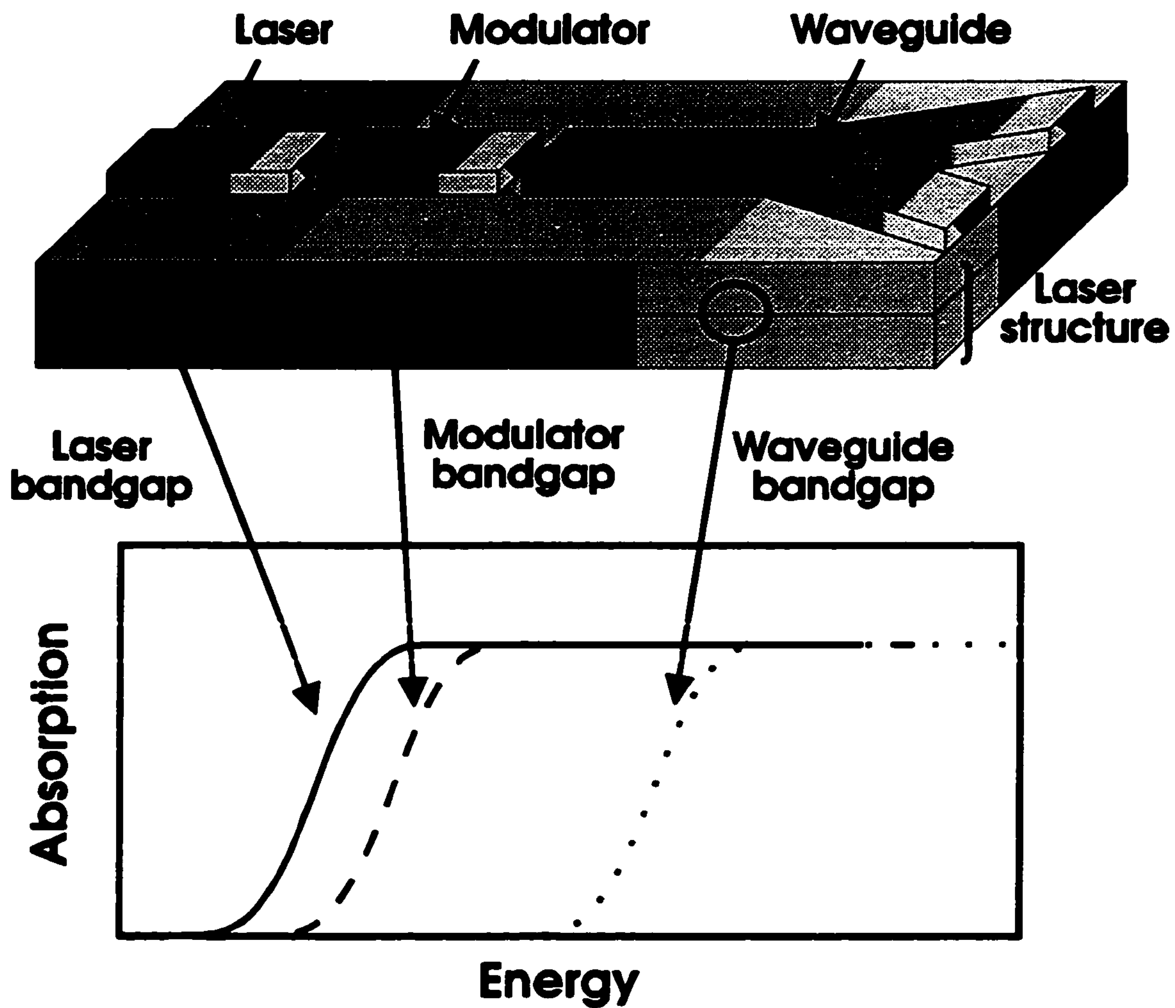

Fig. 2.1: Bandgap requirement for the optimal integration of a laser, modulator and passive waveguide section on a single substrate.

As QW structures are grown epitaxially, all devices fabricated from the same wafer will share a common QW, and hence emit or absorb light at identical wavelengths (ignoring minor fluctuations resulting from asymmetries in growth conditions across the wafer). Many different techniques have been attempted to circumvent this problem.[2.2] One method uses etching and epitaxial regrowth to create a single structure which possesses an active QW layer only in the desired regions.[2.3] Alternatively, if several different sets of active QW layers are required, they may be grown on top of each other, and the structure designed so that light couples vertically from one layer to another (using etched gratings).[2.4] These methods, however, require complex processing, and as such suffer the low yields traditionally associated with regrowth techniques.

Another scheme is to vary the width of a single QW across the wafer by partially masking the deposition surface prior to growth.[2.5,2.6] Growth species encountering the masked region will diffuse some distance, and eventually settle into openings onto the growth surface. Thus local growth rates (and hence well widths) become dependent upon the widths of the openings and the patterning of the masks. As in the previous case, this technique suffers from low yields due to the sophisticated processing required. As the growth of the QW structures must be interrupted for the deposition and subsequent removal of the masking, the crystalline quality of the QW and following epilayers is compromised by presence of contaminants introduced during the ex-situ processing.

2.2 Quantum Well Intermixing

Most promising is the technique of quantum well intermixing (QWI).[2.2] In this scheme, the bandgap of the QW structures is modified in selected regions after growth by interdiffusing the barrier and well species to form an alloy semiconductor. The bandgap of the intermixed QW is then usually larger than that of the original QW[2.7] (see figure 2.2). This provides a method of producing low loss optical waveguides and modulators as well as variably intermixed lasers and detectors possessing differing operating wavelengths.

A number of different techniques for achieving QWI have been developed. Among the most notable are laser-induced disordering (LID), impurity-free vacancy disordering (IFVD), and ion implantation induced disordering (IIID). Laser induced disordering is achieved by focusing a high power laser onto the surface of a QW structure.[2.2] If the power density is sufficient, the sample surface melts momentarily (as the laser sweeps over it) and the sample then recrystallizes with the well and barrier species interdiffusing into one another. This method, however, does not allow for very precise control over the degree of intermixing of the QWs and also tends to cause undesirable redistribution of dopant ions outside of the active region. A modified version of this technique called photo-absorption induced disordering (PAID) exploits the low thermal stabilities of the InGaAs/InGaAsP and InGaAs/AlGaInAs material systems.[2.8,2.9] By selecting a light source possessing photons with energies high enough to be absorbed by the well but not by the barrier material, heating in the sample only takes place in the QW regions. To decrease

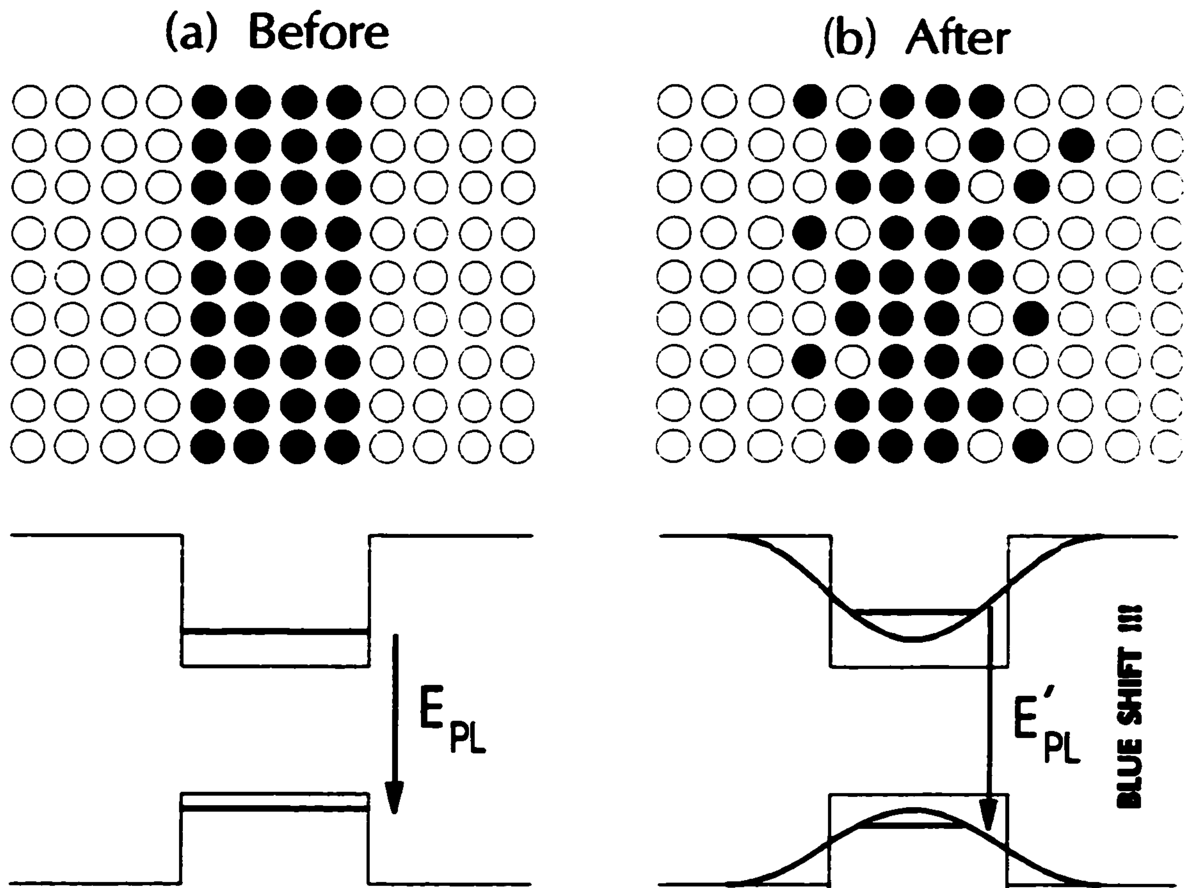

Fig. 2.2: Schematic of QW crystal structures (above) and associated energy band diagrams (below) - (a) as grown; (b) after intermixing.

the incident laser power density required to initiate intermixing, the sample is heated by an external source (such as a hot plate) during its exposure to the laser radiation. The sample temperature is maintained just below that required for the onset of thermal interdiffusion of the QW material without irradiation.

This variant of LID has the advantage of being self-limiting, in that once the QW has blue-shifted in wavelength to just beyond the energy of the heating laser, energy transfer to the QW ceases and the intermixing stops. PAID yields high quality material after intermixing, yet its application is somewhat restricted by its reliance on material systems with low thermal stabilities, and the availability of relatively high power tunable laser sources. Recently, PAID was successfully employed to bandgap shift functional multi-quantum well InGaAs/InGaAsP lasers.[2.8]

IFVD achieves intermixing of QW structures by supplying the QW region with a flux of vacancies during an oven anneal or rapid thermal anneal. These vacancies are produced by the migration of atomic species from the crystalline lattice into a dielectric capping layer deposited on the sample surface after growth.[2.2] In the case of GaAs/AlGaAs for example, SiO_2 acts as a gallium getter. During annealing, Ga atoms diffuse into the SiO_2 and leave behind empty lattice sites on the group III sub-lattice. These lattice vacancies are then free to diffuse across the underlying QW, increasing the diffusivity of barrier and well constituents during the anneal.[2.10,2.11] Capping materials like SrF_2 and Si_3N_4 have been shown to effectively block the out-migration of Ga during

thermal processing, and so can be used in conjunction with SiO_2 to create intermixed and non-intermixed areas on a same sample.[2.2] Control over the extent of intermixing is achieved by varying the thickness of the SiO_2 overlayer.

IFVD has been successfully employed to bandgap shift active devices such as GaAs/AlGaAs QW lasers[2.12] indicating that (as in the case of PAID) the crystal quality is largely unaffected by this method of intermixing. Concerns arise, however, regarding the reproducibility of this technique. As vacancy production relies upon soluble atoms in the crystalline matrix being able to migrate into the dielectric capping material, this technique remains very sensitive to both the interface quality (between the dielectric cap and the QW structure) and the quality of the deposited dielectric films.[2.13] Also, strain produced by the thermal expansion differential existing between the dielectric cap and the semiconductor sample has been shown to be responsible for both the initial injection of vacancies into the semiconductor (if strain is absent, the vacancies accumulate into macroscopic defect structures at the interface without diffusing into the sample), and for the trajectories they follow during diffusion.[2.13] Thus, one must also be able to guarantee the reproducibility of the strain fields experienced by the sample during thermal processing.

Ion implantation induced intermixing is similar to IFVD in that it relies on vacancy production to enhance QW intermixing. In this technique, collisional damage produced by ion beam implantation supplies excess vacancies to the regions where the QW bandgap of the structure is to be modified.[2.14] These vacancies are then free to diffuse through the

sample during an RTA and provoke enhanced intermixing across the barrier-QW interfaces (see figure 2.3).

As this technique relies upon ion implantation for vacancy production, it possesses great spatial selectivity and reproducibility. Since ion penetration depth is insensitive to the presence of minute surface contaminants, this method does not suffer from the repeatability problems traditionally associated with IFVD. Also, broad area implantation coupled with an appropriate masking procedure, allows for rapid spatially selective implantation of large areas.[2.15] Focused ion beam implantation, however, may be utilized in implanting very fine resolution structures (such as QW wires and dots[2.16,2.17]).

Repeatability aside, there exists a complex interplay between the implantation parameters, annealing times, temperatures, and intrinsic properties associated with the material system of a particular QW structure that will affect the extent of intermixing taking place in it. Ion implantation energies and doses for instance, will clearly affect the depth distribution and total number of vacancies and other defects created during implantation. Also, the masses of the implanted species for a given energy will alter the penetration depth and number of defects created on average by each ion.[2.18]

Many of these parameters will also have an effect on the defect generation taking place during the initial ion implantation. Factors such as ion beam flux densities, mobility of point defects in the sample (temperature and system dependent), as well as mass/cross-

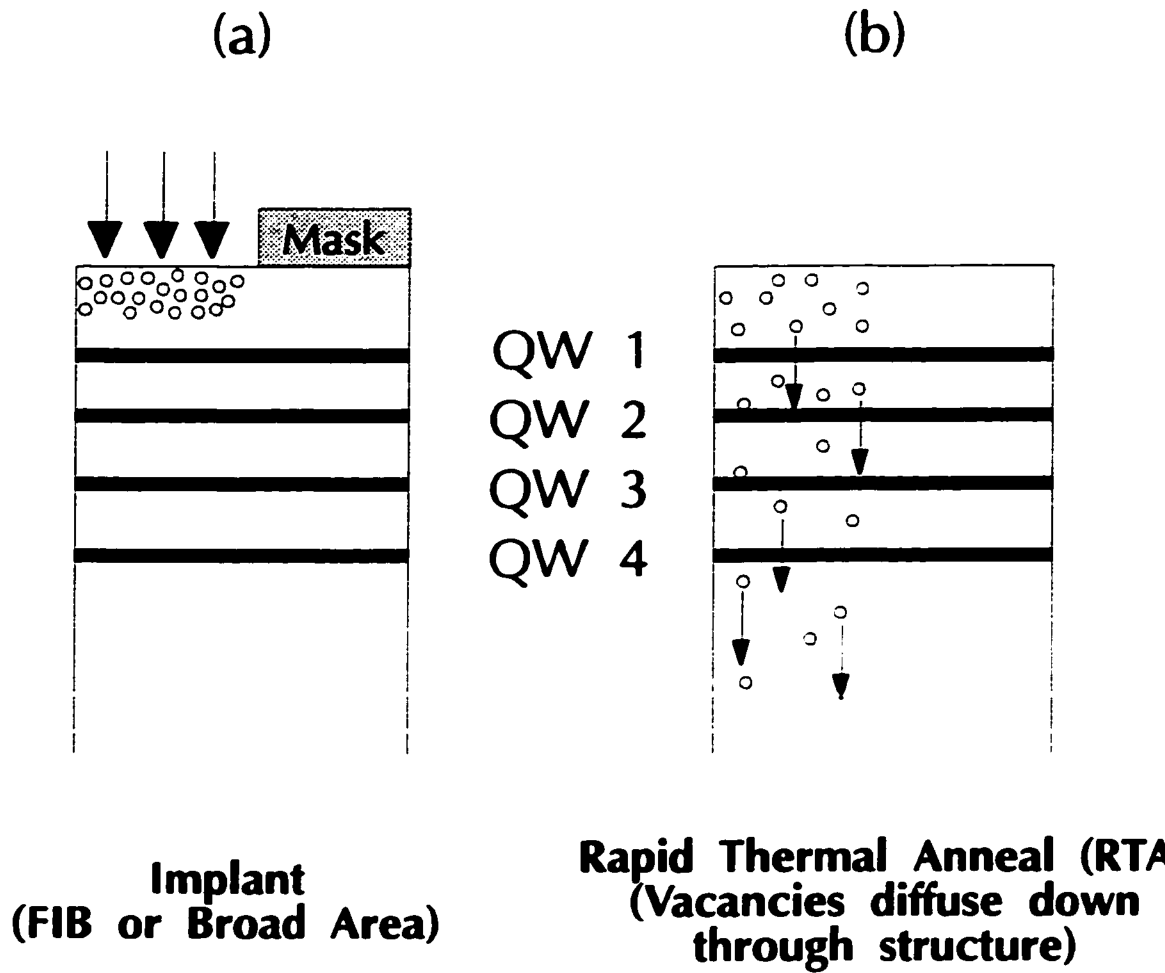

Fig. 2.3: Ion implantation induced intermixing of a QW structure: (a) initial damage produced by implantation; (b) diffusion of vacancies during rapid thermal anneal.

section of the implanted ions, are known to contribute to the extent of dynamic annealing taking place in the sample during irradiation.[2.19]

These effects can be understood in terms of a model first put forth by Morehead and Crowder.[2.20] According to this model, each ion track is initially surrounded by a cylinder of high density defects. During the lifetime of this cylindrical damage cascade, a certain proportion of the enclosed point defects (dependent on their mobility in the host sample) will be able to diffuse out of this high concentration volume and remain in existence outside the damage cylinder as lattice vacancies. Those remaining within a certain critical radius, however, will relax into stable defect structures. The diffusion rate of the defects within the crystalline lattice is temperature dependent, so that the amount of point defects surviving the initial damage cascade is temperature dependent. As the defect complexes formed at the cores of the damage cylinders remain largely fixed during subsequent thermal processing, anything enhancing their creation will do so at the expense of point defect production (the type of damage supposed to be responsible for the enhancement of QW intermixing during annealing[2.14]). Dose rate effects can be seen as arising from reactions between mobile point defects escaping from nearby damage cascades. At low ion beam fluxes, relaxation of individual damage cascades take place in relative isolation. At high fluxes there is an increased probability that adjacent damage cascades will be created simultaneously, resulting in the possible coalescence of point defects (escaping their respective damage cylinders) into larger, more stable defect complexes.[2.21]

Other effects may involve the electronic charge state of the implanted species in the lattice. Through the generation of free carriers, the equilibrium concentration of vacancies at the annealing temperature can be increased.[2.22] These effects, however, are not significant much below concentrations of 10^{18} cm^{-3}, and the incorporation of electrically active impurities into the as-grown QW structures is generally undesirable as the implanted ions would modify the desired doping profiles of the structure. For this reason, our work makes use of implantation species already present in the semiconductor crystal (such as As for GaAs/AlGaAs or P for InGaAs/InP).

2.3 A model for QW interdiffusion

We shall now attempt to derive a model for the interdiffusion of QWs. We begin by considering the problem of diffusion for a distribution of particles dissolved in some medium. If we assume that the concentration gradient for these particles exists in only one dimension (a condition satisfied by our QW structures), say the 'z' direction, we need only consider the net current density (J_z) of such particles which cross a unit surface (oriented in x-y plane) during some time interval Δt. If we assume the system to be at constant temperature, this takes the form

$$J_z = (D^{\cdot} n_{-} v\Delta t - D^{\cdot} n_{+} v\Delta t)/ \Delta t \qquad (2.1)$$

where v is the average speed of the particles, n_- (n_+) is the average concentration of particles within $v\Delta t$ below (above) of the unit surface, and D^* is the fraction of them being able to cross the surface in the prescribed time. If Δt is small enough, '$(n_- - n_+)$' may be approximated by $2v\Delta t(-\partial n/\partial z)$, where '$\partial n/\partial z$' is recognized as being the concentration gradient perpendicular to the surface. Grouping all coefficients into D, we write

$$J_z = -D(\partial n/\partial z) \tag{2.2}$$

where D takes on the role of an effective diffusion coefficient for our dissolved particles. This relation is known as Fick's law. Equation 2.2 combined with the continuity equation

$$\frac{\partial C}{\partial t} + \bar{\nabla} \cdot \bar{J} = 0 \tag{2.3}$$

yields for a concentration gradient existing only along the z-axis

$$\frac{\partial C}{\partial t} = D \frac{\partial^2 C}{\partial z^2} \tag{2.4}$$

This result is known as Fick's second law,[2.23] and is valid for systems with D independent of position or concentration (for example, our use of the continuity equation with D constant requires that we do not have trapping of the diffusing species). If we assume that the interdiffusion of our quantum wells satisfies these conditions, we need only solve this

equation with the appropriate boundary conditions to find an expression describing the shape of our QW structures after intermixing. We have as a solution to equation 2.4

$$C(z,t) = \frac{A}{\sqrt{t}}\exp(\frac{-z^2}{4Dt}) \longrightarrow \frac{M}{\sqrt{\pi\ Dt}}\exp(\frac{-z^2}{4Dt}) \qquad (2.5)$$

with A being an arbitrary constant. The second expression in 2.5 arises from requiring the integral of C(z,t) over all space yield a constant amount of substance 'M'. Taking $t \rightarrow 0$, we recognize that equation 2.5 takes the form of a delta function. Thus, to find the evolution for C(z,t) for any arbitrary initial (1D) distribution, we need only partition $C(z,t_o)$ into infinite number of equally thin slices (perpendicular to the z-axis in this case) and sum the contributions of the form of equation 2.5 arising from each of them.

For a QW (of width w) with an initial concentration of C_o restricted to $-w/2 \leq z \leq w/2$, we have at an arbitrary point (z,t) a contribution of

$$\frac{C_o\ dz}{\sqrt{\pi\ Dt}}\exp(\frac{-z^2}{4Dt}) \qquad (2.6)$$

due to an infinitesimally thin slab within the well. Integrating over the contributions from -w/2 to w/2 allows us to obtain

$$C(z,t) = \frac{C_o}{2}\left\{erf\left(\frac{w/2 - z}{2\sqrt{Dt}}\right) + erf\left(\frac{w/2 + z}{2\sqrt{Dt}}\right)\right\} \tag{2.7}$$

where *erf* is the error function and is defined as

$$erf(z) = \frac{2}{\sqrt{\pi}}\int_0^z \exp(-t^2)dt \tag{2.8}$$

In scientific literature, this result is often written with $(Dt)^{1/2}$ being defined as the interdiffusion coefficient, Δ_i. Δ_i has units of length, and $4\Delta_i$ corresponds to the distance over which the concentration C(z) drops from 90% to 10% of its original value. In light of equation 2.7, we may interpret the effect of introducing vacancies (by implantation or otherwise) in the vicinity of the QW as increasing the effective diffusivity 'D' of the well and barrier atoms during the subsequent thermal anneal.

Figure 2.4 shows the evolution of equation 2.7 with time for an originally uniform concentration of particles located within a slab oriented in the yz plane. (In this diagram the 1-D concentration gradient was taken along the x-axis.). Assuming the vacancy enhanced diffusion of our QW species to be governed by Fick's second law; these curves reveal the expected compositional profiles for varyingly intermixed QWs.[2.24]

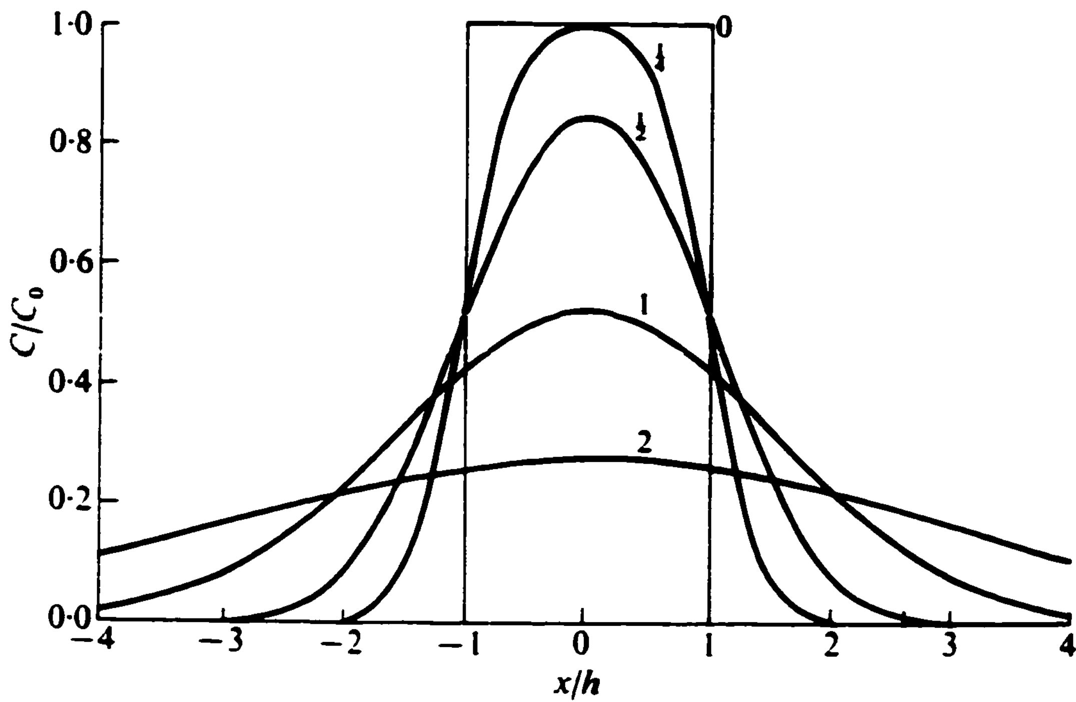

Fig. 2.4: Time evolution of concentration-distance curves for a QW initially of width 2h and concentration C_o. Numbers on curve correspond to time given in units of $(Dt/h^2)^{1/2}$. [Taken from reference 2.23]

CHAPTER 3

Experimental Setup

3.1 Introduction

The aim of this chapter is to present and describe the operation of the hardware employed in preparing and characterizing the various samples appearing in this study. The main elements comprising the experimental setup shall be described in the order in which they are encountered by the samples. Among the topics presented will be; 1) sample growth, 2) ion-implantation, 3) thermal processing, and 4) PL characterization of intermixed samples. Alongside our discussion of ion-implantation sources, will be offered a brief description of TRIM, a computer simulation package employed in predicting the distributions of ion ranges and damage in solids.

3.2 Samples

The low and high energy ion implantation induced intermixing experiments were carried out on a series of QW samples based on various material systems, GaAs/AlGaAs (sample #1198 and #1555), strained InGaAs/GaAs (#1020) and unstrained InGaAs/InP (#170). Both the GaAs/AlGaAs and InGaAs/GaAs structures were grown by molecular beam epitaxy in a Vacuum Generators V80H system using solid sources of Ga, In, Al and

As_4. The GaAs and AlGaAs layers were grown at 650 °C at a growth rate of 0.7 μm/hr, while the InGaAs/GaAs layers were grown after the substrate temperature was lowered rapidly to 565 °C to minimize desorption of indium. The InGaAs/InP sample was grown by chemical beam epitaxy in a Riber 32P system equipped with a cryopump and a turbomolecular pump that allows growth rates of 1 μm/hr in the low 10^{-5} Torr range. The growth temperature for this structure was fixed at 465 °C. For individual growth structures, the reader is invited to consult the 'Experiment' sections of the publications appearing in chapter 4.

3.3 Ion Implantation

Over the course of the present work, use was made of three separate ion beam facilities. Low energy implantation experiments were carried out on QW samples grown in the three different material systems of the preceding section, GaAs/AlGaAs, InGaAs/GaAs and InGaAs/InP. Low energy focused ion-beam (FIB) implantations were performed using a JIBL-104 FIB facility only on samples from the first two material systems. A constant source current of 40 pA of 100 keV Ga^+ ions was used to implant doses ranging from 4×10^{12} to 2×10^{14} ions/cm^2. Square regions (0.5mm×0.5mm) separated from each other by 1mm were patterned across the specimens. Implantations in both samples took place (nominally) at normal incidence to the [100] surfaces. FIB induced intermixing has been studied for several years as a possible technique for the fabrication of lateral confinement nanostructures.[3.1,3.2]

Low energy broad area implantations were carried out in all three material systems using the Varian Extrion 200-CF ion implanter located at the University of Sherbrooke. Ion currents ranged from 0.1 μA to 100 μA for the doses studied here. Ions (As^+ for InGaAs/GaAs, GaAs/AlGaAs and P^+ for InGaAs/InP) were implanted at 32 keV, 7° normal to the [100] surfaces. This practice minimises channeling effects.[3.3] A matrix of 5 ×5 1mm diameter implant regions was formed using Al masks with each row receiving a different dose, and each column receiving a different number of exposures of the specific dose for the row. In both the FIB and broad area experiments, the implant species were selected among those already present in the lattice in order to leave the samples undoped after implantation. Intermixing experiments were carried out with a broad area implanter as a demonstration of the commercial viability of this technique. Broad area implanters are relatively inexpensive compared to FIB systems and, when coupled with an appropriate masking procedure, allow rapid spatially selective implantation of large areas.

High energy ion implantations were accomplished using the 1.7 MeV Tandem Accelerator located at the University of Western Ontario. These experiments were performed on $In_{.23}Ga_{.77}As$/GaAs GRINSCH laser structures containing two 60Å QWs. High energy implantation (8 MeV As^{4+}) was used to create vacancies immediately in the vicinity of the QWs. The low energy techniques of the previous section are ineffective here due the depths of the QWs in these samples (2 μm below the surface). Also, at these energies the implanted ions are buried roughly a micron beneath the QWs (corroborated by TRIM simulations[see next section]) in the event that these might, as interstitial atoms,

degrade the performance of future devices. In the first series of experiments, the dose dependence of the high energy implant method was investigated. Doses were varied from 2×10^{11} to 2×10^{13} ions/cm^2. In a second series of experiments, the dose was maintained at a fixed level (2×10^{13} ions/cm^2) while the temperature of the sample during the implantation procedure was varied from 25 to 200 °C (all previous implants were performed at 25 °C). This experiment was carried out for two ion beam current densities (26 and 240 nA/cm^2) to examine the effects of dose-rate in the regimes studied. Lastly, a series of 50 angstrom GaAs/AlGaAs QW samples were implanted with 8.56 MeV As ions to investigate the effect of implantation dose on carrier lifetimes. Implant doses ranged from 10^{10} to 10^{15} cm^{-2}, and were performed (with the exception of the lowest and highest doses) using an ion flux of 5 nA/cm^2. Given the large range in doses studied here, the 10^{10} and 10^{15} cm^{-2} samples were implanted using ion current densities of 0.3 nA/cm^2 and 24 nA/cm^2, respectively. This maintained accurate dose monitoring for the low fluence sample and kept the time required to complete the highest dose implantation within acceptable bounds.

3.3.1 TRIM

As stated earlier, the TRIM (Transport of Ions in Matter) program is a numerical Monte Carlo simulation program that allows the predictive determination of ion ranges and damage distributions resulting from the implantation of ions of varying energy into amorphous targets. The approach used by the program is to follow a large number of

implanted ion trajectories into a target. Each implanted particle begins with a specific energy, position and direction. Each of these is then assumed to change direction as a result of individual nuclear collisions with atoms in the host material, and move in straight free flight paths between collisions. The kinetic energy of each incident ion is incrementally tabulated at each collision event and is reduced by successive inelastic collisions with host nuclei. Losses due to ion-electron interactions (most significant for lighter ions), are approximated as being continuous processes. To reduce the computational task, analytic expressions with accuracies on the order of one percent are used to determine the scattering angles, cross sections, and energy losses involved in the various collisions. Each ion is tracked until its kinetic energy falls below a specified value - usually the displacement energy for a host atom. TRIM also keeps track of the displaced atoms, produced vacancies, backscattered and transmitted ions, as well as the depth distribution of energy transferred to phonons. Each of these distributions can be viewed separately during program execution and saved to disk as text files for later consultation. A minor weakness of TRIM is that it does treat the possible crystallinity of the host material. This means that the importance of such effects as the channeling of ions along low index crystallographic directions (which result in a non-negligible portion of ions penetrating far beyond the mean range expected in an amorphous material of identical composition) are totally ignored. In most applications though, this discrepancy is of little consequence as implantations are carried out at 7° from normal incidence to minimize this very effect. For an in depth treatment of the physical theory behind TRIM, the reader is

referred to 'The Range and Stopping of Ions in Solids' by Ziegler, Biersack and Littmark.[3.4]

For both low and high energy implantations, TRIM was used to obtain projected ion ranges (see fig. 3.1) in the QW structures. This was done to guarantee that the bulk of the implanted ions were kept from the immediate vicinity of the QWs to minimize the production of non-radiative recombination centres.[3.5] For the time-resolved PL study, additional use of TRIM was made to scale the known intermixing threshold dose for 8 MeV Bi ions in GaAs/AlGaAs to that expected for 8.56 MeV As. This was done by scaling the required As dose by the ratio of the two differing vacancy production efficiencies (evaluated at their respective QW depths - see fig. 3.2). The result obtained in this manner agreed favorably with the actual value.[3.6]

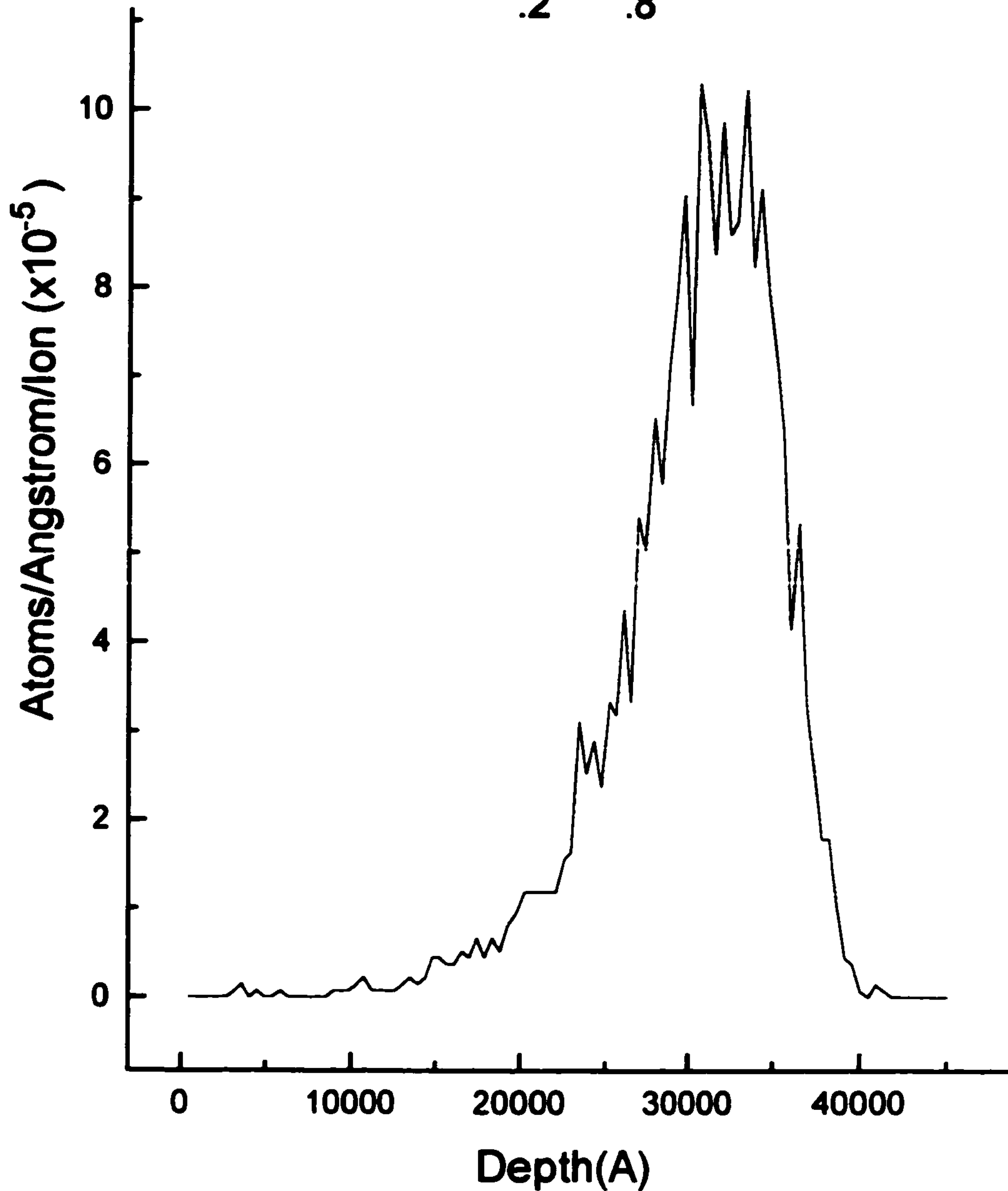

Fig. 3.1: Projected ion ranges by TRIM for 8.56 MeV As^{4+} ions in bulk $Al_{0.2}Ga_{0.8}As$ incident at 7° off-normal. In this structure, the GaAs QW (not shown) was situated at a depth of 4500 Å.

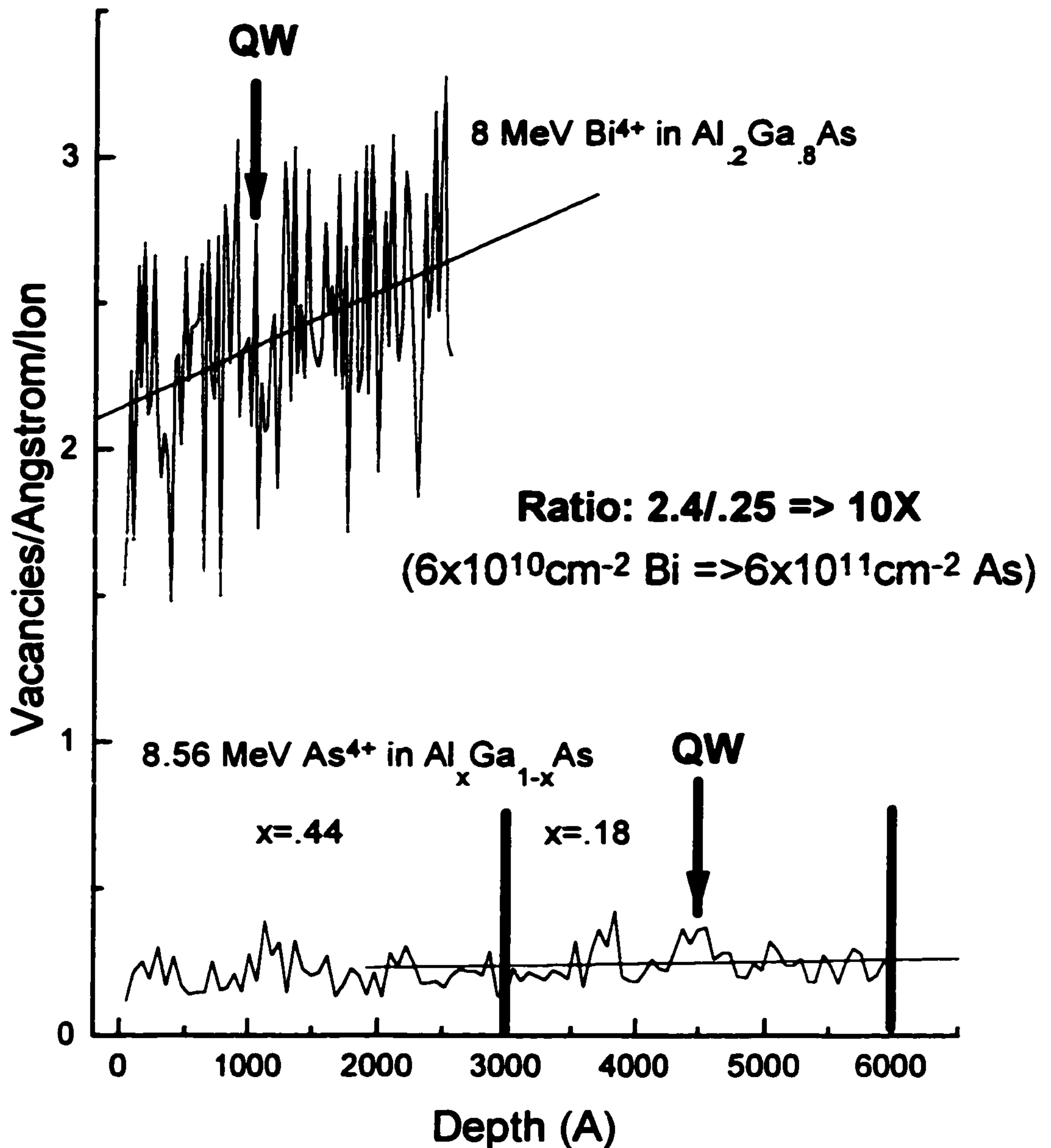

Fig. 3.2: Plot showing differing vacancy production efficiencies (as projected by TRIM) for 8 MeV Bi^{4+} and 8.56 MeV As^{4+} in their respective structures. Calculation in the inset shows an expected As^{4+} threshold dose of $6x10^{11}$ cm^{-2}. The threshold dose for 8 MeV Bi^{4+} ions ($6x10^{10}$ cm^{-2}) was taken from reference 2.7.

3.4 Thermal annealing

After ion beam implantation the QW samples were annealed using an AG Associates Heatpulse 610 Rapid Thermal Annealer (see fig. 3.3). The sample chamber is heated by upper and lower banks of regularly spaced tungsten-halogen lamps. These allow for rapid control over the radiant energy reaching the centre of the chamber. An optical pyrometer is employed to measure the temperature of the silicon support wafer. Temperature control is achieved by tying the pyrometer response into the lamp control circuitry. The system can perform rapid thermal anneals at temperatures ranging between 400 °C and 1400 °C with an accuracy and repeatability of +/- 3.5 °C.

Samples to be annealed are centred face up, on a five inch silicon wafer and introduced into the central heating chamber on a quartzware tray. To prevent against desorption of group V elements during the rapid thermal anneal (RTA), the samples are covered with face down pieces of GaAs or InP (GaAs for GaAs/AlGaAs - InGaAs/GaAs QWs and InP for InGaAs/InP QWs). To protect against excessive oxidation of the samples during thermal processing, the central chamber is continually flushed with nitrogen gas. Annealing temperatures for the various material systems used in this study were determined empirically. The annealing temperatures were selected to maximize the interdiffusion of the implanted regions of the QWs while leaving the unimplanted regions unshifted (see fig. 3.4 for determination of InGaAs/GaAs anneal temperature). Optimal annealing temperatures of 700 °C and 850 °C were found for InP and GaAs based

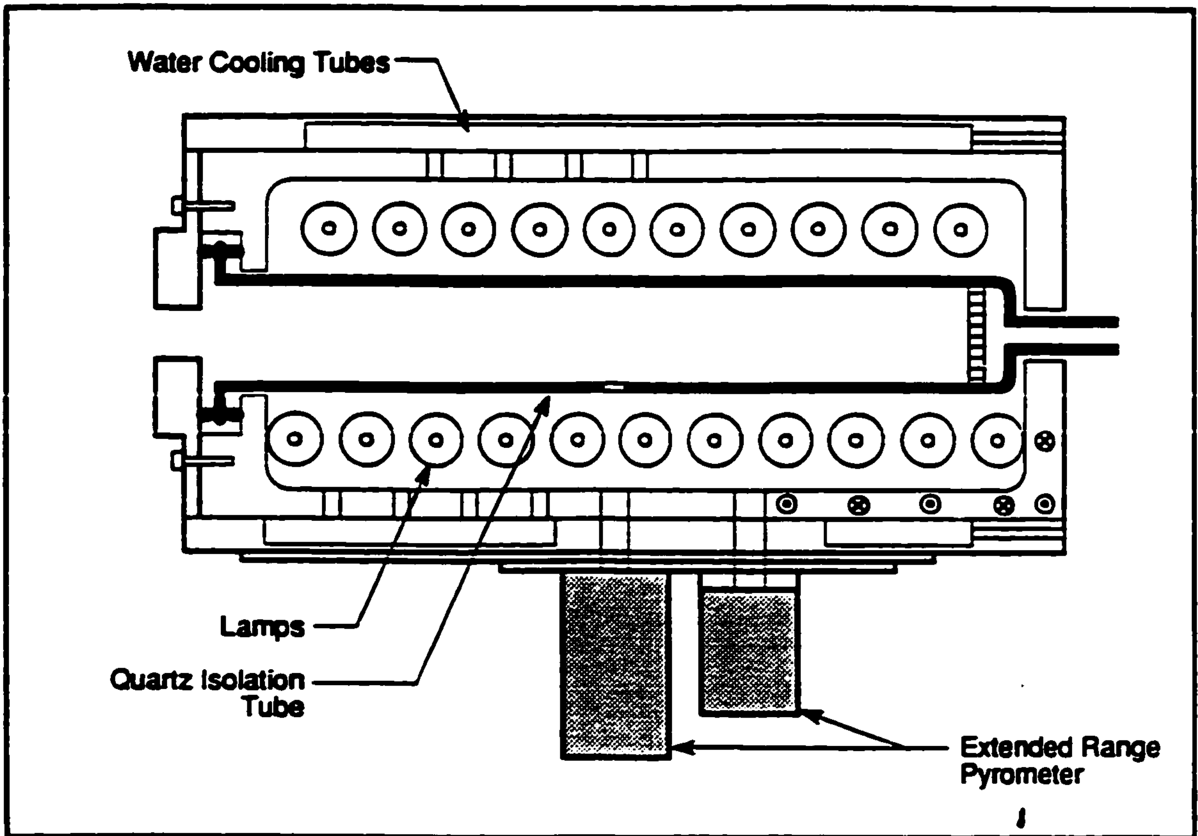

Fig. 3.3: Cross-sectional diagram of the RTA heating chamber and associated components.

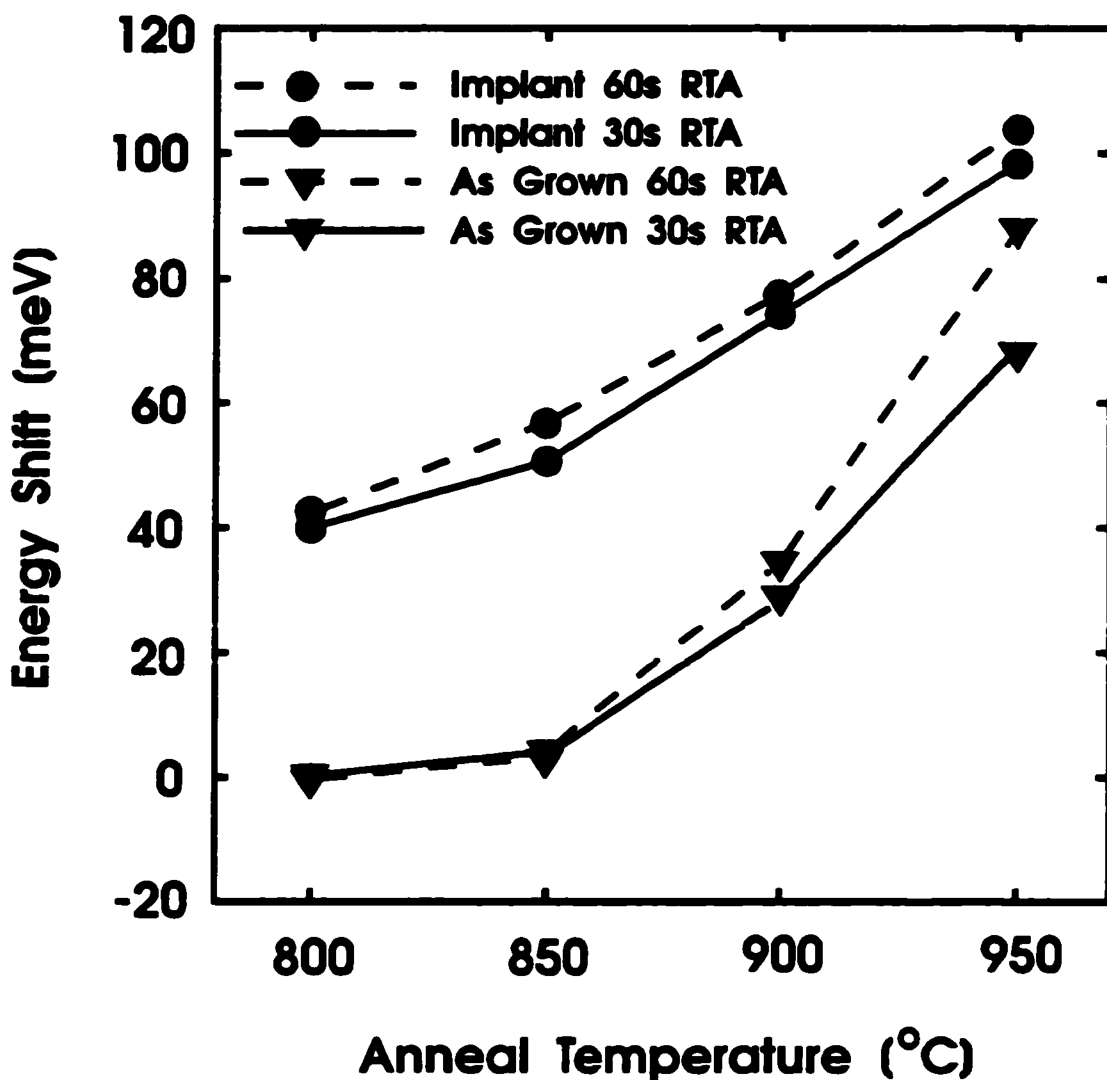

Fig. 3.4: RTA temperature determination for InGaAs/GaAs QW structures. From this graph, an RTA temperature of 850 °C was selected to maximize intermixing of implanted regions whilst minimizing that of the unimplanted areas.

systems respectively. Required annealing times for all systems (resulting in a saturation of the interdiffusion in the implanted areas) were on the order of one minute.

3.5 PL Characterization

In this study, two different PL techniques were used to study the effect of intermixing on QW structures. Continuous-wave photoluminescence (CWPL) measurements comprise the bulk of the results presented in the following chapter. It was used as a direct measure of the modification of the QW bandgap resulting from the intermixing process. Time resolved photoluminescence (TRPL) was employed as a means of investigating the residual damage present in the QWs after disordering. This section will look at both the excitation sources and spectroscopic instrumentation employed in implementing these techniques.

3.5.1 Excitation Sources

In spectroscopy, lasers offer many advantages over their conventional predecessors (e.g. glow discharge lamps). Characteristics such as increased spectral energy densities and extremely small bandwidths allow experiments to be performed with lasers that until their appearance were deemed impossible. One such application of laser technology lies in the area of transient spectroscopy. Techniques such as Q-switching and mode locking have allowed for the creation of very short optical pulses (μs to ns duration

for Q-switching, and ns to fs for mode locking).[3.7] Coupled with ultra rapid and sensitive detectors, these pulsed laser systems allow experimenters direct observation of the radiant relaxation of photo-excited carriers in semiconductors.

In our CWPL experiments, a 5mW helium-neon (HeNe) laser was employed as an above bandgap excitation source. Its principal emission line is at 632.8 nm. (To exclude excitation arising from secondary plasma lines, a Fabry-Perot 632.8 nm narrow bandpass filter was placed at the output of the HeNe laser.)

The laser setup used in the time-resolved PL experiments is significantly more complex than that of the single HeNe laser described above (see fig. 3.5). In our experiments, 100 ps pulses of 1.064 μm light are originally produced at a rate of 76 MHz by a Coherent Antares 76-S mode locked Nd:YAG laser. This light is then frequency doubled in a LiB_3O_5 crystal and used to synchronously pump a Coherent 700 series dye laser. The pulse width emerging from the output of the dye laser is reduced down to the order of a couple of picoseconds.

At the core of the Nd:YAG laser is a neodymium (Nd) doped yttrium aluminum garnet (YAG) rod. The YAG rod is optically pumped by two linear halogen lamps. To increase the optical coupling of the lamps to the crystal, the lamps are each positioned along one of the focal axes of their own elliptical reflecting tubes. These two cavities are then positioned on either side of the YAG rod, separated by a distance which

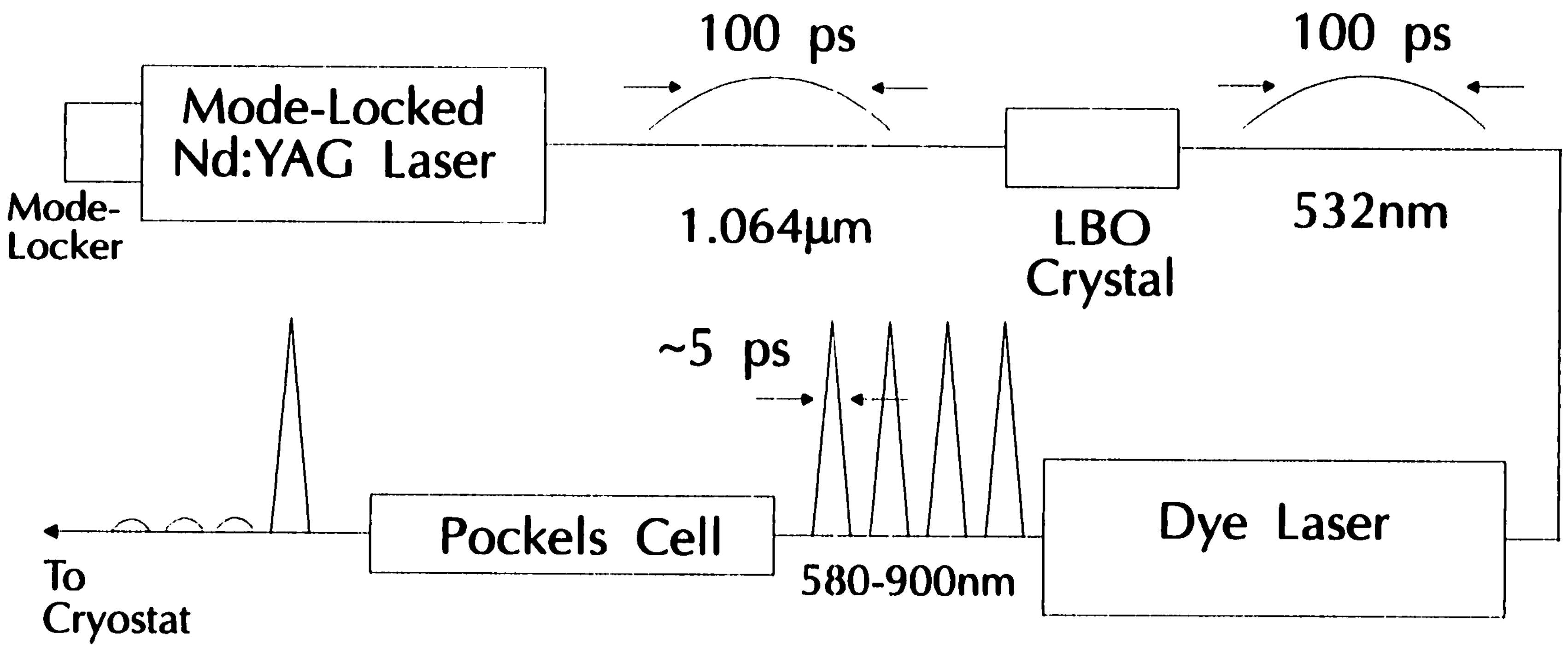

Fig. 3.5: Schematic layout of pulsed laser system employed in performing time-resolved PL experiments.

places both their unoccupied foci onto the YAG element. This then focuses all the radiation emanating from the flash lamps onto the laser rod. Lasing takes place as a result of stimulated radiative recombination between optically excited levels in the Nd^{3+} ions present in the YAG matrix.[3.8]

Output from the laser cavity is converted into short pulses by means of a technique called 'mode locking'. In mode locking, the mode phases are correlated and the total intensity at a fixed point in the cavity will fluctuate with time. There are two principle methods of achieving mode locking - frequency modulation and amplitude modulation (AM).

In our system, AM mode locking is achieved by means of an acousto-optical modulator incorporated into the laser cavity. The crystal is driven at half the mode separation frequency. This produces a standing acoustical wave in the crystal, which modulates the index of refraction of the material in a periodic fashion through the structure. This periodic structure can then diffract a certain portion of the radiation out of the lasing plane. As the standing wave vanishes momentarily twice every cycle, enhanced transmission occurs through the crystal at a rate of twice the driving frequency (i.e. at the mode spacing frequency). This produces the desired temporal modulation of the cavity transmission necessary to initiate mode-locking. For a good review on the subject, the reader is referred to "Lasers" by P. Miloni and J. Eberly.[3.8]

At this point, we have from the output of our mode locked Nd:YAG laser, 100 ps wide pulses of 1.064 μm light emitted at a rate of 76 MHz. Photons at this wavelength, however, are not sufficiently energetic to generate luminescence in the GaAs/AlGaAs quantum well samples we wish to study later. To circumvent this problem, use is made of the second harmonic of the 1.064 μm line generated in a LiB_3O_5 (LBO) crystal.

After frequency doubling in the LBO crystal, we possess 100 ps wide pulses of 532 nm light. This light is used to pump dye laser in order to achieve significantly shorter pulses over a tunable range of lasing wavelengths. Dye lasers employ organic dye solutions as a gain medium. As these dyes exhibit gain over a large spectral region, they may support the generation of much shorter pulses. To do so, however, the dye laser cavity length must be a multiple of the mode-locked pump laser cavity length. This situation is referred to as synchronous pumping.[3.8] Wavelength tuning of the dye laser is achieved by introducing a wavelength selective element into the dye laser cavity.

Pulses arrive from the Nd:YAG pumped dye laser at a rate of 76Mhz. This corresponds to a separation of merely 13ns between successive laser pulses. In order to perform time-resolved photoluminescence experiments on systems possessing radiative lifetimes in excess of this value, some scheme must be devised to keep successive excitation pulses from reexciting the samples before the samples have relaxed. In our system, we employ a Conoptics Laser Modulation System Model 50. Its operation is based on an electro-optic effect known as the Pockel effect. In this case, birefringence is

electrically induced by an applied electric field which sets up an optic axis in a direction perpendicular to the applied field. The difference in the index of refraction between the ordinary and extraordinary modes of light propagation is proportional to the magnitude of the applied fields. By modulating the electrically induced birefringence, a proportion of the laser pulses can be deflected away from the target. In our case, the time between successive pulses is increased from 13 to 250 ns (i.e. repetition rate decreases from 76 MHz to 4 MHz).

3.5.2 Spectroscopic Instrumentation

Two different spectrometer systems were employed to analyze the spectral content of the PL emitted by our samples under continuous-wave excitation. One system consisted of a 600 groove/mm, 0.64m grating spectrometer mated to a charge coupled device detector array (CCD). By virtue of the lateral extent of the CCD, acquisition of the PL spectra consists of reading the intensity of the dispersed light from the individual detector elements across the array. (This is in contrast to the more traditional practice of placing a single narrow detector at the output of the spectrometer and rotating the internal grating assembly.) The resolution of this system was better than 0.4 meV. The other was a BOMEM Michelson - 102 FTIR (Fourier Transform Infra-Red) spectrometer. It has a resolution of 2 cm^{-1} ($\approx$ 0.5meV) and allows detection of light in the 650 nm to 1100 nm range for the silicon avalanche photodetector, and from the 900 nm to 1700 nm range for the thermoelectrically cooled InGaAs detector.

Instead of spatially separating all the different optical frequencies as in a grating spectrometer, the FTIR determines the spectral content of light sent into it by modulating all the wavelengths simultaneously. This is done by means of a variable interference effect which alters the net intensity of the PL light reaching the detector. This modulation is achieved by separating the incoming beam into two different branches and varying the path length in one of the branches by moving a mirror. The light is then recombined at the detector head and the resulting variation in intensity is recorded as a function of optical path difference (see fig. 3.6). As light of any given frequency going through the apparatus will interfere destructively whenever the path difference is equal to an odd half-multiple of its wavelength, short wavelength components of the spectrum will be responsible for rapid modulations in the signal intensity at the detector head as the path difference is varied. Similarly, longer wavelength components will produce relatively slower intensity variations. A Fourier transform is then taken of the data and the intensity vs. path difference data is mapped into wavenumber space allowing one to recover the spectrum in the more familiar 'intensity vs. wavelength' (or frequency) format. Data in the latter format is sent over a data bus to an IBM-PC compatible computer where the user may analyze the collected PL spectra.

Transient PL measurements were made using a Mepsicron MCP-RA (micro-channel plate) detector model F4146M attached to a double 0.75 m Czerny-Turner spectrometer. The MCP detector itself is a 25 mm diameter multialkali photocathode disk containing 400 by 400 individual detector pixels and is sensitive over the 400 to 900 nm

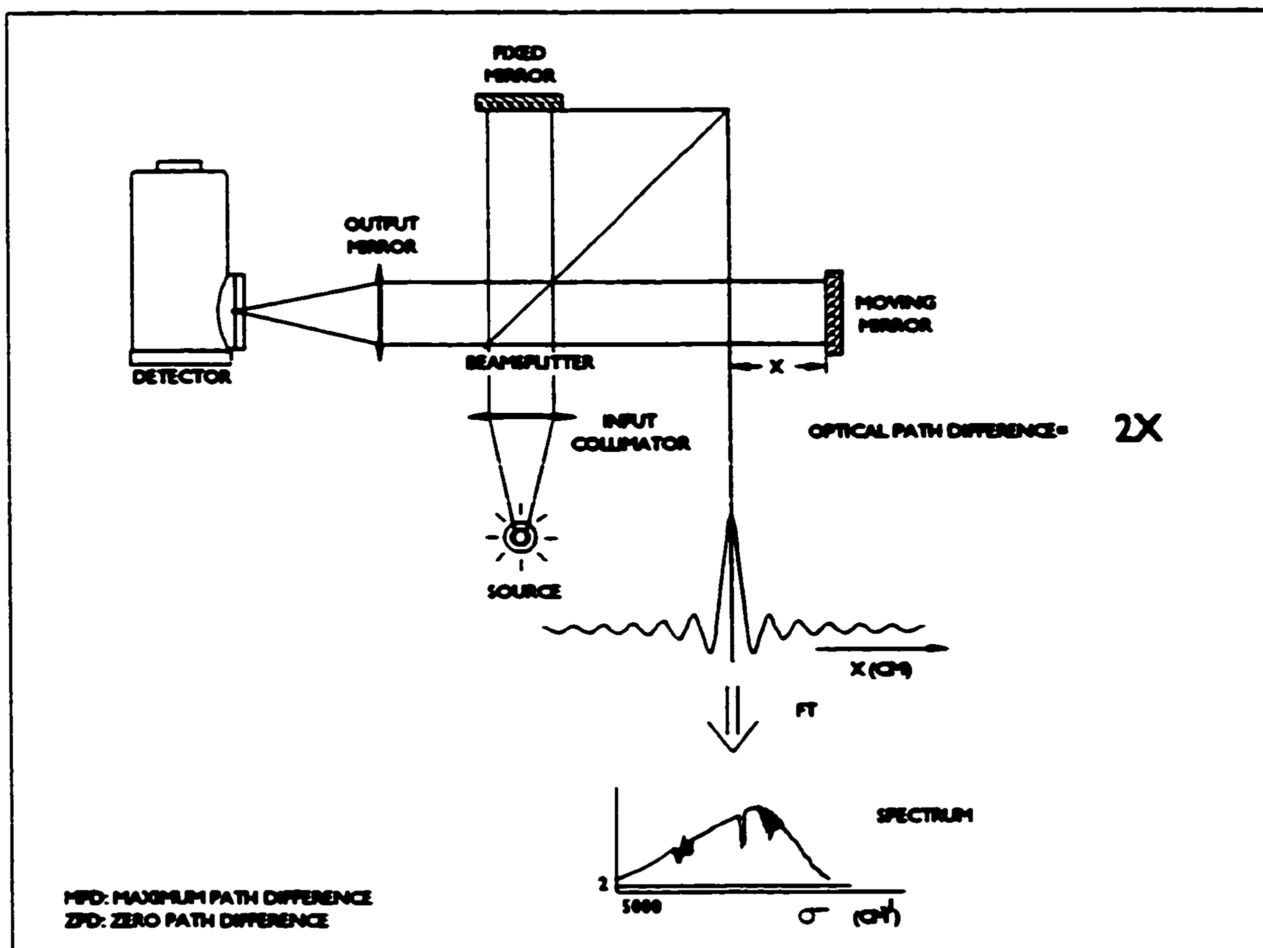

Fig. 3.6: Schematic diagram of the Bomem Michelson spectrometer employed in performing the continuous-wave PL experiments. [Taken from reference 3.9]

range. Coupled with a 1200 groove/mm grating (blazed at 500 nm), this results in a linear dispersion of 5 Å/mm when operated in the first order. When configured for TRPL experiments, one may gate the detector so as to only integrate photon counts coming from a specific region on the detector surface (corresponding to a specific spectral range). Timing information is obtained from a small RC circuit placed between the output biasing lead and ground of the MCP detector. When a luminescence photon (resulting from the excitation pulse) is registered by the detector array, a transient voltage pulse is produced in the RC circuit. This signal is then amplified, and if it is large enough (indicating a true photon capture), it is compared with a similar timing signal from the pump beam (i.e. the stop pulse). The stop pulse is provided by the output from an avalanche photodiode, which samples a small portion of the light from the pump beam. The data is then sent over a bus to an IBM-PC compatible computer for manipulation. (For a more thorough description of the TRPL detection system, the reader is referred to reference 3.10)

During the PL experiments, samples were mounted in a Cryo Industries Model 8 CN liquid helium cryostat. This allowed cooling of the samples down to 4.2 K. Intermediate temperatures (between liquid helium and room temperatures) were achieved by means of a resistive heater built into the sample mount. Figure 3.7 shows a schematic of the acquisition system employed in the PL measurements.

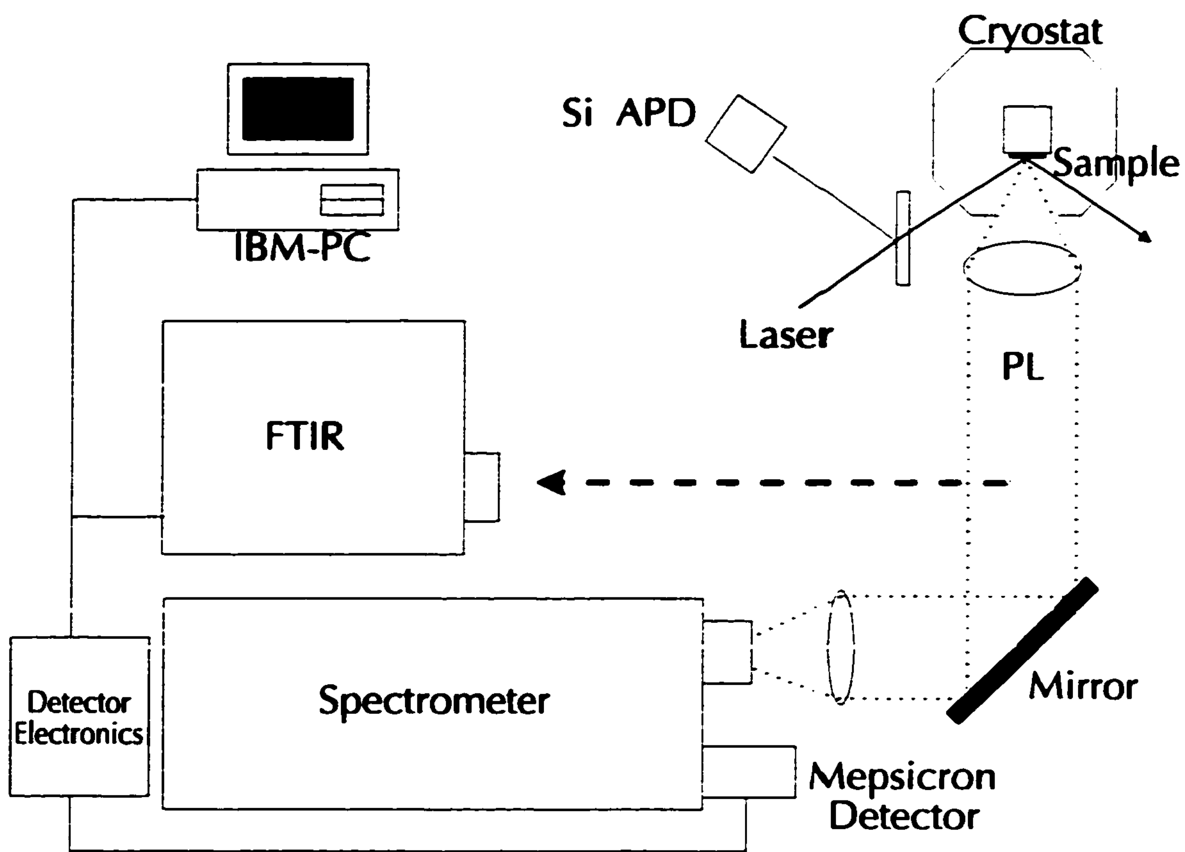

Fig. 3.7: Photoluminescence setup employed to obtain spectra in continuous-wave and time-resolved PL experiments.

CHAPTER 4

Results

4.1 List of presented papers:

Appendix A: Bandgap Tuning of Semiconductor Quantum Well Structures Using Ion Implantation. P.G. Piva, P.J. Poole, S. Charbonneau, E.S. Koteles, M. Buchanan, G. Aers, A.P. Roth, Z.R. Wasilewski, J. Beauvais, R.D. Goldberg. *Superlattices and Microstructures*, **15** (4) 385, 1994.

Appendix B: Enhanced Compositional Disordering of Quantum Wells in GaAs/AlGaAs and InGaAs/GaAs Using Focused Ga^{+} Ion Beams. P.G. Piva, P.J. Poole, M. Buchanan, G. Champion, I. Templeton, G. Aers, R. Williams, Z.R. Wasilewski, E.S. Koteles, S. Charbonneau. *Applied Physics Letters*, **65** (5) 621, 1994.

Appendix C: The Enhancement of Quantum Well Intermixing Through Repeated Ion Implantation. P.J. Poole, P.G. Piva, M. Buchanan, G. Aers, A.P. Roth, M. Dion, Z.R. Wasilewski, E.S. Koteles, S. Charbonneau, J. Beauvais. *Semiconductor Science and Technology*, **9** 2134, 1994.

Appendix D: Enhanced Quantum Well Intermixing Using Multiple Ion Implantation. P.J. Poole, P.G. Piva, M. Buchanan, G. Champion, I. Templeton, G. Aers, R. Williams, A.P. Roth, Z.R. Wasilewski, E.S. Koteles, S. Charbonneau. *SPIE Conference Proceedings*, Vol. 2139 103, 1994.

Appendix E: Effect of Implantation Dose on Photoluminescence Decay Times in Intermixed GaAs/AlGaAs Quantum Wells. P.G. Piva, S. Charbonneau, I.V. Mitchell, R.D. Goldberg. *Applied Physics Letters*, **68** (16) 2252, 1996.

APPENDIX -A-

Bandgap Tuning of Semiconductor Quantum Well Structures Using Ion Implantation

P G. Piva, P.J. Poole, S. Charbonneau, E.S. Koteles,
M. Buchanan, G. Aers, A.P. Roth, Z.R. Wasilewski,
Institute for Microstructural Sciences
National Research Council Canada
Ottawa, Ontario, K1A 0R6
and
J. Beauvais
University of Sherbrooke, QC, Canada
and
R.D. Goldberg
University of Western Ontario, London, ON, Canada

(Received 22 August 1994)

Ion induced QW intermixing using broad area and focused ion beam (FIB) implantation was investigated at low energy (32 and 100 keV respectively) in three different material systems (GaAs/AlGaAs, InGaAs/GaAs, and lattice matched InGaAs/InP). Repeated sequential ion implants and rapid thermal anneals (RTAs) were successful in delivering several times the maximum QW bandgap shift achievable by a single implant/RTA cycle. The effectiveness of broad area high energy implantation (8 MeV As^{4+}) on QW intermixing was also established for GRINSCH (graded-index separate confinement heterostructure) QW laser structures grown in InGaAs/GaAs. Lastly, preliminary work illustrating the effects of implant temperature and ion current density was carried out for InGaAs/GaAs QWs.

1. Introduction

Vacancy diffusion enhanced quantum well (QW) intermixing, induced by ion implantation, has shown itself to be a useful technique for achieving spatially selective tuning of the QW bandgap[1-4]. It promises a method for monolithically integrating optoelectronic devices of differing functionality on a single semiconducting substrate[5]. In integrating lasers, detectors and waveguides on a single chip, performance as a whole is improved by having detectors operate with smaller bandgaps than the lasers, while waveguides benefit from larger bandgaps to minimise losses due to absorption. For commercial applications, a technique is needed that will allow the tuning of the bandgap by different amounts in different regions of the wafer in a simple and repeatable manner. QW intermixing achieved via low or high energy ion implantation and annealing holds the potential for fulfilling these requirements.

With this technique, tuning of the QW bandgap is believed to be achieved by the thermally assisted diffusion of vacancies (created by the ion implantation) across the interfaces of the QW structures. As a result, the cladding and well alloys interdiffuse across the interfaces and the confinement profile of the QW is altered (from a square to a more or less parabolic shape). This generally results in a blue shift of the interband transition energy which can then be monitored using low temperature photoluminescence (PL). One drawback with this technique is that there is a maximum vacancy concentration (and ultimately a maximum achievable energy shift) that may be delivered to the crystal during the implantation process [6,7]. Beyond this threshold, vacancies begin to group themselves into defect clusters and do not diffuse sufficiently during the subsequent rapid thermal anneal (RTA) to participate in the intermixing process[8]. Furthermore, these vacancy complexes may remain in the active regions of fabricated devices after the RTA and degrade performance. Here we report on a method found effective in overcoming the damage processes responsible for limiting QW intermixing. Results are presented for GaAs/AlGaAs, InGaAs/GaAs and InGaAs/InP QWs using multiple sequential low energy broad area and focused ion beam (FIB) implantation

0749-6036/94/040385 + 05 $08.00/0

© 1994 Academic Press Limited

followed by rapid thermal annealing. Also reported here are results from high energy broad area implantation on GRINSCH (graded-index separate confinement heterostructure) QW laser structures grown in InGaAs/GaAs along with a preliminary study of the effects of implant temperature and ion current density on the intermixing of these structures.

2. Experiment

2.1 Low energy implantation

The low energy implantation experiments were carried out on QW samples grown in three different material systems, GaAs/AlGaAs, InGaAs/GaAs and InGaAs/InP. FIB implantations were performed using a JIBL-104 FIB facility only on samples from the first two material systems. A constant source current of 40 pA of 100 keV Ga^+ ions was used to implant doses ranging from 4×10^{12} to 2×10^{14} ions/cm^2. Square regions (0.5mm×0.5mm) separated from each other by 1mm were patterned across the specimens. Implantations in both samples took place (nominally) at normal incidence to the [100] surfaces. FIB induced intermixing has been studied for several years as a possible technique for the fabrication of lateral confinement nanostructures[1,9,10].

Low energy broad area implantations were carried out in all three material systems using the Varian Extrion 200-CF ion implanter located at the University of Sherbrooke. Ion currents ranged from 0.1 μA to 100 μA for the doses studied here. Ions (As^+ for InGaAs/GaAs, GaAs/AlGaAs and P^+ for InGaAs/InP) were implanted at 32 keV, 7° normal to the [100] surfaces. This practice minimises channelling effects. A matrix of 5×5 1mm diameter implant regions was formed using Al masks with each row receiving a different dose, and each column receiving a different number of exposures of the specific dose for the row. In both the FIB and broad area experiments, the implant species were chosen to match those present in the cladding material in order to leave samples undoped after implantation. Intermixing experiments were carried out with a broad area implanter as a demonstration of the commercial viability of this technique. Broad area implanters are relatively inexpensive compared to FIB systems and, when coupled with an appropriate masking procedure, allow for rapid spatially selective implantation of large areas.

After implantation all samples were annealed in a N_2 atmosphere using a Heatpulse 410 Rapid Thermal Annealer. They were annealed from 15 to 30 seconds at settings of 800 to 850°C on the RTA unit. This initiated compositional disordering of the QWs and removed non-radiative recombination sites. In each system, RTA times and temperatures were selected to maximise intermixing of the implanted regions (reflected by a saturation in the shift) without inducing thermal QW disordering in unimplanted material (PL spectrum remaining unchange The sample surfaces were protected from desorpt (capable of producing additional vacancies) during anneals by placing large pieces of substrate material f down upon them.

2.2 High energy implantation

High energy ion implants were accomplished using the MeV Tandem Accelerator located at the University Western Ontario. These experiments were performed $In_{.23}Ga_{.77}As$/GaAs GRINSCH laser structures contain two 60A QWs. High energy implantation (8 MeV As was used to create vacancies immediately in the vicinity the QWs. The low energy techniques of the previ section are ineffective here due the depths of the QWs these samples (2 μm below the surface). Also, at th energies the implanted ions are buried roughly a mic beneath the QWs (corroborated by TRIM simulations[1 in the event that these might, as interstitial atoms, degr the performance of future devices. RTAs were carried as described earlier. In the first series of experiments, dose dependence of the high energy implant method investigated. Doses were varied from 2×10^{11} to 2×1 ions/cm^2 In a second series of experiments, the dose maintained at a fixed level (2×10^{13} ions/cm^2) while temperature of the sample during the implantat procedure was varied from 25 to 200°C (all previ implants were performed at 25°C). This final experim was carried out for two ion beam current densities (26 240 nA/cm^2) to examine the effects of dose-rate in regimes studied.

In all experiments, the shift in peak energy of PL fr each of the various QWs was used as a direct measure the achieved shift in the optical bandgaps of the sampl PL spectra were obtained at 4.2 K using weak He excitation. The PL was dispersed by a spectrometer collected using a CCD detector with a resolution of meV for the GaAs/AlGaAs and InGaAs/GaAs samples. Bomem FTIR with a resolution of 0.5 meV was employ for the InGaAs/InP samples. The PL shifts were measu with respect to the as-grown QW PL peak positions. correct for variations in QW thicknesses across the sampl the peak PL values for the as-grown wells were determin by interpolating between values measured on either side the implanted areas. In all these measurements, significant shifts in the unimplanted areas were observ resulting from the RTAs.

3. Discussion of Results

3.1 Low energy implantation

Figure 1 shows the FIB results obtained for a typi QW in the GaAs/AlGaAs sample over four consecut

implants and 5 RTAs. After the first implant/RTA cycle, the bottom curve shows how, for doses beyond 8×10^{13} ions/cm^2, the QW intermixing saturates and upon further irradiation diminishes. This effect is believed to be the result of the creation of vacancy complexes which limit the amount of mobile vacancies able to diffuse across the QW interfaces during the subsequent RTA. Also present at higher doses, for the FIB case of figure 1, are ion de-channelling effects which further impede the creation of vacancies deeper down into the samples. A separate study[12] showed how compositional disordering had occurred in QWs at depths corresponding to nearly ten times the mean range (500nm as compared to 50 nm projected by TRIM in amorphous material for 100 keV As^+ ions) yet decreased radically after implantation through a thin amorphous Si_3N_4 cap. In the present study, as the doses are increased, the cystallinity of the lattice degrades and channelling of ions along the [100] direction becomes less likely due to scattering.

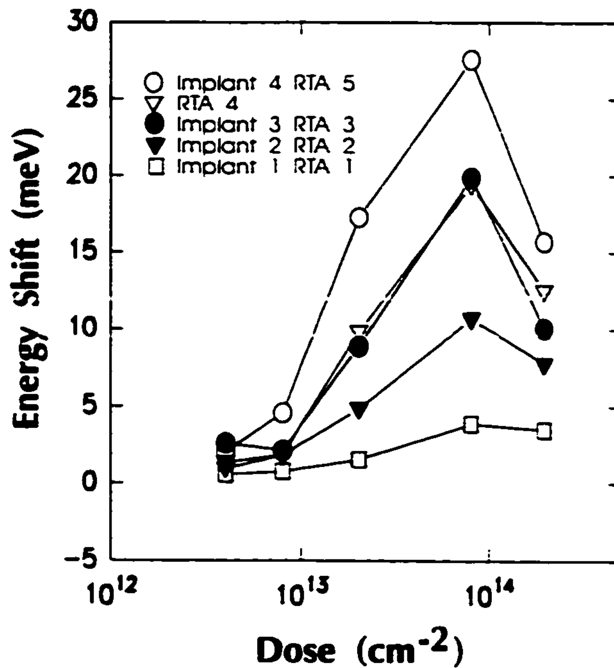

Fig.1. Multiple implant/RTA results for FIB implanted $GaAs/Al_xGa_{(1-x)}As$ QWs. L_z = 95A, x = 0.35, Depth=250nm. The empty triangles show the negligible effect of an RTA performed without prior implantation.

After the first RTA, sample crystallinity is greatly restored (as indicated by the return of the PL intensity to its level prior to implantation), and freed of many of the defects acquired during the implantation process[8]. This allows the following implantation to create new vacancies without immediately adding to the growth of undesirable vacancy complexes. Figure 1 shows how after 4 implants (8×10^{13} cm^{-2} As^+ ions each time) and 5 RTAs the QW's PL peak has shifted by roughly 30 meV, compared with the less than 5 meV attainable with a single implant/RTA. To demonstrate the effectiveness of the selected RTA times and temperatures in completely intermixing the QWs after a round of implantation, we show the negligible effect of an additional RTA (#4), performed after three implant/RTA cycles. Selected results for QWs in other material systems are given in Table I. All systems studied yielded qualitatively similar results to those presented in Figure 1.

Generally, FIB implantation was more effective in disordering the more deeply buried QWs regardless of material system. This is consistent with the presence of ion channelling. Also, for any particular implantation method and material system, the relative energy shifts of the QWs could be explained in terms of well compositions, widths and distances from the surface. A more detailed presentation of these results will be given elsewhere[6,7]

3.2 High energy implantation

Figure 2 shows the results from high energy (8 MeV As^{4+}) broad area implantation induced intermixing of GRINSCH QW laser structures grown in InGaAs/GaAs. Doses from 2×10^{11} to 2×10^{13} cm^{-2} were delivered to the samples and corresponding shifts in the PL spectra were observed ranging from 6.5 meV for the lowest dose, to 32

Table I. Selected results from QW intermixing experiments in InGaAs/GaAs, InGaAs/InP and GaAs/AlGaAs. L_z and Depth correspond to QW thickness and depth below surface respectively.

Well/Barrier - Implantation Source	Max Energy Shift 1 Implant 1 RTA (meV)	Corresponding Dose (cm^{-2})	Shift After 4 Impl/RTAs (meV)	Comments
$In_{.18}Ga_{.82}As/GaAs$ - FIB	20	2×10^{13}	34	L_z=30A Depth=450nm
$GaAs/Al_{.35}Ga_{.65}As$ - Broad Area	26	4×10^{13}	49	L_z=35A Depth=50nm
$In_{.53}Ga_{.47}As/InP$ - Broad Area	94	1×10^{14}	180	L_z=15A Depth=200A

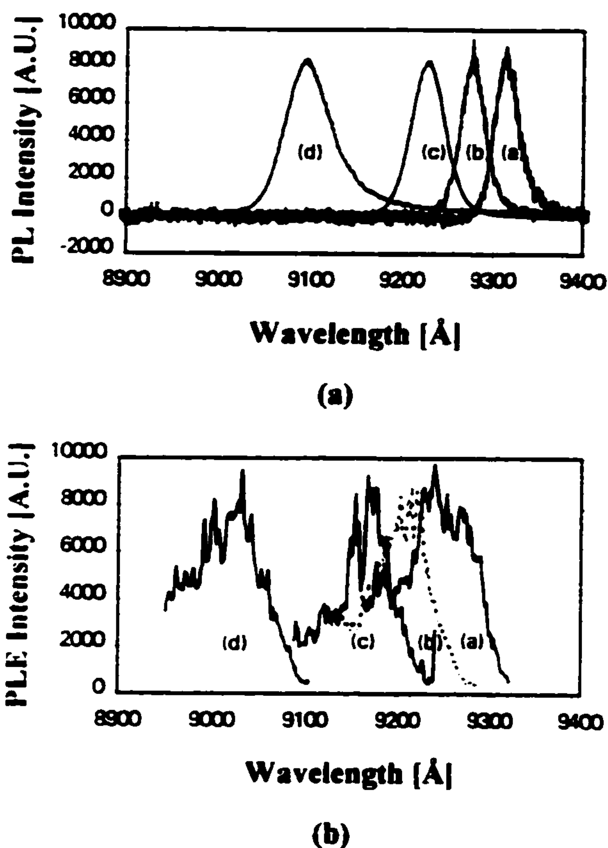

Fig.2. Effect of high energy broad area implantation/RTA on InGaAs/GaAs GRINSCH QW laser structures. (a) Resulting PL spectra for various doses (b) Corresponding PLE spectra. Peak labels indicate following doses: [a] as-grown, [b] 2×10^{11} ions/cm^2 [c] 2×10^{12} ions/cm^2 [d] 2×10^{13} ions/cm^2. All intensities are given in arbitrary units.

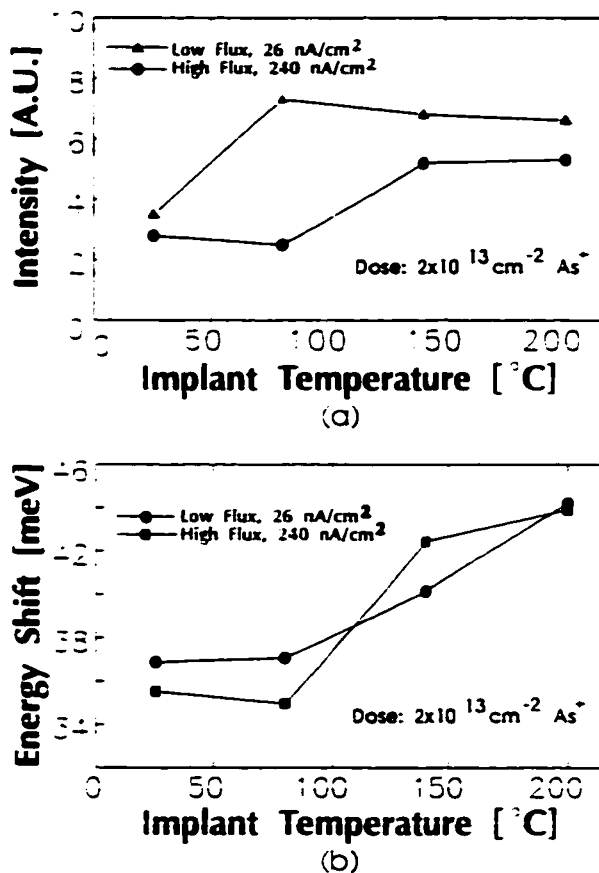

Fig.3 Effects of sample temperature and current density during implantation on (a) PL intensity, and (b) intermixing efficiency for InGaAs/GaAs GRINSCH QW laser structures. All intensities are given in arbitrary units.

meV for the highest dose. PL excitation (PLE) measurements were also performed on these samples and indicate a slight Stokes shift of the absorption spectra relative to the emission spectra. Of relevance here to waveguide applications is the success of this technique in blue-shifting the absorption of these structures while maintaining a sharp absorption edge.

Figures 3 (a) and (b) present the results of the implant temperature study. The first points involving implantation at 25 and 80 °C show little change in intermixing efficiency (fig. 3(b)). Data points taken at 140 and 200 °C, however, demonstrate a marked increase. This most probably is due to the dependence of defect production efficiencies and types on lattice temperature[13].

Data for low and high flux implantation also appear in both figures 3 (a) and (b). While the intermixing efficiencies seem comparable (to within 2 meV error bars), the intensity measurements suggest that better quality material (possessing fewer non-radiative recombination sites) results from the lower flux implantation at temperatures below perhaps 100°C. This advantage seems to lessen for higher implant temperatures and probably reflects the increasingly important role played by dynamic annealing at these temperatures[14].

4. Conclusions

The effectiveness of multiple implants and RTAs in delivering several times the maximum energy shift attributable to a single implant and RTA has been demonstrated in GaAs/AlGaAs, InGaAs/GaAs and InGaAs/InP QWs. These results were obtained at low energy using either FIB or the more commercially viable broad area implanter. Also studied was the effectiveness of high energy implantation induced intermixing on GRINSCH QW laser structures. PLE measurements confirmed the success of this technique in blue shifting the absorption edges of these structures. Lastly, the effects of implant

temperature and dose-rate were briefly investigated. From this we conclude that future work will most likely involve low ion implantation current densities and sample implant temperatures above 25°C.

Acknowledgement - This work was partially supported by the Natural Sciences and Engineering Research Council of Canada.

REFERENCES

[1] L.B. Allard, G.C. Aers, S. Charbonneau, T.E. Jackman, R.L. Williams, I.M. Templeton, M. Buchanan, D. Stevanovic, F.J.D. Almeida, J. Appl. Phys. 72 (2), (1992), pp. 422-428.

[2] F. Laruelle, Y.P. Hu, R. Simes, R. Kubena, W. Robinson, J. Merz, P.M. Petroff, J. Vac. Sci. Technol. B 7 (6), (1989), pp. 2034-2038.

[3] Y. Hirayama, S. Tarucha, Y. Suzuki, H. Okamoto, Phys. Rev. B37 (5), (1988), pp. 2774-2777.

[4] E.S. Koteles, A.N.M. Masum Choudhury, A. Levy, B. Elman, P. Melman, M.A. Koza, R. Bhat, Mat. Res. Soc. Symp. Proc. Vol. 240, (1992) pp.171-176.

[5] A.N.M. Masum Choudhury, P. Melman, A. Silletti, E.S. Koteles, B. Foley, B. Elman, IEEE Phot. Tech. Lett. 3 (9), (1991) pp. 817-820.

[6] P.J. Poole, P.G. Piva, M. Buchanan, G.C. Aers, A.P. Roth, Z.R. Wasilewski, E.S. Koteles, S. Charbonneau, J. Beauvais, submitted to Semiconductor Sc. and Tech.

[7] P.G. Piva, P.J. Poole, M. Buchanan, G. Champion, I. Templeton, G.C. Aers, R. Williams, Z.R. Wasilewski, E.S. Koteles, S. Charbonneau, accepted for publication in Appl. Phys. Let.

[8] J. Cibert, P.M. Petroff, D.J. Werder, S.J. Pearton, A.C. Gossard, J.H. English, Appl. Phys. Let. 49, (1986), pp. 223-225.

[9] F. Laruelle, A. Bagchi, M. Tsuchiya, J. Merz, P.M. Petroff, Appl. Phys. Let. 56, (1990), pp. 1561-1563.

[10] F.E. Prins, G. Lehr, H. Schweizer, G.W. Smith, Appl. Phys. Let. 63, (1993), pp. 1402-1404.

[11] J.F. Ziegler, J.P. Biersack, TRIM-90 Simulator , Pergamon, (1990).

[12] T.E. Jackman, S. Charbonneau, L.B. Allard, R.L. Williams, I.M. Templeton, M. Buchanan, M. Vos, I.V. Mitchel, J.A. Jackman, Appl. Phys. Let. 59, (1991), pp. 27-33.

[13] T.E. Haynes, O.W. Holland, U.V. Desnica, Mat. Res. Soc. Symp. Proc. Vol. 240, (1992), pp. 823-828.

[14] J.S. Williams, H.H. Tan, R.D. Goldberg, R.A. Brown, C. Jagadish, Mat. Res. Soc. Symp. Proc. Vol. 316, (1994), pp. 15-25.

APPENDIX -B-

and InGaAs/GaAs using focused Ga^+ ion beams

P. G. Piva,[a] P. J. Poole, M. Buchanan, G. Champion, I. Templeton, G. C. Aers, R. Williams, Z. R. Wasilewski, E. S. Koteles, and S. Charbonneau[b]
Institute for Microstructural Sciences, National Research Council, Ottawa, Ontario K1A 0R6, Canada

(Received 17 March 1994; accepted for publication 23 May 1994)

Spatially selective compositional disordering induced by focused Ga^+ ion beam implantation in GaAs/AlGaAs and strained InGaAs/GaAs quantum well structures has been studied using photoluminescence. We find that beyond a certain implantation dosage, the degree of intermixing imparted to a given quantum well saturates and may eventually decline as a result of damage to the semiconductor surface. We overcome this limitation by thermally annealing the sample after implantation to repair the crystalline surface. We show that multiple successive implants interspersed with rapid thermal anneals (RTAs) are successful in locally shifting the optical band gap of quantum wells by many times that attributed to a single implant and RTA.

Most optoelectronic devices utilize quantum wells (QWs) in their active regions, mainly because of their ability to produce a number of different components, such as lasers, amplifiers, detectors, and modulators in both waveguide and transverse configuration. Monolithic integration of such components in photonic integrated circuits (PICs) and optoelectronic integrated circuits (OEICs) is, in general, desirable due to the advantages gained in terms of cost, size, reliability, and performance. Integration of diverse optical devices can, however, give rise to problems. For example, the optimum operating wavelength of a laser is not that of a modulator or passive waveguide. What is required for optimization of an OEIC is a method of selective-area band-gap control. One of the most promising methods to achieve such a goal is QW intermixing.

Intermixing of QW structures by focused ion beam (FIB) has been shown to be a useful tool for spatially selective tuning of the QW band gap.[1-4] This technique promises not only the fabrication of optoelectronic structures of reduced dimensionality, but also the means to monolithically integrate devices of differing functionality on a single substrate without requiring additional lithography.[5] Ion beam induced intermixing is achieved by supplying excess neutral vacancies to the region where the band gap of the structure is to be modified. These vacancies are then free to diffuse through the sample during a RTA and provoke intermixing across the barrier-QW interfaces. FIB is not the only implantation technique capable of achieving the results of this study (see broad area implantation) but was readily available.

For FIB implantation at normal incidence to the epilayer surface, the depth distribution of the implanted ions and the resulting vacancy distribution have been shown to result from ion channeling.[6] As implantation doses are increased, damage to the sample surface gradually impedes the channeling of ions to the QWs. This process ultimately limits the amount of vacancies (necessary for QW intermixing) that can be delivered to a given QW by channeling durin[g a] single implantation.

Other studies have shown[4] that QW intermixing can a[lso] be achieved by using low energy (35 keV) broad area [im]plantation at orientations other than the [100] direct[ion]. These low energy implants were used to ensure that the i[ons] were stopped in the first few hundred Angstroms, spati[ally] removed from the QWs. The number of vacancies genera[ted] at the surface are a function of the mass of the ions, t[heir] energy, and the fluence. These vacancies were then dri[ven] down to the QW by thermally induced diffusion and, onc[e at] the QW-barrier interfaces, their presence enhanced the in[ter]diffusion of well and barrier atoms. It was pointed out tha[t at] large ion doses, the density of single vacancies decrease[s at] the expense of the vacancy complexes.[7] These diffuse a[t a] much slower rate than single vacancies, and do not reach [the] QWs on the time scale of the RTA resulting in a decreas[e in] the intermixing of the QWs.

In this letter we demonstrate an effective technique [to] overcome the damage processes limiting QW intermixing [by] either channeling or vacancy in-diffusion. This techni[que] consists of performing a RTA after each FIB exposure [in] order to recrystallize the sample surface. Subsequent exposure to the FIB then provokes further defect generat[ion] near the QWs via channeling or vacancy in-diffusion fr[om] the surface region. This then allows one to impart to a Q[W] by repeated implantation and RTAs, many times the ma[xi]mum shift attributable to a single implant/RTA.

These ion implantation experiments were carried out [in] two different material systems, GaAs(wells)/AlGa[As] (#1198) and strained InGaAs(wells)(#1020). Details rega[rd]ing the growth of these samples have been presen[ted] elsewhere.[1,6] Relevant sample parameters are shown in Ta[ble] I.

Ion implantation in both samples was carried out us[ing] 100 keV Ga^+ ions from a JIBL-104 Focused Ion Beam [fa]cility. A constant source current of 40 pA was used to impl[ant] doses ranging from 4×10^{12} to 2×10^{14} ions/cm^2 at room te[m]perature. Implantation in both samples took place (no[mi]nally) at normal incidence to the [100] surfaces to maxim[ize] ion channeling. Square regions (0.5 mm$\times$0.5 mm) separa[ted]

[a]Graduate student with the Ottawa-Carleton Institute for Physics, Dept. of Physics, University of Ottawa, Ottawa, Ontario, K1N 6N5.
[b]Also an Adjunct Professor, Dept. of Physics, University of Ottawa.

© 1994 American Institute of Physics
NRC 37

TABLE I. Nominal growth parameters and the measured (as-grown) PL peak positions for the samples used in the FIB implantation experiments.

	$GaAs/Al_xGa_{1-x}As$ #1198 (x=0.35)			$In_xGa_{1-x}As/GaAs$ #1020 (3 nm QWs)		
	Well width (nm)	Peak position (nm)	Well depth (nm)	Indium conc. (%)	Peak position (nm)	Well depth (nm)
QW1	3.5	757.3	50	7.0	828.0	50
QW2	5.6	779.1	100	10.3	837.3	100
QW3	9.5	798.9	250	14.7	848.1	250
QW4	18.5	811.8	450	18.0	858.3	450

from each other by 1 mm were patterned across the samples.

After each implantation, the samples were annealed at 850 °C for 30 s using a Heatpulse 410 Rapid Thermal Annealer. It is during the RTA process that intermixing occurs in the implanted regions. The annealing also acts to remove nonradiative recombination sites created in the lattice during implantation. During the RTA, the specimen surfaces were protected from arsenic desorption by placing a second large piece of GaAs substrate up against them.

As the barrier and QW materials intermix, the confinement profile of the QW is assumed to depart from that of a square well and to take on the shape of a double error function.[1] The net result of this QW disordering is manifested by a blue shift of the photoluminescence (PL) peak emission. The blue shift observed depends on many parameters such as QW thickness, indium concentration (in the case of InGaAs QWs) the ion fluence and energy, and the angle at which the implantation is performed. Lattice relaxation in the InGaAs QWs would lead to a red shift[1] and considerable broadening and loss of PL signal[8] not observed in these experiments.

We used the shift of the peak energy of the PL from each QW to monitor the compositional disordering. The PL measurements were carried out at 4.2 K using weak HeNe excitation. The emission spectra were dispersed by a spectrometer and detected using an imaging array with a resulting resolution of 0.2 meV. The QW peak positions in the nonimplanted regions were also monitored to determine how much, if any, of the shift was due to the RTA process itself.

The observed energy shifts as a function of ion fluences for each of the four QWs in both GaAs/AlGaAs and InGaAs/GaAs samples are summarized in Figs. 1(a) and 2(a), respectively. The non-monotonic behavior of the energy shifts as a function of QW depth in Fig. 2(a) is understood[1] in terms of a convolution of the effects of QW depth, width, and ternary composition and is of secondary importance to this study. Missing datapoints in Figs. 1(a) and 2(a) at higher doses indicate conditions where no luminescence was observed (i.e., complete disordering of the QW, particularly for QWs nearest to the surface, and/or incomplete removal of nonradiative recombination sites). As previously reported,[1] the mean range and straggling of 100 keV Ga^+ ions in randomly aligned GaAs are 50 and 25 nm, respectively. However, for sample 1020, substantial compositional disordering has been initiated even for the QW which is 450 nm below the surface, a distance nearly ten times the mean range. A separate study[6] showed that appreciable intermixing occurred in deep QWs only when a significant ion dose had been de ered to the QW regions, as measured by secondary ion-m spectroscopy (SIMS) before annealing. This was clear dence of channeling as opposed to vacancy in-diffusion ing annealing.

As the dose is increased to 8×10^{13} cm^{-2}, the en shift saturates (QW1, #1198), or slows down significa (QW2, #1198; QW3, #1020) and even decreases (Q #1198; QW4, #1020). These effects are believed to be du a convolution of channeling effects, single vacancy and cancy complex in-diffusion following RTA. In any c there is a maximum single dose beyond which further in mixing of the QWs is impeded by damage to the semic ductor surface.

To overcome this limitation, we implanted the sampl

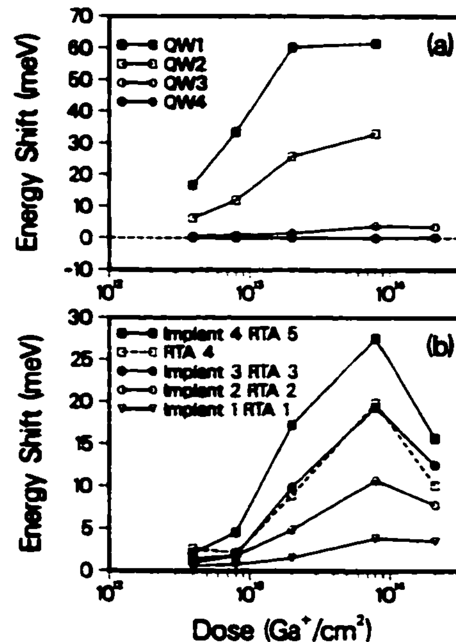

FIG. 1. Plots of energy shifts in peak PL emission vs implant dosage fo QWs 1–4 sample #1198 (GaAs/AlGaAs) for a single implant/RTA QW3 of the same sample over multiple implant/RTAs. The solid lines s the effect of consecutive implants and RTAs demonstrating that this pro can be used to enhance the energy shifts. The dotted line shows the effe a RTA on its own, leading to no significant change in the energy of th emission.

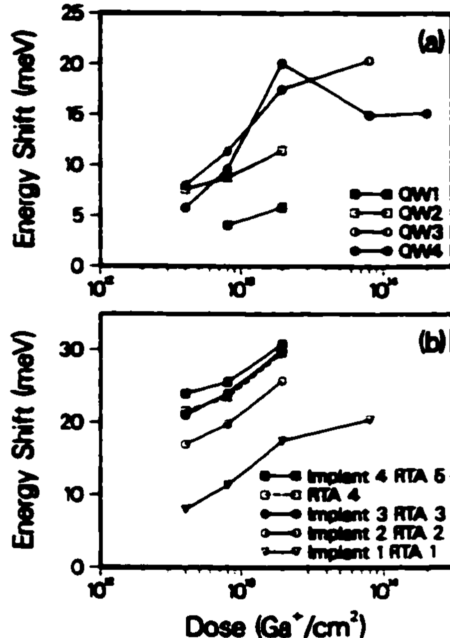

FIG. 2. Plots of energy shifts in peak PL emission vs implant dosage for (a) QWs 1–4 in sample #1020 (InGaAs/GaAs) for a single implant/RTA. (b) QW3 of the sample over multiple implants/RTAs. The dotted line shows the negligible effect of a single RTA, performed without prior implantation, on the intermixing process.

second time after the first implant/RTA and then performed a second RTA. The first RTA annealed out the damage created by the first implant, at least partially repairing the surface and allowing another successful implant to take place. We performed a total of four implant/RTA sequences. Figures 1(b) and 2(b) show the results of this process for QW3 of the GaAs/AlGaAs and InGaAs/GaAs samples, respectively. After the third implant/RTA sequence, we performed an additional (fourth) RTA without prior implantation to confirm that the RTA by itself was not affecting the energy shifts (the dashed line). A fourth implant and fifth anneal were then performed resulting in yet another shift in peak energy. The same conclusions were reached for the other QWs.

The process of sequential implant and RTA to further shift the band-gap energy of QWs is clearly demonstrated, with additional shifts of the order of 8 meV for each additional implant at a dose of 8×10^{13} cm^{-2} being observed for

meV) at a dose of 2×10^{13} cm^{-2}) for sample #1020. fourth RTA causes no significant change in the PL peak position and shows the previously observed shifts to be dependent upon the combination of ion implantation and RTA not merely a consequence of the RTA process. The integ PL emission intensity of implanted and annealed mater of the same order as the untreated material, indicating essentially all the damage is successfully annealed out o sample by the RTA process. These results show that the repairs much of the surface damage acquired during th plantation process. This allows a larger integrated degr intermixing to be produced in the QWs for a given tota dose than can be obtained by a single implantation wit dose.

We have studied the intermixing of GaAs/AlGaAs InGaAs/GaAs QWs by focused Ga^+ ion beams. In each we found that the maximum disordering that could be d ered to the QWs was limited by ion damage to the crysta surface. By performing RTAs after the implantation, it possible to repair the sample surfaces and, by virtue of tiple subsequent implantations and RTAs, deliver many the maximum possible disordering typically accompl by a single implant/RTA. Successful demonstration o hanced compositional disordering of QW using this nique suggests that a variety of integrated optoelect structures may be fabricated with submicron scale preci

This work was partially supported by the Natural ences and Engineering Research Council of Canada.

[1] L. B. Allard, G. C. Aers, S. Charbonneau, T. E. Jackman, R. L. Wi I. M. Templeton, M. Buchanan, D. Stevanovic, and F. J. D. Alme Appl. Phys. 72, 422 (1992).
[2] F. Laruelle, Y. P. Hu, R. Simes, R. Kubena, W. Robinson, J. Merz, M. Petroff, J. Vac. Sci. Technol. B 7, 2034 (1989).
[3] Y. Hirayama, S. Tarucha, Y. Suzuki, and H. Okamoto, Phys. Rev. 2774 (1988).
[4] E. S. Koteles, A. N. M. Masum Choudhury, A. Levy, B. Elman, P man, M. A. Koza, and R. Bhat, Mater. Res. Soc. Symp. Proc. 24 (1992).
[5] A. N. M. Masum Choudhury, P. Melman, A. Silletti, E. S. Kotel Foley, and B. Elman, IEEE Photon. Tech. Lett. 3, 817 (1991).
[6] T. E. Jackman, S. Charbonneau, L. B. Allard, R. L. Williams, Templeton, M. Buchanan, M. Vos, I. V. Mitchel, and J. A. Jackman, Phys. Lett. 59, 27 (1991).
[7] F. Laruelle, Y. P. Hu, R. Simes, W. Robinson, J. Merz, and P. M. P Surf. Sci. 228, 306 (1990).
[8] B. Elman, E. S. Koteles, P. Melman, C. Jagannath, C. A. Armiento, Rothman, J. Appl. Phys. 68, 1351 (1990).

Published without author corr

APPENDIX -C-

The enhancement of quantum well intermixing through repeated ion implantation

P J Poole†, P G Piva†‡, M Buchanan†, G C Aers†, A P Roth†, M Dion†, Z R Wasilewski†, Emil S Koteles†, S Charbonneau†§ and J Beauvais‖

† Institute for Microstructural Sciences and Solid State Optoelectronic Consortium, National Research Council, Ottawa, Canada, K1A 0R6
‖ Department of Electrical Engineering, University of Sherbrooke, Sherbrooke, Quebec, Canada J1K 2R1

Received 3 May 1994, in final form 29 June 1994, accepted for publication 18 July 1994

Abstract. Quantum well (QW) intermixing has been performed using low-energy broad-area ion implantation to increase the bandgap energy in a spatially selective manner. There is a maximum single dose beyond which further intermixing of the QWs is impeded by damage to the semiconductor surface. We demonstrate that this problem can be overcome by using a series of implants and rapid thermal anneals, with each rapid thermal anneal repairing the crystal surface. Using this technique we have observed shifts in optical bandgap for multiple implants greater than 2.5 times that observed for a single implant.

Ion-beam induced intermixing of quantum well (QW) structures has been shown to be a useful technique for the spatially selective tuning of the QW bandgap [1–4]. It can also be used as a technique for monolithically integrating optoelectronic devices of differing functionality (for example lasers, detectors, waveguides, modulators etc) on a single semiconductor wafer [5]. The most fundamental aspect of this integration is the requirement that different devices must have different bandgaps in order to operate efficiently. For example the creation of a detector, laser and transparent waveguide on one wafer requires three different optical bandgaps, the smallest for the detector to absorb the laser light, and the largest for the waveguide to minimize absorption. For commercial devices a technique is then needed that will allow the tuning of the bandgap by different amounts in different regions of the wafer using as simple a process as possible. Ion implantation and annealing is an effective process for initiating QW intermixing, and hence bandgap tuning, and can be used on a finished wafer without further reprocessing such as regrowth. For this technique to be as useful as possible we must ha[ve] the ability to shift the QW bandgap a significant dista[nce] in energy in a well controlled manner.

In this paper we report on the use of low-ene[rgy] broad-area ion implantation and rapid thermal anneal (RTA) to selectively tune the bandgap of a quant[um] well. We use a commercial low-energy broad-area [ion] implanter and a series of metal masks to allow us [to] selectively implant different regions of a sample. T[his] process is easier and more commercially viable th[an] the use of a focused beam facility as used in so[me] previous studies [1].

The ion implantation experiments were carried [out] on two QW samples based on different material syste[ms:] GaAs/AlGaAs (sample no 1198) and lattice-match[ed] InGaAs/InP (sample no 170). The GaAs/AlGa[As] structure was grown by molecular beam epitaxy i[n a] Vacuum Generators V80H system, using solid sour[ces] of Ga, Al and As_4. The GaAs and AlGaAs lay[ers] were grown at 650 °C at a growth rate of 0.7 μm h[$^{-1}$]. The lattice-matched InGaAs/InP sample was grown [by] chemical beam epitaxy in a Riber 32P system equipp[ed] with a cryopump and a turbomolecular pump that allo[w] typical growth rates of 1 μm h^{-1} in the low 10^{-5} T[orr] range. The growth temperature for this structure w[as] fixed at 465 °C. The sample parameters are shown [in] table 1.

The two samples were implanted with 32 keV io[ns:] arsenic for the GaAs/AlGaAs sample and phosphor[us]

‡ Graduate student with the Ottawa-Carleton Institute for Physics, Department of Physics, University of Ottawa, Ottawa, Ontario, Canada, K1N 6N5.

§ Also an Adjunct Professor, Department of Physics, University of Ottawa.

0268-1242/94/112134+04$19.50 © 1994 IOP Publishing Ltd

Table 1. Sample parameters for the GaAs/AlGaAs and InGaAs/InP QW structures. The peak positions correspond to the $n = 1$ heavy-hole exciton obtained at 4.2 K.

	GaAs/AlGaAs. sample 1198. 33% Al			InGaAs/InP. sample 170. 53% In		
	Well width (Å)	Peak position (Å)	Well depth (Å)	Well width (Å)	Peak position (μm)	Well depth (Å)
QW 1	35	7537	500	15	1.708	200
QW 2	56	7791	1000	25	1.296	365
QW 3	95	7989	2500	50	1.346	530
QW 4	185	8118	4500	70	1.412	730
QW 5	—			120	1.465	950

for the InGaAs/InP sample, from a Varian Extrion 200-CF ion implanter. These particular ions were chosen to avoid doping effects. Ion currents ranging from 0.1 μA for the lowest doses to 100 μA for the highest doses were used. An implantation angle of 7° to the normal minimized the effects of channelling [1, 6]. A lattice of 5×5 1 mm diameter implant regions was formed using metal masks with each row being given a different dose. The samples with the masks were mounted on 3″ silicon wafers in order to use the automatic loading system of the ion implanter.

After implantation the samples were annealed in an N_2 atmosphere using a Heatpulse 410 rapid thermal annealer. The GaAs/AlGaAs sample was annealed at 850 °C for 15 s, and the InGaAs/InP sample at 800 °C for 15 s. This initiated the compositional disordering of the QWs and removed non-radiative recombination sites. The sample surfaces were protected during the anneal by placing on top of them a second, larger piece of a wafer of the same material as the sample substrate.

The energy of the ion beam is small enough that implantation introduces vacancies and defects only into a thin region at the semiconductor surface (the ion penetration depth is a few hundred angstroms). When the sample is subsequently annealed these diffuse down through the structure. As they pass through the QWs they increase the magnitude of the intermixing of the QW and barrier materials driven by the elevated temperatures. This leads to a change in the shape of the QW confining potential and the bandgap of the QW. From the information here it is not possible to determine the exact species responsible for the interdiffusion, but we will talk in terms of both vacancies and defects [7].

The shift in peak energy of the photoluminescence (PL) from each QW corresponding to ground state transitions between conduction and valence band quantized levels was used to monitor the degree of QW shape change. This was performed at 4.2 K using weak HeNe excitation. The PL was dispersed by a spectrometer and detected using a CCD detector with a resolution of 0.2 meV in the case of the GaAs/AlGaAs sample, and with a Bomem FTIR with a resolution of 0.5 meV for the InGaAs/InP sample. The QW PL peak positions in the non-implanted regions were also measured to determine how much, if any of the shift was just due to intrinsic intermixing resulting from the

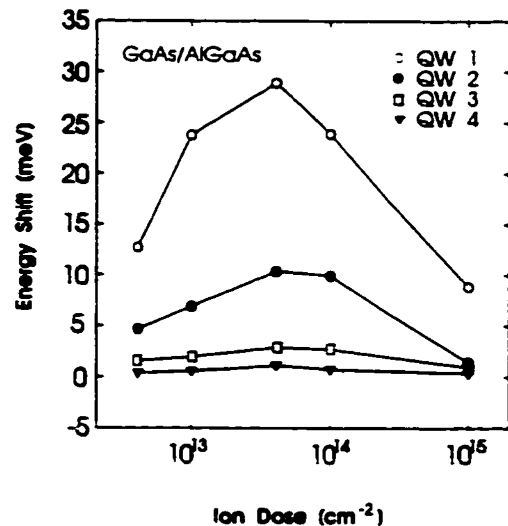

Figure 1. A plot of the energy shifts observed in the photoluminescence peaks for the four quantum wells in GaAs/AlGaAs sample after ion implantation and anneal. The narrowest well (QW 1) nearest the surface has the largest energy shift, and all the wells demonstrate a pe[ak] in energy shift against ion dose of 4×10^{13} cm^{-2}.

elevated temperatures experienced by the samples du[ring] the RTA process. In all these measurements there wa[s] significant shift observed for just the RTA process.

Figure 1 presents the energy shifts observed for four QWs in the GaAs/AlGaAs sample after diffe[rent] ion doses and a single anneal (further annea[ls] caused no significant additional shift in the PL [peak] positions). It should be noted that the four wells [have] significantly different energy shifts, with the narro[west] well demonstrating the largest shift. This is expected, only since this QW is nearest the surface but also bec[ause] a fixed degree of intermixing of the QW interfaces [will] be a small perturbation on the transition energy in a l[arge] well, and a large perturbation for a narrow well. [This] is true until one gets to extremely narrow wells w[here] the lowest energy state in the well is very close to conduction band levels in the barriers. More impor[tant] for this study is the strong peak observed in the en[ergy] shift versus ion dose curve. This means that there [is a] maximum energy shift possible for a single implanta[tion] and RTA.

The cause of the peak in the observed energy s[hift]

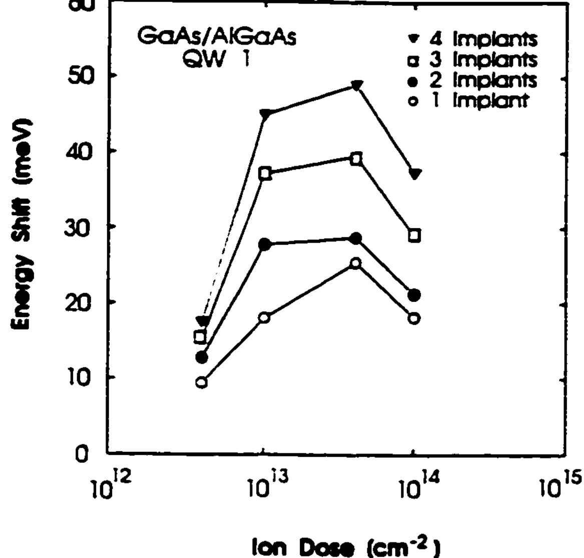

Figure 2. A plot of the energy shift for QW 1 of the GaAs/AlGaAs sample after one, two, three and four consecutive implants and anneals. Each additional implant and anneal causes an extra energy shift allowing energy shifts significantly greater than those observed for a single ion implant and anneal. Similar behaviour is observed for the other three QWs.

as a function of dose is believed to be the formation of highly immobile defect complexes and vacancy complexes in the implanted region of the sample when the dose is large. These do not diffuse through the QWs during the 15 s anneal, and hence cause no intermixing. At low ion doses the single vacancy and defect density will be low enough for very few complexes to be formed. As the dose increases, more complexes will be created until a critical dose is reached (in this case 4×10^{13} cm^{-2}). Above this dose the single vacancy and defect density will actually be decreasing with increasing dose, leading to a decreasing energy shift.

To overcome this problem we re-implanted the samples and annealed them after performing the first implant and anneal. Annealing results in a repaired crystal surface suitable for re-implantation. The result of this for QW 1 is shown in figure 2 for one, two, three and four consecutive implants and anneals. These energy shifts were observed in a different region of the sample from those in figure 1. Owing to sample non-uniformity, the two regions do not give the same energy shifts for a single ion dose and RTA, but the trend always remains the same. This clearly illustrates how the anneal repairs the surface of the crystal, allowing further successful implantations and energy shifts. The energy shift observed at a dose of 1×10^{13} cm^{-2} after four consecutive implants and anneals is 2.5 times greater than that for a single implant and anneal.

Figure 3 shows the energy shifts observed in the InGaAs/InP sample after similar treatment. Again the re-implantation and anneal causes an additional energy shift. The energy shifts observed for this sample are considerably greater than for the GaAs/AlGaAs sample, and show no sign of a peak with ion dose, up to a dose of

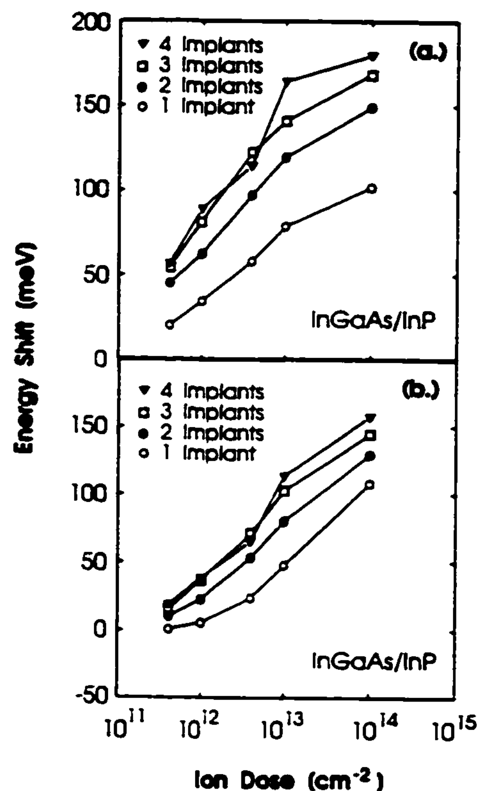

Figure 3. A plot of the energy shift observed for (*a*) QW 2 and (*b*) QW 3 of the InGaAs/InP sample after one, two, three and four consecutive implants and anneals. As observed in the GaAs/AlGaAs system each additional implant and anneal causes an extra energy shift.

1×10^{14} cm^{-2}. The lack of a peak in energy shift in t[he] InGaAs/InP sample is most likely due to the differen[ce] in the materials where the ion implantation damage [is] created (GaAs for sample no 1198 and InP for samp[le] no 170), and the ion used for implantation. It wou[ld] appear that InP requires a larger dose of phosphorus io[ns] before the formation of complex defects and vacanci[es] becomes significant, possibly due to the lower ma[ss] of phosphorus ions relative to the arsenic ions us[ed] for the GaAs/AlGaAs system. The intermixing of t[he] QWs and the surrounding barrier material in this syste[m] is more complicated than in the GaAs/AlGaAs syste[m] due to strain effects, and is not yet well understoo[d]. The QWs are initially lattice matched to the InP, b[ut] after intermixing occurs strain may be present. Rece[nt] work seems to indicate that the QWs will in fa[ct] remain unstrained after intermixing [8, 9], being a lattic[e] matched alloy of InGaAsP, and will have sharp interfac[es] with the InP resulting in narrow linewidths in PL a[nd] minimal Stokes shift. This is consistent with the [PL] linewidths observed in our sample after intermixin[g]. Further work is in progress to clarify the effect of stra[in] after disordering has taken place.

We have shown that the use of sequential multip[le] ion implants and RTAs can enhance the bandgap tunin[g] of semiconductor QW structures beyond that possib[le] with a single implant. This technique has been show[n] to work in two very different material systems, wi[th]

the largest tuning observed for the technologically important InGaAs/InP system which has bandgap in the wavelength region 1–1.5 μm. This process is potentially very useful for the monolithic fabrication on one wafer of optoelectronic devices performing different functions.

References

[1] Allard L B. Aers G C. Charbonneau S. Jackman T E. Williams R L. Templeton I M. Buchanan M. Stevanovic D and Almeida F J D 1992 *J. Appl. Phys.* **72** 422–8

[2] Laruelle F. Hu P. Simes R. Kubena R. Robinson W. Merz J and Petroff P M 1989 *J. Vac. Sci. Technol.* B **7** 2034–8

[3] Hirayama Y. Tarucha S. Suzuki Y and Okamoto H 198 *Phys. Rev.* B **37** 2774–7

[4] Koteles E S. Masum Choudhury A N M. Levy A. Elm B. Melman P. Koza M A and Bhat R 1992 *Mater. R Soc. Symp. Proc.* **240** 171–6

[5] Masum Choudhury A N M. Melman P. Silletti A. Kote E S. Foley B and Elman B 1991 *IEEE Photon. Tech Lett.* **3** 817–20

[6] Jackman T E. Charbonneau S. Allard L B. Williams R Templeton I M. Buchanan M. Vos M. Mitchell I V a Jackman J A 1991 *Appl. Phys. Lett.* **59** 2733–5

[7] Hirayama Y 1989 *Japan. J. Appl. Phys.* **28** L162–5

[8] Yu S J. Asahi H. Emura S and Gonda S 1991 *J. Appl. Phys.* **70** 204–8

[9] Temkin H. Chu S N G. Panish M B and Logan R A 19 *Appl. Phys. Lett.* **50** 956–8

APPENDIX -D-

Enhanced Quantum Well Intermixing Using Multiple Ion Implantation

P. J. Poole, P. G. Piva†, M. Buchanan, G. Champion, I. Templeton, G. Aers, R. Williams, A. P. Roth, Z. R. Wasilewski, E. S. Koteles, S. Charbonneau*

Institute for Microstructural Sciences, National Research Council
Ottawa K1A OR6, Canada

J. Beauvais

Dep. Electrical Engineering, University of Sherbrooke, Sherbrooke, Quebec, J1K 2R1, Canada

†Graduate student with the Ottawa-Carleton Institute for Physics, Dep. Of Physics, Univ. of Ottawa, Ottawa, Ontario, K1N 6N5

*Also an Adjunct Professor, Dep. of Physics, University of Ottawa.

ABSTRACT

Quantum well intermixing has been performed using ion implantation techniques to increase the optical bandgap in a spatially selective manner. We show that there is a maximum single dose beyond which further intermixing of the QWs is impeded by damage to the semiconductor surface. We overcome this problem by using a series of implants and rapid thermal anneals, with each rapid thermal anneal repairing the crystal surface. Using this technique we have demonstrated shifts in optical bandgap for multiple implants greater than seven times that observed for a single implant.

1. Introduction

Ion-beam induced intermixing of quantum well (QW) structures has shown itself to be a useful technique for the spatially selective tuning of the QW bandgap[1-4]. It can also be used as a technique for monolithically integrating optoelectronic devices of differing functionality (e.g.

0-8194-1434-4/9

lasers, detectors, waveguides, modulators, etc.) on a single semiconductor wafer[5]. The most fundamental aspect of this integration is the requirement that different devices must have different bandgaps in order to operate efficiently.

The ion-beam induced intermixing process operates by supplying excess, neutral vacancies (in the region where the bandgap of the structure is to be shifted) which are free to diffuse through the sample during a rapid thermal anneal (RTA). The maximum energy shift observed by this process is not limited by the maximum ion dose but by the amount of damage created in the sample by the ion implantation. In this paper we demonstrate an effective technique for overcoming this problem which consists of performing sequential ion implants followed by RTAs.

2. Experiment

The ion implantation experiments were carried out on a series of QW samples based on different material systems, GaAs/AlGaAs (sample #1198), strained InGaAs/GaAs (#1020) and unstrained InGaAs/InP (#170). Both the GaAs/AlGaAs and InGaAs/GaAs structures were grown by molecular beam epitaxy in a Vacuum Generators V80H system, using solid sources of Ga, In, Al and As_4. The GaAs and AlGaAs layers were grown at 650°C at a growth rate of 0.7 µm/h, while the InGaAs layers were grown after the substrate temperature was lowered rapidly to 565°C to minimise desorption of indium. The InGaAs/InP sample was grown by chemical beam epitaxy in a Riber 32P system equipped with a cryopump and a turbomolecular pump that allows typical growth rates of 1 µm/h in the low 10^{-5} Torr range. The growth temperature for this structure was fixed at 465°C. The sample parameters are shown in table I.

	GaAs/AlGaAs #1198 35% Al			InGaAs/GaAs #1020 30Å QWs			InGaAs/InP #170 53% In		
	Well Width	Peak Position	Well Depth	Indium Conc.	Peak Position	Well Depth	Well Width	Peak Position	Well Depth
QW 1	35 Å	7573 Å	500 Å	7%	8280 Å	500 Å	15 Å	1.156 µm	200 Å
QW 2	56 Å	7791 Å	1000 Å	10.3%	8373 Å	1000 Å	25 Å	1.272 µm	365 Å
QW 3	95 Å	7989 Å	2500 Å	14.7%	8481 Å	2500 Å	50 Å	1.317 µm	530 Å
QW 4	185 Å	8118 Å	4500 Å	18%	8583 Å	4500 A	70 Å	1.388 µm	730 Å
QW 5	-	-	-	-	-	-	120 Å	1.445 µm	950 Å

TABLE I

The nominal growth parameters and the measured PL peak positions for the samples used in the ion implantation experiments. The depth of the wells below the surface is also given.

Two techniques were used for implanting ions to induce the compositional disordering. The first was using 100 keV Ga^{+} ions implanted by a JIBL-104 UHV Focused Ion Beam (FIB) facility and was performed on samples #1198 and #1020. A constant current of 40 pA was used to implant doses ranging from 0.4 to 20×10^{13} ions/cm^2. The geometry of the target stage and ion column is such that the implantation direction is normal to the epilayer surface (allowing channelling of the ions to occur). Square regions (0.5 mm × 0.5 mm) separated from each other by 1 mm were patterned across the sample.

The second technique used was a broad area implant of 32 keV ions from a Varian Extrion 200-CF ion implanter. Ion currents ranging from 0.1 μA for the lowest doses to 100 μA for the highest doses were used. An implantation angle of 7° to the normal minimised the effects of channelling. A lattice of 5×5 1 mm diameter implant regions was formed using metal masks with each row being given a different dose. The samples with the masks were mounted on 3" silicon wafers in order to use the automatic loading system of the ion implanter.

After implantation the samples were annealed as shown in table II in a N_2 atmosphere using a heatpulse 410 Rapid Thermal Annealer (RTA). This initiated the compositional disordering of the QWs and removed non-radiative recombination sites. The sample surfaces were protected during the anneal by placing a second, larger piece of a wafer on top of them of the same material as the sample substrate.

	#1198 FIB	#1198 Broad Area	#1020 FIB	#170 Broad Area
Implant Species	Gallium	Arsenic	Gallium	Phosphorus
Implant Energy (keV)	100	32	100	32
RTA Temperature (°C)	850	850	850	800
RTA Time (seconds)	30	15	30	15
Cap Material	GaAs	GaAs	GaAs	InP

Table II

The parameters used for each sample in the ion implantation and rapid thermal anneal. The ion species was chosen so as not to act as a dopant in the structure. The RTA temperatures and times were chosen to allow a complete disordering of the structure without causing degradation of the QWs. The cap material protected the sample surfaces during the anneal.

The ion implantation process causes a blue shift in the QW bandgap energy by enhancing compositional disordering, a mixing of the QW material with the barrier material. Figure 1 shows schematically the band structure of a QW before and after implantation and RTA. The intermixing of the QW and barrier changes the shape of the QW, and leads to a blue shift in the bandgap of the well. The size of the energy shift depends in part on the well width, the difference between the barrier and QW bandgaps, and the concentration of defects delivered to the QWs by the implantation.

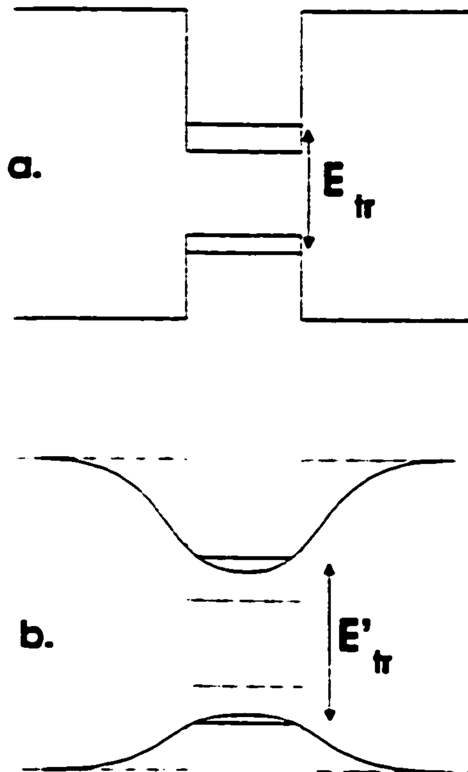

Fig. 1 : A schematic of the band structure of a quantum well before (a.) and after (b.) intermixing has occurred. The change in shape of the well causes the bandgap transition energy E_{tr} to increase (E'_{tr}).

The shift in peak energy of the PL from each QW was used to monitor the degree of compositional disordering. This was performed at 4.2 K using weak HeNe excitation. The PL was dispersed by a spectrometer and detected using an imaging detector with a resolution of 0.2 meV (or in the case of sample #170 a Bomem FTIR was used with a resolution of 0.5 meV). The QW PL peak positions in the non-implanted regions were also measured to determine how much, if any, of the shift was just due to the RTA process.

3. Results

Fig. 2 shows the resulting shift in PL peak position for sample #1198 after one dose and RTA, using the broad area implantation. The narrowest well displays the largest energy shift, the shift decreasing as the well width increases. The energy shift observed with dose peaks at a density of 4×10^{13} cm^{-2}, any dose higher than this results in a smaller shift in energy for all the QWs. This gives the maximum energy shift possible with a single implant process. This behaviour is also observed for the FIB implanted samples.

Intermixing of the QW material with the barriers can be caused by a number of different mechanisms depending on the material system, dose regime and QW depth below the surface. In the GaAs/AlGaAs system, the effect is believed to be due predominantly to the production of vacancies at the surface of the crystal during implantation[4]. The details of these processes are not particularly relevant to the present study since, in either case, damage in the surface region is understood to be the limiting factor in the QW interdiffusion process. The RTA then causes these to diffuse down through the crystal resulting in the intermixing of QWs. At large ion doses, vacancy complexes start to form which diffuse at a slower rate than single vacancies and so do not reach the QWs on the time scale of the RTA. Therefore at large doses the density of single vacancies decrease at the expense of the vacancy complexes, resulting in a decrease in intermixing of the QWs.

The situation in InGaAs/GaAs QWs is more complicated, at least in part, because of the ion damage threshold dosage in this strained system is much lower than for GaAs/AlGaAs QWs[6]. In this case, the few ions that may penetrate even to QWs deep below the surface due to channelling[7] have been shown to lead to significant interdiffusion upon annealing. Here the energy shifts for the deep QWs saturate with increasing dose (up to $\approx 10^{14}$ Ga^+ ion/cm^2) due to dechannelling of the ions in the surface region as it is damaged. The shallow QWs are completely disorded at doses higher than $\approx 2\text{-}4\times 10^{13}$ Ga^+ ion/cm^2.

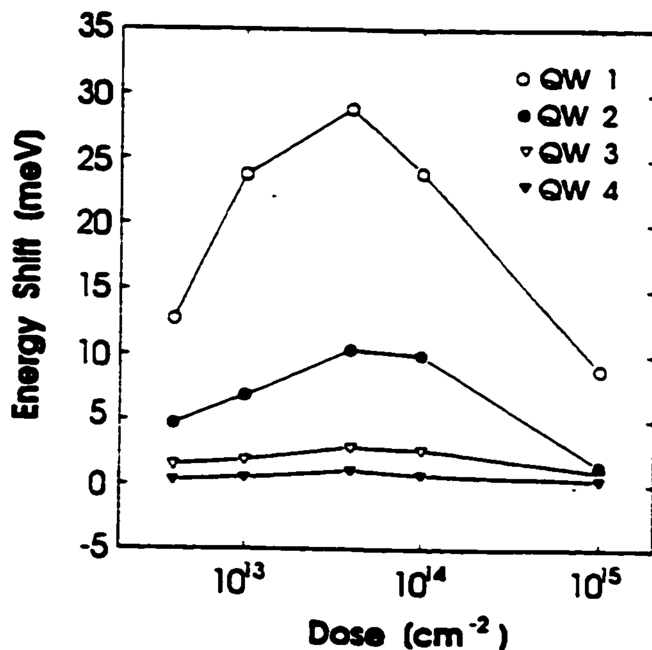

Fig. 2 : A plot of the energy shifts in the PL emissions due a single broad area ion implant and RTA for sample #1198 (GaAs/AlGaAs). Note how the shifts peak at 4×10^{13} cm^{-2}.

To overcome this limitation, by whatever mechanism, in the generation of damage at the crystal surface (and hence, ultimately the maximum energy shift) we re-implanted the samples after the first RTA and then performed a second RTA. The first RTA annealed out the damage caused by the first implant, repairing the surface and allowing another successful implant to take place. Figure 3 shows the results of this sequential implantation and RTA process for QW 3 of the GaAs/AlGaAs sample (#1198) and

the InGaAs/GaAs sample (#1020) using FIB implantation. For these samples we performed a fourth RTA without prior implantation to confirm that the RTA by itself was not affecting the energy shifts (the dashed line). A fourth implant and fifth anneal were then performed resulting in yet another shift in peak energy. The same conclusions were reached for the other QWs regardless of the ion source being used.

The process of sequential implant and RTA to further shift the bandgap energy of QWs is clearly demonstrated, with additional shifts of the order of 8 meV for each additional implant at a dose of 8×10^{13} cm^{-2} being observed for sample #1198. The fourth RTA causes no significant change in the PL peak position and shows the previously observed shifts to be dependent upon the ion implantation followed by an RTA, and not merely an artefact of the RTA process. The integrated PL emission intensity of implanted and annealed material is of the same order as the untreated material, indicating that all the damage is successfully annealed out of the sample by the RTA process. These results show very clearly that the RTA is repairing the surface of the samples allowing a larger effective dose to be delivered to them.

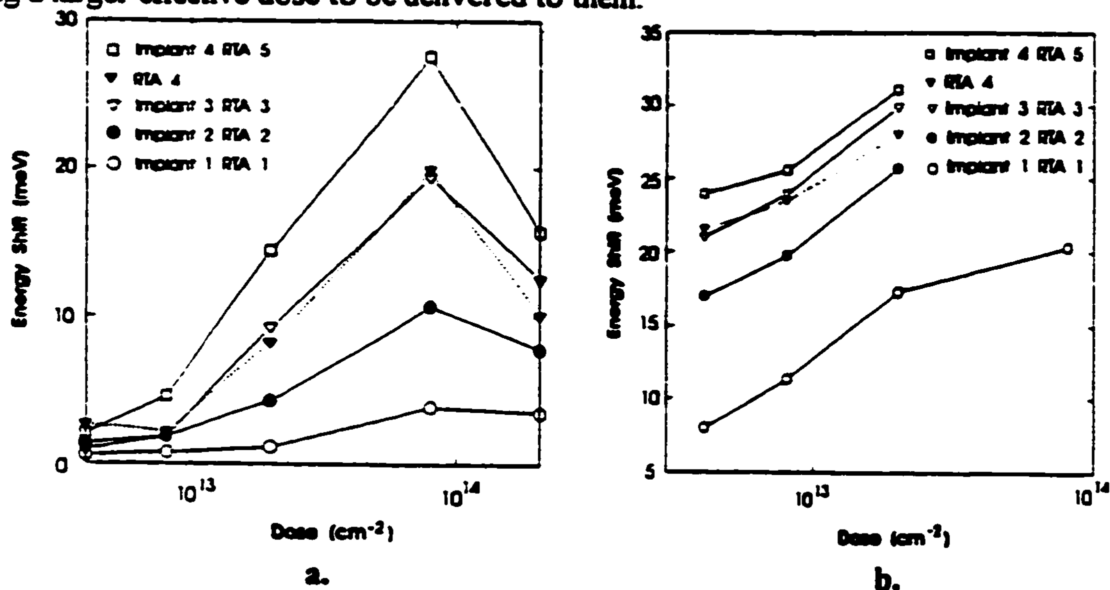

Fig. 3 : A plot of the energy shifts observed in the PL emission from (a.) QW 3 of sample #1198 (GaAs/AlGaAs) and (b.) QW 3 of sample #1020 (InGaAs/GaAs) implanted using the FIB. The solid lines show the effect of consecutive implants and RTAs demonstrating that this process can be used to enhance the energy shifts. The dotted line shows the effect of an RTA on its own, and leads to no significant change in the energy of the PL emission.

This technique was also very effective for the InGaAs/InP sample which is working at wavelengths suitable for optoelectronic applications. Figure 4 shows the energy shifts observed

for multiple implants and RTAs for this sample (QW 2) using the broad area implant summarise in table II. The same general trend was observed for the other QWs. A summary of these finding will be reported in a following publication[8].

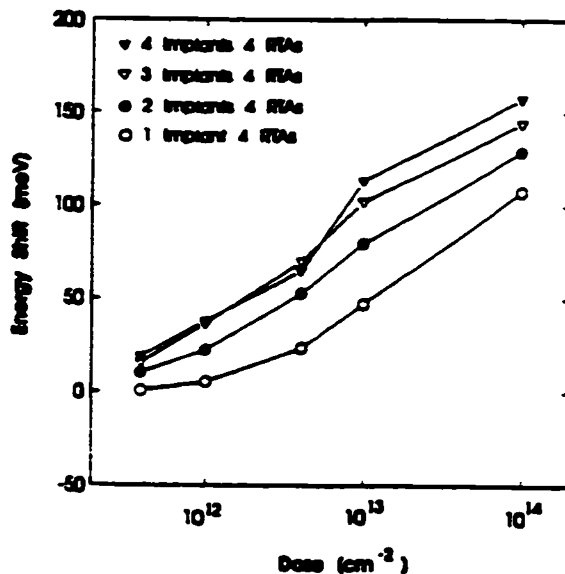

Fig. 4 : A plot of the energy shif observed in the PL emission from QW 2 c sample #170 (InGaAs/InP) implanted usin the broad area implantation. All implar regions receive the same amount c annealing, but different numbers of repea implants. The shifts observed for th materials system are very large due to th large difference between QW and barrie bandgap energies.

4. Summary

We have shown that the use of sequential multiple ion implants and RTAs has enhance the bandgap tuning of semiconductor QW structures beyond that possible with a single implan This technique has been shown to work in different material systems, with the largest tunin observed for the technologically important InGaAs/InP system which operates in the 1-1.5 μr wavelength region. This process works both for the FIB and broad area implanting method making it very useful for the monolithic fabrication of optoelectronic devices performing differer functionalities on one wafer.

5. Acknowledgements

The authors would like to acknowledge the help of Michel Dion in the careful cleaving c the samples, and Pierre Lafrance for assistance with the broad area ion implantation. This wor was partially supported by the Natural Sciences and Engineering Research Council of Canada.

References

[1] L. B. Allard, G. C. Aers, S. Charbonneau, T. E. Jackman, R. L. Williams, I. M. Templeton, M. Buchanan, D. Stevanovic, F. J. D. Almeida, J. Appl. Phys. 72 (2), (1992), pp. 422-428

[2] F. Laruelle, P. Hu, R. Simes, R. Kubena, W. Robinson, J. Merz, P. M. Petroff, J. Vac. Sci. Technol. B 7 (6), (1989), pp. 2034-2038

[3] Y. Hirayama, S. Tarucha, Y. Suzuki, H. Okamoto, Phys. Rev. B37 (5), (1988), pp. 2774-2777

[4] E. S. Koteles, A. N. M. Masum Choudhury, A. Levy, B. Elman, P. Melman, M. A. Koza, R. Bhat, Mat. Res. Soc. Symp. Proc. Vol. 240, (1992) pp.171-176

[5] A. N. M. Masum Choudhury, P. Melman, A. Silletti, E. S. Koteles, B. Foley, B. Elman, IEEE Phot. Tech. Lett. 3 (9), (1991) pp. 817-820

[6] L. B. Allard, J. C. Aers, P. G. Piva, P. J. Poole, M. Buchanan, T. E. Jackman, S. Charbonneau, M. Vos, I. V. Mitchell, submitted to Appl. Phys. Lett. (1993)

[7] T. E. Jackman, S. Charbonneau, L. B. Allard, R. L. Williams, I. M. Templeton, M. Buchanan, M. Vos, I. V. Mitchell, J. A. Jackman, Appl. Phys. Lett. 59 (1991), p. 2733

[8] P. J. Poole, P. G. Piva, M. Buchanan, G. Champion, I. Templeton, G. Aers, R. Williams, A. P. Roth, Z. R. Wasilewski, E. S. Koteles, S. Charbonneau, to be submitted to J. Appl. Phys.

APPENDIX -E-

in intermixed GaAs/AlGaAs quantum wells

P. G. Piva[a),b)] and S. Charbonneau[c)]
Institute for Microstructural Sciences, National Research Council Canada, Ottawa, Ontario K1A 0R6, Canada

I. V. Mitchell and R. D. Goldberg
University of Western Ontario, London, Ontario N6A 3K7, Canada

(Received 11 December 1995; accepted for publication 12 February 1996)

The effect of ion implantation induced intermixing on the effective radiative lifetimes in GaAs/AlGaAs quantum wells is investigated using the technique of time-resolved photoluminescence (TRPL). Below the critical dose, the carrier lifetimes appear enhanced by the processing although no changes are discernible in the continuous wave photoluminescence (CWPL) spectra. Above the critical dose, carrier lifetimes are reduced by residual defects created in the intermixed wells by the implantation procedure. These observations demonstrate the greater sensitivity of TRPL over CWPL in detecting residual damage produced by processing quantum well material. [S0003-6951(96)02516-1]

Vacancy enhanced compositional mixing of quantum well (QW) structures induced by ion beam implantation has shown itself to be a useful technique for achieving spatially selective tuning of the QW band gap.[1–4] As QWs form the active region of most optoelectronic devices, this method is being pursued as a means of monolithically integrating many such components onto a single substrate. There are, however, concerns regarding the degradation in the crystalline quality of QWs subjected to this form of processing.[5]

In this letter, we look at the degradation resulting in the GaAs/AlGaAs system as reflected by changes in the effective decay rates of photo-excited carriers in the intermixed QWs. We find that below the critical dose required to initiate QW interdiffusion,[6] the carrier lifetimes in the QW structures are increased. Implantation doses above the critical dose, however, clearly result in reduced carrier lifetimes in the QWs.

The test samples used in this experiment were grown by molecular beam epitaxy in a Vacuum Generators V80H system using solid sources of Ga, Al, and As_4. The QW structure was grown on a (100) oriented undoped GaAs wafer, and comprised (from bottom up) a 400 Å GaAs buffer layer, 20 periods of 20-Å-thick layers of AlAs and GaAs, a second 5000-Å-GaAs buffer layer, 1.49 μm of $Al_{0.44}Ga_{0.56}As$, 1500 Å of $Al_{0.18}Ga_{0.82}As$, a 50-Å-thick GaAs QW, 1500 Å of $Al_{0.18}Ga_{0.82}As$, 3000 Å of $Al_{0.44}Ga_{0.56}As$, and a 20 Å GaAs capping layer.

The implantations were carried out using the 1.7 MV Tandem accelerator facility located at the University of Western Ontario. Six samples were cleaved from the growth wafer and implanted at room temperature with 8.56 MeV As^{4+} ions. The expected range of such ions in our structures is 3.2 μm as estimated by TRIM-91.[7] Implant doses ranged from 10^{10} to 10^{15} cm^{-2}, and were performed (with the exception of the lowest and highest doses) using an ion flux of 5 nA/cm^2. Given the large range in doses studied here, 10^{10} and 10^{15} cm^{-2} samples were implanted using fluxes of 0.3 and 24 nA/cm^2, respectively. This mainta[ined] accurate dose monitoring for the low fluence sample[s and] kept the time required to perform the highest dose impla[nta]tion within acceptable bounds. To determine the rang[e of] implantation doses, the critical dose for arsenic impla[nted] GaAs/AlGaAs QWs was estimated from that reported in [Ref.] 8 for 8 MeV bismuth implanted GaAs/AlGaAs QWs. [This] was done by scaling the required arsenic dose by the rat[io of] the two differing vacancy production efficiencies (evalu[ated] at their respective QW depths) as calculated by TRIM. The extrapolated value for the critical dose required to [ini]tiate a detectable shift in the QW photoluminescence [spec]trum was 1×10^{12} cm^{-2} and compared reasonably wit[h the] actual value (see Fig. 1). To allow for a direct compar[ison] between implanted and as-grown material, only half of [each] sample was implanted.

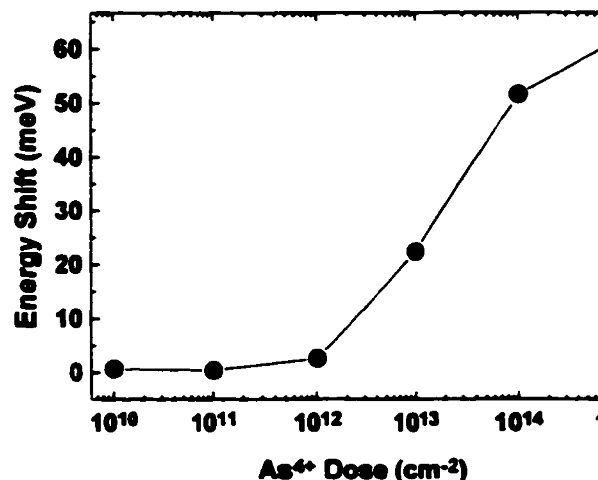

FIG. 1. Plot of PL emission energy shifts as a function of implantation [dose]. The critical dose is located between 10^{11} and 10^{12} cm^{-2} for 8.56 [MeV] As^{4+}.

[a)]Graduate student with the Ottawa-Carleton Institute for Physics, Dept. of Physics, University of Ottawa, Ottawa, Ontario K1N 6N5, Canada.
[b)]Present address: Dept. of Physics, University of Western Ontario, London, Ontario N6A 3K7, Canada. Electronic mail: pgpiva@julian.uwo.ca
[c)]Also an Adjunct Professor, Dept. of Physics, University of Ottawa.

(RTA). It is during this stage that damage produced by the ion implantation serves to enhance the interdiffusion of barrier and well species, typically resulting in a blueshifting of the QW band gap in the implanted region.[1] The samples were annealed at 850 °C for 90 s, as these conditions were previously found to saturate interdiffusion in the implanted regions while leaving the unimplanted material unshifted.[9] During annealing, the sample surfaces were protected from arsenic desorption by means of a GaAs proximity cap.

Continuous-wave photoluminescence (CWPL) measurements were used to monitor the extent of the quantum well disordering achieved in each of the samples. These measurements were performed at 4.2 K, and spectra were collected using a Bomem FTIR. PL recombination rates were determined by time-resolved photoluminescence (TRPL), and used to monitor the quality of the QWs after intermixing. The experimental set-up has been described elsewhere.[10] The temperature evolution of the carrier lifetimes in the intermixed QWs was determined from 4.2 to 100 K. In all experiments, photo-excitation was provided by a dye laser pumped by a frequency doubled mode-locked Nd:YAG, which produced 5 ps pulses of 625 nm light. The excitation intensity was 10 W/cm^2 over an excitation diameter of 100 μm.

Figure 1 shows the corresponding blue-shift of the QW band gap in each of the samples as determined by the PL emission peaks. Energy shifts in the intermixed regions were referenced to the peak emission energies of the unimplanted halves of each sample. These data indicate a critical dose situated between 10^{11} and 10^{12} cm^{-2} for our 8.56 MeV arsenic implanted GaAs/AlGaAs QWs. PL signal intensity largely recovered after annealing for implantation doses between 10^{10} and 10^{12} cm^{-2}. Significant reduction in PL efficiency, however, was observed for the 10^{14} and 10^{15} cm^{-2} As^{4+} implanted samples (increasingly pronounced at higher temperatures).

At 4.2 K, all samples in both intermixed and nonintermixed regions yielded PL decay times in the vicinity of 0.4 ns (see Fig. 2). Observed lifetime fluctuations in the implanted regions follow those in the adjacent nonintermixed regions, and reflect inhomogeneity of growth conditions across the substrate during deposition of the epitaxial layers. At 100 K, recombination times for the as-grown material are on the order of 1 ns, with fluctuations following the same pattern revealed at 4.2 K. The recombination rates in the intermixed regions, however, deviate significantly from those of the as-grown material. For implantation doses near, or in excess of the critical dose, carrier lifetimes are found to diminish rapidly. For doses of 10^{14} and 10^{15} cm^{-2}, values for the 100 K PL lifetimes fall near or below the instrumental response of our system (110 ps), and as such reflect upper limits on their actual values.

From 4.2 to 100 K, the nonimplanted QW regions demonstrate a monotonic increase of decay times with sample temperature (Fig. 3). In particular, we obtain a reasonably linear increase between 4.2 and 60 K which has been observed by others.[11,12] This has been explained as resulting from the temperature dependent distribution of kinetic en-

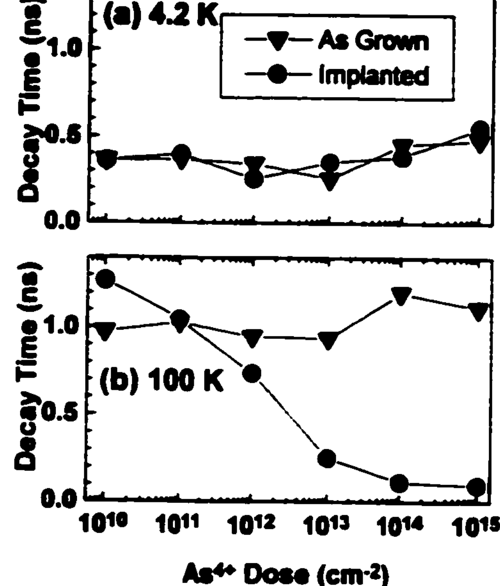

FIG. 2. Dose dependence of the recombination times evaluated at (and (b) 100 K. Uncertainties for these points are on the order of :

ergy among excitons in the QW. As only free exciton near the Brillouin-zone center can recombine, increa tice temperatures decrease the portion of them whic readily recombine.[13]

At low temperatures, intermixed and noninte wells possess similar recombination rates. As impla doses are increased, the temperature at which the li begin to fall away from the as-grown curve decrease behavior may be explained by the formation of an inc number of nonradiative recombination sites in the inte QW structures resulting from the ion bombardment. creasing the density of defects through implantation, erage separation (ΔS) between nonradiative recomb

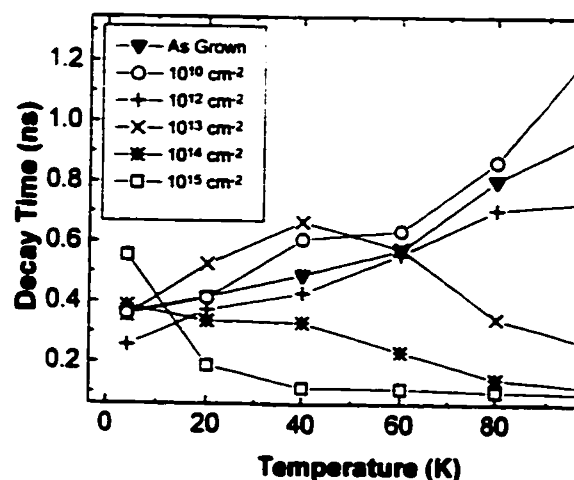

FIG. 3. Decay times for as-grown and intermixed QW structures as tion of sample temperature. The trace for 10^{11} cm^{-2} overlaps with grown data (to within ±0.06 ns) and has been omitted for clarity of tation. Error bars for any given trace are on the order ±0.05 variations between the "as-grown" curves from sample to sample b the order of 0.1 ns.

the average PL displacement before recombination is significantly smaller than ΔS, fewer encounters with nonradiative centers result. This may explain why lifetimes at low temperature seem unaffected by the intermixing process. At higher temperatures, FE diffusivities increase,[14] and a greater number of nonradiative defects may be encountered (in the case of the higher dose samples) thus reducing the carrier lifetimes. This would also be consistent with the decreases observed in PL intensity for these samples at increased temperatures.

For the 10^{10} cm^{-2} As^{4+} implanted sample, lifetimes are actually enhanced beyond 40 K. Other isolated points show this behavior (4.2 to 40 K for 10^{13} cm^{-2}, and 4.2 K for 10^{15} cm^{-2}). This could perhaps be attributed to the formation of defects in the QWs which localize excitons, and widen their spread in momenta. This increases the population of higher momentum states, and hence the recombination times.[15] The appearance of such points at lower temperatures for higher doses, could then be seen as resulting from the combined effects of the dose-dependent densities of these sites, with the temperature dependence of excitonic diffusivities. Taking excitonic diffusivities from Ref. 14, coupled with our PL-lifetime measurements yield diffusion lengths of 0.19 μm (at 4.2 K) and 1.8 μm (100 K) for FE in our 10^{10} cm^{-2} implanted sample. This would imply that for this sample, the average separation between these proposed binding sites would be on the order of a micron. The increase in PL-lifetime observed at 4.2 K for the 10^{15} cm^{-2} sample may reflect the higher density of trapping centers created at this dose. The rapid drop in lifetime observed at 20 K, however, would suggest a defect with a weaker binding potential than those present at lower doses. This might be expected if the excitonic binding sites result from local fluctuations in the QW widths caused by the intermixing process. For narrower QWs (in our case corresponding to the low dose intermixed wells), width fluctuations of a given amplitude will have a more substantial effect on the local QW band gap,[15] and in such a way perhaps allow for the formation of binding sites with greater localization potentials.

To summarize, the temperature dependence of the PL recombination rates of intermixed GaAs/AlGaAs QW structures [...] dose required to initiate a detectable shift in the QW CWPL spectrum. Below the critical dose, the observed PL-lifetimes are greater or equal to those of the as-grown material between 4.2 and 100 K. Above the critical dose lifetimes are reduced with increasing fluence. The temperature for which this difference becomes apparent is found to be dose-dependent. In both cases we suggest these behaviors can be understood in terms of the temperature dependence of the excitonic diffusivities, and the dose-dependent defect densities and types present in the QWs after annealing.

The authors wish to thank Z. R. Wasilewski for growth of the samples. This work was partially supported by the Natural Sciences and Engineering Research Council of Canada.

[1] L. B. Allard, G. C. Aers, S. Charbonneau, T. E. Jackman, R. L. Williams, I. M. Templeton, M. Buchanan, D. Stevanovic, and F. J. D. Almeida, J. Appl. Phys. 72, 422 (1992).
[2] F. Laruelle, Y. P. Hu, R. Kubena, W. Robinson, J. Merz, and P. M. Petroff, J. Vac. Sci. Technol. B 7, 2034 (1989).
[3] Y. Hirayama, S. Tarucha, Y. Suzuki, and H. Okamoto, Phys. Rev. B 37, 2774 (1988).
[4] E. S. Koteles, A. N. M. Masum Choudhury, A. Levy, B. Elman, P. Melman, M. A. Koza, and R. Bhat, Mater. Res. Soc. Symp. Proc. 240, 171 (1992).
[5] J. H. Marsh, Semicond. Sci. Technol. 8, 1136 (1993).
[6] R. Kalish, L.-Y. Kramer, K.-K. Law, J. L. Merz, L. C. Feldman, D. C. Jacobson, and B. E. Weir, Appl. Phys. Lett. 61, 2589 (1992).
[7] J. F. Ziegler, J. P. Biersack, and U. Littmark, *The Stopping and Ion Range of Ions in Matter* (Pergamon, New York, 1985).
[8] L. B. Allard, G. C. Aers, P. G. Piva, P. J. Poole, M. Buchanan, I. M. Templeton, T. E. Jackman, S. Charbonneau, U. Akano, and I. V. Mitchell, Appl. Phys. Lett. 64, 2412 (1994).
[9] S. Charbonneau, P. J. Poole, P. G. Piva, G. C. Aers, E. S. Koteles, M. Fallahi, J.-J. He, J. P. McCaffrey, M. Buchanan, M. Dion, R. D. Goldberg, and I. V. Mitchell, J. Appl. Phys. 78, 3697 (1995).
[10] S. Charbonneau, L. B. Allard, J. F. Young, G. Dyck, and B. J. Kyle, Rev. Sci. Instrum. 63, 5315 (1992).
[11] J. Feldmann, G. Peter, E. O. Göbel, P. Dawson, K. Moore, and C. Foxon, Phys. Rev. Lett. 59, 2337 (1987).
[12] H. Akiyama, S. Koshiba, T. Someya, K. Wada, H. Noge, Y. Nakamura, T. Inoshita, A. Shimizu, and H. Sakaki, Phys. Rev. Lett. 72, 924 (1994).
[13] L. C. Andreani, Solid State Commun. 77, 641 (1991).
[14] H. Hillmer, A. Forchel, S. Hansmann, M. Morohashi, E. Lopez, H. P. Meier, and K. Ploog, Phys. Rev. B 39, 10901 (1989).
[15] M. A. Herman, D. Bimberg, and J. Christen, J. Appl. Phys. 70, R1 (1991).

CHAPTER 5

Conclusions

We have demonstrated the effectiveness of multiple implants and RTAs in delivering several times the maximum energy shift attributable to a single implant/RTA in GaAs/AlGaAs, InGaAs/GaAs, and InGaAs/InP QW structures. These results were obtained at low energy (32 & 100 keV) using both a focused ion beam facility, and a more commercially viable broad area implanter. For these samples, the limitations encountered in intermixing the QWs with a single implant/RTA cycle were attributed to the creation of damage in the crystals by the ion implantation. Beyond a certain dose, the effective number of single vacancies able to participate in the intermixing process during the RTA was supposed to be reduced in favor of the creation of stable defect complexes (SDCs). Subsequent annealing was found to restore the samples' capacities to support elevated single vacancy concentrations without the preferential formation of SDCs during the following RTA. This allowed intermixing of the QWs beyond the single dose limit.

We also demonstrated the effectiveness of high energy broad area implantation (8 MeV As^{4+}) in intermixing an InGaAs/GaAs laser structure possessing a QW 2 μm below the sample surface. The influence of ion beam current and sample temperature were briefly investigated using this structure, and results indicated that dynamic annealing

during implantation clearly affects the extent of intermixing achieved, as well as the amount of residual damage present in the QWs after thermal processing.

Lastly, a series of time-resolved photoluminescence (TRPL) experiments were performed on 8.56 MeV As^{4+} implanted GaAs/AlGaAs QW structures. Below the critical dose, the observed PL lifetimes were greater or equal to those of the as-grown material between 4.2 K and 100 K. Above the critical dose lifetimes were increasingly reduced by the higher dose implantations. The temperature for which this difference became apparent was found to be dose-dependent. In both cases we suggested these behaviors could be understood in terms of a convolution of the temperature dependence of the excitonic diffusivities, with the dose-dependent densities and defect-types present in the QWs after annealing.

At the time of the writing of this thesis, ion implantation induced QW intermixing remains an actively pursued project in Dr. Charbonneau's group at the NRC. Some of the group's successful applications of this technique have included the creation of bandgap shifted QW waveguides[5.1], superluminescent laser diodes, and most recently, bandgap tuned InGaAs/InGaAsP/InP QW lasers.[5.2] This latter result can be expected to play a key role in the future development of multiplexing/demultiplexing laser/detector arrays by the telecommunications sector.

Ongoing experiments by the author include InGaAs/GaAs QW lasers with intermixed passive cavity sections, and attempts at the passivation of implantation damage in GaAs/AlGaAs QW structures by hydrogen plasma exposure. Preliminary results suggest that the addition of intermixed passive sections to the InGaAs/GaAs QW laser diodes has been successful in lowering the temperatures of the laser facets during device operation.[5.3]

The prospects for future work in this area remain extremely promising. In the search for applications of this technique, many qualitative effects are beginning to be mapped out by researchers in this area (segregation of lattice species by implantation, differential damage accumulation in layers, the monolayer progression of interdiffusion in InGaAs/InP, etc.). Recent experiments by Poole and coworkers[5.4] indicate substantial differences in the diffusion properties of vacancies between the GaAs/AlGaAs and InGaAs/InP systems. In most cases, however, the detailed microscopic models invoked to explain many of these observations remain to be substantiated experimentally. This final point will comprise the central aim of the author's work during the tenure of his Ph.D. position with Dr. Mitchell's group at the University of Western Ontario.

REFERENCES

1.1 M. Gershenzon in Semiconductors and Semimetals, Vol 3, Edited by R.K. Willardson and A.C. Beer, Academic Press, London, 1966, 432 p.

1.2 C. Kittel, Introduction to Solid State Physics, 6th Edition, Wiley and Sons, New York, 1986, 646 p.

1.3 H. Hillmer, A. Forchel, S. Hansmann, M. Morohashi, E. Lopez, Phys. Rev. B 39 (13) 10901 (1989)

1.4 B.C. Cavenet in Luminescence Spectroscopy, Edited by M. Lumb, Academic Press, London, 1978, 375 p.

1.5 G.W. 't Hooft, W.A.J.A van der Poel, L.W. Molenkamp, C.T. Foxon. Phys Rev. B. 35 (15) 8281 (1987)

1.6 D. Bimberg and J. Christen in Two Dimensional Systems, Heterostructures and Superlattices, Edited by H.J. Queisser, Springer-Verlag, New York, 1984, 293p.

1.7 G. Bastard, Wave Mechanics Applied to Semiconductor Heterostructures, John Wiley and Sons, New York, 1994, 427p.

1.8 R. Dingle, W. Wiegmann, C.H. Henry, Phys. Rev. Lett. 33 (14) 827 (1974)

1.9 M.A. Herman, D.Bimberg, J. Christen, J. Appl. Physics 70 (2) R1 (1991)

2.1 T. Imai, M. Murakami, Y. Fukada, M. Aiki, T. Ito, *Conf. Procs. - Topical Meeting on Optical Amplifiers and their Applications*, Paper PD12, 24-26 June 1992.

2.2 J.H. Marsh. Semicond. Sci. Technol. 8, 1136 (1993)

2.3 R.C. Alferness, U. Koren, L.L. Buhl, B.I. Miller, M.G. Young, T.L. Koch, G. Raybon, C.A. Burrus, Appl. Phys. Lett. 60 (26) 3209 (1992)

2.4 J.E. Zucker, K.L. Jones, M.A. Newkirk, R.P. Gnall, B.I. Miller, M.G. Young, U. Koren, C.A. Burrus, B. Tell, Electron. Lett. 28 (20) 1888 (1992)

2.5 P. Demeester, L. Buydens, P. Van Daele, Appl. Phys. Lett. 57 (2) 168 (1990)

2.6 E. Colas, C. Caneau, M. Frei, E.M. Clausen Jr., W.E. Quinn, M.S. Kim, Appl. Phys. Lett. 59 (16) 2019 (1991)

2.7 L.B. Allard, G.C. Aers, P.G. Piva, P.J. Poole, M. Buchanan, I.M. Templeton, T.E. Jackman, S. Charbonneau, U. Akano, I.V. Mitchell, Appl. Phys. Lett. 64 (18) 2412 (1994)

2.8 A. McKee, C. J. McLean, A.C. Bryce, R. M. De La Rue, J.H. Marsh, C. Button, Appl. Phys. Lett. 65 (18) 2263 (1994)

2.9 G. Lullo, A. McKee, C. J. McLean, A.C. Bryce, C. Button, J.H. Marsh, Electron. Lett. 30 (19) 1623 (1994)

2.10 E.V.K. Rao, A. Hamoudi, Ph. Krauz, M. Juhel, H. Thibierge, Appl. Phys. Let 23 (17) 2096 (1995)

2.11 J.D. Ralston, W.J. Schaff, D.P. Bour, L.F. Eastman, Appl. Phys. Lett. 54 (6) 534 (1989)

2.12 S.G. Ayling, A.C. Bryce, I. Gontijo, J.H. Marsh, J.S. Roberts, Semicond. Sci. Technol. 9 2149 (1994)

2.13 A. Pepin, Conference given at NRC - Montreal Road Campus, Sept., 1995

2.14 K.B. Kahen, G. Rajeswaran, S.T. Lee, Appl. Phys. Let. 53 (17) 1635 (1988)

2.15 P.G. Piva, P.J. Poole, S. Charbonneau, E.S. Koteles, M. Buchanan, G. Aers, A.P. Roth, Z.R. Wasilewski, J. Beauvais, R.D. Goldberg, Superlat. and Microstruct., 15 (4) 385 (1994)

2.16 F.E. Prins, G. Lehr, H. Schweizer. Appl. Phys. Let. 63 (10) 1402 (1993)

2.17 Y. Hirayama, S. Tarucha, Y. Suzuki, H. Okamoto. Phys. Rev. B. 37 (5) 2774 (1988)

2.18 P.D. Townsend, J.C. Kelly, N.E.W. Hartley, Ion Implantation, Sputtering and Their Applications, Academic Press, New York, 1976, 333p.

2.19 J.S. Williams, H.H. Tan, R.D. Goldberg, R.A. Brown, C. Jagadish, Mat. Res. Soc. Symp. Proc., Vol. 316, 15 (1994)

2.20 T.E. Haynes, O.W. Holland, U.V. Desnica, Mat. Res. Symp. Proc. Vol 240, 823 (1992)

2.21 N.A.G. Ahmed, C.E. Christodoulides, G. Carter. Rad. Eff. (52) 211 (1980)

2.22 T.Y. Tan, U. Gosele, Appl. Phys. Lett., 52 (15) 1240 (1988)

2.23 J. Crank, The Mathematics of Diffusion, Oxford University Press, London, 1956, 347 p.

2.24 J. Cibert, P.M. Petroff, Phys. Rev. B. 36 (6) 3243 (1987)

3.1 L.B. Allard, G.C. Aers, S. Charbonneau, T.E. Jackman, M. Buchanan, D. Stevanovic, FLD Almeida. J. Appl. Phys. 72 (2) 422 (1992).

3.2 F. Laruelle, A. Bagchi, M. Tsuchiya, J. Merz, P.M. Petroff. Appl. Phys. Let. 56 (10) 1561 (1990)

3.3 J.W. Mayer, L. Eriksson, J.A. Davies, Ion Implantation In Semiconductors, Academic Press, New York, 1970, 280p.

3.4 J.F. Ziegler, J.P. Biersack, U. Littmark, The Stopping and Range of Ions in Solids, Vol 1, Pergamon Press, Great Britain, 1985, 321p.

3.5 P.J. Poole, S. Charbonneau, G.C. Aers, T.E. Jackman, M. Buchanan, M. Dion, R.D. Goldberg, I.V. Mitchell. J. Appl. Phys. 78 (4) 2367 (1995)

3.6 P.G. Piva, S. Charbonneau, I.V. Mitchell, R.D. Goldberg. Appl. Phys. Lett. 68 (16) 2252 (1996)

3.7 D. Heiman and A.V. Nurmikko in The Spectroscopy of Semiconductors, Vol. 36, Edited by R.K. Willardson and A.C. Beer, Academic Press, United Kingdom, 1992, 435 p.

3.8 P. Milonni and J.Eberly, Lasers, John Wiley & Sons, New York, 1988, 731 p.

3.9 Hartmann & Braun, The Michelson Series FT-IR Spectrometer User's Guide, Version 1.50, Bomem Inc., Quebec, Canada, 1992.

3.10 S. Charbonneau, L.B. Allard, Rev. Sci. Instruments, 63 (11) 5315 (1992)

5.1 J.-J. He, Y. Feng, E.S. Koteles, P.J. Poole, M. Davies, M. Dion, R.D. Goldberg, I.V. Mitchell, S. Charbonneau, Electron. Lett. 31 (24) 2094 (1995).

5.2 S. Charbonneau, P.J. Poole, Y. Feng, G.C. Aers, M. Dion, M. Davies, R.D. Goldberg, I.V. Mitchell, Appl. Phys. Lett., 67 (20) 2954 (1995)

5.3 P.G. Piva, S. Fafard, M. Dion, M. Buchanan, S. Charbonneau, R.D. Goldberg, I.V. Mitchell, *To be submitted to Appl. Phys. Lett.*

5.4 P.J. Poole, S. Charbonneau, G.C. Aers, T.E. Jackmann, M. Buchanan, M. Dion, R.D. Goldberg, I.V. Mitchell, J. Appl. Phys. 78 (4) 2367 (1995).

TEST TARGET (QA-3)

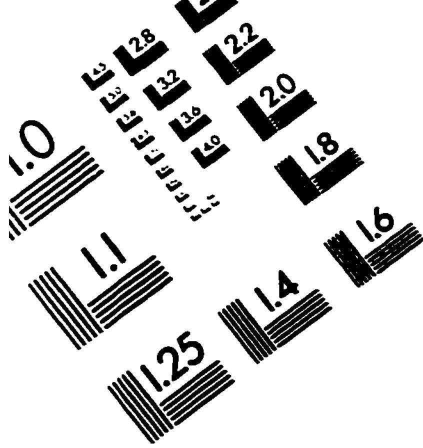

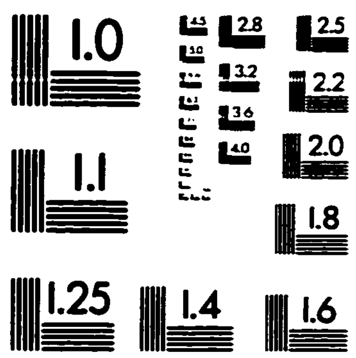

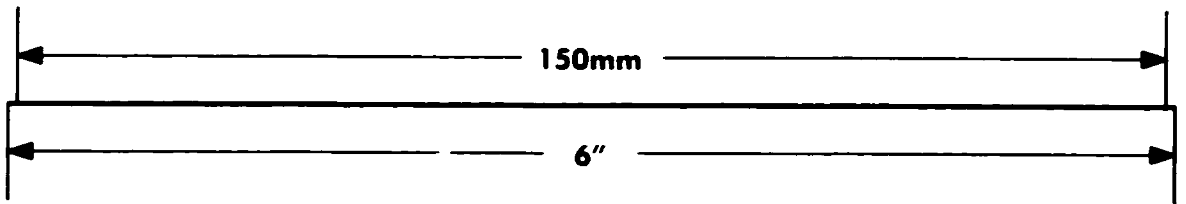

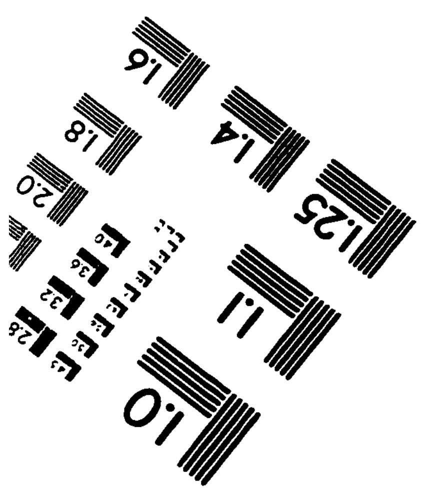
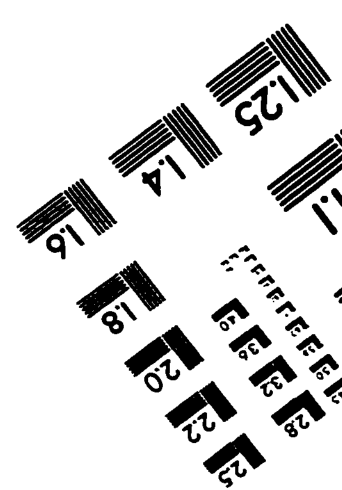

APPLIED IMAGE . Inc
1653 East Main Street
Rochester, NY 14609 USA
Phone: 716/482-0300
Fax: 716/288-5989

© 1993, Applied Image, Inc., All Rights Reserved